ADDRESSING FACIAL NERVE STIMULATION IN COCHLEAR IMPLANTS USING MODEL-BASED DIAGNOSTICS

by

Jacques van der Westhuizen

Submitted in partial fulfilment of the requirements for the degree
Master of Engineering (Bioengineering)

in the

Department of Electrical, Electronic and Computer Engineering
Faculty of Engineering, Built Environment and Information Technology

UNIVERSITY OF PRETORIA

February 2020

SUMMARY

ADDRESSING FACIAL NERVE STIMULATION IN COCHLEAR IMPLANTS USING MODEL-BASED DIAGNOSTICS

by

Jacques van der Westhuizen

Supervisor:	Prof T. Hanekom
Co-supervisor:	Prof J.J. Hanekom
Department:	Electrical, Electronic and Computer Engineering
University:	University of Pretoria
Degree:	Master of Engineering (Bioengineering)
Keywords:	model-based diagnostics, facial nerve stimulation, 3D cochlear implant modelling, user-specific model

Post-implantation facial nerve stimulation is a common side-effect of cochlear electrical stimulation. Facial nerve stimulation can often be resolved through adjustments in speech processor fitting but, in some instances, exhibit limited benefit or may have a detrimental effect on speech perception. In this study, the apical reference stimulation mode was investigated as a potential intervention to facial nerve stimulation. Firstly, a model refinement software tool was developed to improve the accuracy of models created by an automated workflow. Secondly, the refined model of the human cochlea, facial nerve and electrode array, coupled with a neural model, was used to predict excitations of auditory and facial nerve fibres. Finally, psychoacoustic tests were used to determine auditory comfort and threshold levels for the apical reference stimulation mode while simultaneously capturing electromyography data. The refinement tool illustrated an improved accuracy compared to measured data. Models predicted a desirable outcome for apical reference stimulation, as facial nerve fibre thresholds were higher and auditory thresholds were lower, in direct comparison to conventional monopolar stimulation. Psychoacoustic tests illustrated decreased auditory thresholds and increased dynamic range during apical reference

stimulation. Furthermore, apical reference stimulation resulted in lower electromyography energy levels, compared to conventional monopolar stimulation, which suggests a reduction in facial nerve stimulation. Subjective feedback corroborated that apical reference stimulation alleviated facial nerve stimulation. This suggests that apical reference stimulation may be a viable strategy to alleviate facial nerve stimulation considering the improvements in dynamic range and auditory thresholds, complemented with a reduction in facial nerve stimulation.

LIST OF ABBREVIATIONS

2IFC	Two-interval forced choice
AAM	Adapted automated method
ALT	Angle between the labyrinthine and the tympanic segments
AN	Auditory nerve
ANF	Auditory nerve fibre
AR	Apical reference
ATM	Angle between the tympanic and mastoid segment
BC	Bone conduction
BCNC	Bony cochlear nerve canal
BP	Bipolar
CI	Cochlear implant
C-level	Comfortable level
CN	Cochlear nerve
CT	Computerised tomography
CU	Current units
DFT	Discrete Fourier Transform
ECE	Extracochlear electrode
EDRR	Effective dynamic range ratio
EF	Meatal foramen
EMG	Electromyography
FN	Facial nerve
FNF	Facial nerve fibre
FNS	Facial nerve stimulation

GG	Geniculate ganglion
GUI	Graphic user interface
HINT	Hearing in noise test
ICE	Intracochlear electrode
LLS	Length of the labyrinthine segment
LMS	Length of the mastoid segment
LO	Labyrinthine ossification
LTS	Length of the tympanic segment
MAE	Mean absolute error
MP	Monopolar
NMT	Nucleus MATLAB toolbox
OC	Organ of Corti
PEST	Parameter estimation by sequential testing
SEMG	Surface electromyography
SG	Second genu
SMF	Stylomastoid foramen
SP	Speech processor
T-level	Threshold level
UBTC	Upper basal turn of the cochlea
WL(1-2)	Width of the labyrinthine segment (1-2)
WM(1-3)	Width of the mastoid segment (1-2)
WT(1-3)	Width of the tympanic segment (1-2)

TABLE OF CONTENTS

LIST OF FIGURES

LIST OF TABLES

CHAPTER 1 INTRODUCTION

1.1 PROBLEM STATEMENT

1.1.1 Context of the problem

A cochlear implant (CI) is a device that uses electrical pulses delivered by an electrode array, which is placed inside the cochlea to directly stimulate surviving and functioning auditory nerve fibres (ANFs) in an attempt to restore the sense of hearing in profoundly deaf people (Clark, 1973). Attempts to restore the sense of hearing by electrical stimulation have been recorded from as early as 1790 (Wilson and Dorman, 2008). One of the first recorded attempts to directly stimulate the auditory nerve (AN) was performed by Djourno and Eyries (1957). A person was implanted with a single electrode into the stump of the AN and could successfully perceive electrical stimuli. Although stimulus intensity discrimination was relatively good, the frequency discrimination was relatively poor, as expected from a single channel implant. The CI user could not understand speech or discriminate between speakers or sounds, however, the presence of environmental sounds was detectable. The device failed after a few months, which led to the reimplantation of a new device.

A few years later, Dr William F. House read the report from Djourno and Eyries (1957) in a newspaper article, which inspired him to create a CI of his own (House, 1987). In 1961, a group of deaf individuals were implanted with a gold wire, which could deliver an electrical stimulus to the impaired cochlea. Although implantees could detect environmental sounds, they could not understand speech. Insufficient biocompatibility of the electrodes caused

complications that required the implants to be removed, which limited long-term testing. Numerous shortcomings still existed with early implants which rendered them unsuitable for long-term use (Clark, 1973).

Dr House temporarily halted his research but resumed his work on implants in 1967, introducing the first CI system that served as a long-term solution, which could be used outside a laboratory environment. This system was seen as a landmark in the history of CIs (Eshraghi et al., 2012). Since this historical event in cochlear implantation, advances in technology allowed the development of sophisticated multichannel devices, which can deliver spectrally rich acoustic content to the hearing-impaired cochlea.

Despite decades of research, advances in CIs are ongoing. Reduced implant size, advances in directional microphone technology, robotic electrode insertion, battery life improvements, improved speech processing strategies, affordability and improved music perception, are all areas which are currently under investigation in CI research to improve user experience and reduce complications associated with CIs (Eshraghi et al., 2012, Seeber et al., 2001, Weissgerber et al., 2019).

A well-known complication experienced by CI users is facial nerve stimulation (FNS) (Smullen et al., 2005). FNS occurs when electrical current intended to stimulate auditory neurons, inadvertently excites the adjacent facial nerve fibres (FNFs) (Berrettini et al., 2011). When this occurs, the CI user may experience facial muscle twitching during intracochlear electrical stimulation. Twitching occurs in the vicinity of the orbicularis oculi and oris muscles, on the same side of the face where the CI resides (Bahmer et al., 2017). The labyrinthine segment of the FN is most likely the branch being stimulated in most implantees (Bigelow et al., 1998). The presence of FNS is specific to the CI user and may be severe, mild or absent, or may be absent in one ear and present in the other in bilateral implantees (Seyyedi et al., 2013). The incidence of FNS has been reported to be as high as 14.63% in adult users (Niparko et al., 1991). Factors that seem to influence the incidence of FNS include otosclerosis, cochlear malformations, cochlear ossification (post-meningitis,

otosyphilis), temporal bone fracture, a narrow bony cochlear nerve canal (BCNC) and osteoporosis (Bahmer et al., 2017, Bigelow et al., 1998, Kelsall et al., 1997, Kempf et al., 1999, Muckle and Levine, 1994, Niparko et al., 1991, Rotteveel et al., 2004). High current levels, which are required in some CI users to achieve adequate loudness perception, have also been reported to influence the incidence of FNS due to high-intensity currents reaching the adjacent FN (Bigelow et al., 1998).

1.1.2 Research gap

Recent attempts to address FNS have been made, but interventions often come with a detrimental effect on either the quality of hearing or the quality of life, and may not eliminate all symptoms. Non-invasive interventions involve the modification of CI fitting parameters such as the lowering of stimulation levels, disabling of offending electrodes, increased stimulation pulse widths, triphasic pulse stimulation and alternative stimulation modes (Alharbi et al., 2012, Berrettini et al., 2011, Seyyedi et al., 2013).

Berrettini et al. (2011) suggested that disabling offending electrodes and reducing stimulation levels often result in a low loudness level which is not sufficient for speech discrimination. Alharbi et al. (2012) presented a case report of a 75-year old male who developed FNS after cochlear implantation. Various alterations in CI fitting parameters did not eliminate FNS. Increased pulse widths used in combination with an alternative stimulation mode was required to eliminate the effects of FNS. These alterations led to the deterioration of hearing and speech understanding to such an extent that reimplantation, together with advanced programming techniques, was required to reduce the effects of FNS.

Triphasic pulse stimulation can also be beneficial to users experiencing FNS. Recent reports indicated that FNF threshold levels (T-levels) could increase when triphasic pulse stimulation is used, presumably because of the highly focused stimulation produced by triphasic stimulation (Bahmer et al., 2017, Bahmer and Baumann, 2016, Schatzer et al., 2014). Triphasic pulse stimulation does not always eliminate FNS but has demonstrated a

reduction in symptoms in most cases. However, ANF excitation is less effective with triphasic pulse stimulation than with conventional biphasic stimulation, and the implementation of triphasic stimulation protocols is only available in a limited number of implants.

When FNS is present and modified CI fitting parameters demonstrate little or no improvement, botulinum toxin injections can be used as a treatment because it induces temporary facial muscle paralysis. Langman et al. (1995) presented a case report of a CI user who experienced FNS on 15 out of 22 electrodes with the result that the 15 offending electrodes had to be turned off. After receiving botulinum toxin treatment, the number of deactivated electrodes was reduced from 15 to 8. An increase in dynamic range was reported from four electrodes which were active prior to the treatment. These improvements considerably increased sound quality and speech understanding. Botulinum toxin treatment interferes with neural transmissions by blocking the release of acetylcholine, which is the principal neurotransmitter at the neuromuscular junction (Nigam and Nigam, 2010). Although implant performance effectively increased in the study done by Langman et al. (1995), the treatment induced facial muscle paralysis, which is an undesired side-effect of botulinum toxin treatment. Furthermore, botulinum toxin treatment is a temporary intervention and requires frequent botulinum toxin injections (Nigam and Nigam, 2010).

In some cases, FNS results in such severe discomfort or non-optimal use of the CI, that it is mostly unusable and leads to explantation or reimplantation (Berrettini et al., 2011, Seyyedi et al., 2013). In these cases, a conventional electrode array may be replaced with an electrode array in which electrode contacts face the modiolus, or the implant may be removed, and implanted in the contralateral ear (Alharbi et al., 2012). Explantation or reimplantation is not the preferred intervention due to trauma inflicted during surgery (Martins et al., 2015).

Due to the complications existing in conventional interventions, it is necessary to further the investigation into possible non-invasive interventions that would ensure optimal CI performance and good quality of life while reducing or eliminating the effects of FNS.

1.2 RESEARCH OBJECTIVES AND QUESTIONS

The objective of intracochlear stimulation is to artificially induce neural excitation that mimics the acoustically elicited neural excitation patterns for a given sound. Computational models of electrical stimulation with a CI should thus predict neural excitation patterns as governed by the many factors that describe the electrical characteristics of the cochlea and surrounding tissue. A three-dimensional (3D) volume conduction description of the implanted cochlea, electrode array and FN, coupled to a nerve fibre model, can be used to predict neural excitation from the potential distribution resulting from intracochlear current injections (Hanekom and Hanekom, 2016). Various 3D CI models have been suggested to describe either the micromechanical or the electrophysiological behaviour of the cochlea. This study utilises 3D electro-anatomical models of the auditory and facial nerve (FN) systems, to facilitate the prediction of electrophysiological behaviour of the electrically stimulated cochlea. The 3D modelling techniques developed by Malherbe et al. (2016), Gross et al. (2017) and Crous et al. (2018) will be used to create person-specific volume conduction models of the cochlea, FN and electrode array.

Malherbe et al. (2016) developed a method in which landmarks are manually identified on CT scans, whereafter a 3D model is created from measured data. This technique, hereafter referred to as the manual method, requires extensive involvement from the investigator and is usually very time-consuming. Since user-specific computational modelling of a CI is envisioned to become part of the clinical maintenance protocol, Crous et al. (2018) developed an automated method, which automates most of the landmark detection process. Furthermore, Gross et al. (2017) included the FN geometry into the cochlear model to investigate the electrical potential distribution characteristics at the FN.

The first objective of this study is to evaluate the accuracy of the automated method and to propose a refinement tool that would allow the investigator to increase the overall accuracy of the model, if discrepancies exist. Increasing the accuracy of the model is essential since cochlear morphology and electrode placement often affect potential distributions in volume

conduction models (Badenhorst et al., 2017, Malherbe et al., 2016). Additionally, modifications to the cochlear model will be investigated to determine how variations in geometry affect neural excitation predictions and to give recommendations regarding future models.

The second objective of this study is to capture the underlying mechanisms of FNS in a computational model to allow assessment of various intervention strategies. The study will seek to identify a non-invasive intervention that addresses FNS while maintaining optimal CI performance and quality of life. Using the refined modelling process, a model-based intervention will be investigated, which aims to increase predicted T-levels of the FN while decreasing T-levels of the AN. Finally, this intervention will be evaluated in clinical testing to determine whether it is effective to reduce FNS and to determine the effects of this intervention on implant performance, in terms of dynamic range and auditory T-levels.

The study's primary objectives have prompted investigation into the following research questions:

1. What is the accuracy of the automated method and can a refinement tool aid to increase the accuracy of 3D person-specific volume conduction models of the human cochlea and electrode array?
2. Which recommendations can be made regarding the 3D modelling of the human cochlea?
3. Can a 3D model be used to rate a selection of FNS interventions based on their effectiveness in reducing FNS?
4. Does a model-predicted intervention prove to be effective in reducing FNS in clinical experiments?
5. What is the effect of this intervention on perceptual T-levels and dynamic range?
6. How successful is this model in predicting measured outcomes?

1.3 APPROACH

Since cochlear morphology and electrode array placement into a model often affects predicted T-levels, it is beneficial to create models which mimic the characteristics of the cochlear anatomy and electrode array placement for a specific person. High-resolution anatomical images can be used for this purpose since it usually contains extensive detail of the microanatomy of the cochlea. However, high-resolution imaging is typically not suitable for living persons due to its destructive nature (e.g. histology) or high doses of radiation (e.g. micro-CT) often associated with it. Therefore, limited anatomical data are obtainable in living persons due to the necessity of using low-resolution clinical imaging. Despite this limitation, Malherbe et al. (2016) illustrated that person-specific 3D models could be constructed using clinical computerised tomography (CT) scans, which typically require lower doses of radiation, compared to high-resolution imaging techniques.

Conventionally, this process required extensive involvement from the investigator, but an automated workflow was developed by Crous et al. (2018) which demonstrated relatively good performance in terms of accuracy. However, the automated workflow may deviate from measured landmarks in some instances. Discrepancies are especially evident when output spirals are registered back onto CT images. In the present study, a refinement tool will be developed to adapt output spirals from the automated method by visually comparing model data against CT images. The refinement tool will enable the investigator to make localised adjustments to the model geometry where the automated placement of landmarks visually deviates from the location of landmarks on the CT images. The landmark data extracted via the automated and adapted methods will be compared to data measured by an experienced anatomist to quantify the accuracy of the two methods, and to determine whether improvements can be made using the refinement tool.

Geometric variations in models can potentially influence the accuracy of predicted T-levels (Malherbe et al., 2016). Therefore, some factors regarding the modelling process should be taken into account when creating a 3D model. A selection of geometric variations will be

investigated to determine how it affects predicted T-levels. Based on these findings, recommendations will be made, which could potentially assist in future modelling work.

To date, numerous 3D CI models have been developed for research purposes, but very few have been employed in the diagnosis of CI complications (Hanekom and Hanekom, 2016). Hanekom and Hanekom (2016) suggested that computational models are ideally suited to inform the diagnosis and treatment of side-effects related to cochlear implantation, e.g. FNS. Incorporating the FN geometry into the model can potentially aid an investigation into the electrical potential distribution at the FN (Gross et al., 2017). Using electrical potential distributions, predicted T-levels for ANFs and FNFs can be calculated. In this study, T-level predictions will be utilised to evaluate an alternative stimulation mode and to rate a selection of interventions according to their effectiveness in reducing FNS. The difference between ANF and FNF T-levels will be used as a measure of the effectiveness of potential interventions.

Once the benefit of the proposed intervention has been established in simulation, it will be evaluated in a clinical experiment. The experiment will be designed to determine the efficacy of the intervention in terms of alleviating FNS symptoms, but also to determine the degree to which auditory T-levels and dynamic range are influenced since hearing performance needs to be maintained. Psychoacoustic tests will be used to find auditory T- and C-levels and will be conducted for the participant's present stimulation mode, as well as the alternative stimulation mode. The results from these tests will aid in quantifying the effects of the intervention on T-levels and dynamic range since these parameters can consequently be used to indicate the degree to which implant performance is influenced. High T-levels usually require high stimulation levels, which are often associated with increased channel interaction, low battery life, voltage compliance problems and may eventually degrade speech perception (Mertes and Chinnici, 2006). Dynamic range will also be used as a measure of implant performance since an increased dynamic range is often associated with an increase in speech perception (Khater et al., 2015).

Furthermore, electromyography (EMG) data will be captured during every stimulus since myogenic responses and artefacts resulting from electrical stimulation are often distinguishable in biosignal recordings (Bahmer and Baumann, 2016). The artefact can potentially quantify the amount of current leaking from the cochlea into the surrounding tissue. As such, the electrical artefact can be used to objectively indicate the degree to which FNS is experienced since artefact reduction is often associated with a reduction of FNS (Bahmer and Baumann, 2016). Additionally, feedback from the participant will be recorded in an attempt to corroborate the findings in EMG data. EMG data will be collected during electrical stimulation using the participant's present stimulation mode, as well as the alternative stimulation mode.

1.4 RESEARCH CONTRIBUTION

The primary objective of this study is to investigate an alternative CI stimulation technique, which aims to address FNS. The objective of the intervention is to alleviate or eliminate FNS, while simultaneously allowing for optimal operation of the CI in terms of auditory T-levels and dynamic range. Should a technique prove to be effective, it could potentially contribute to the cluster of present interventions, or become the preferred method for mitigating FNS in CI users. Additionally, this study aims to affirm the known origins of FNS and attempts to rate the intervention against a selection of existing FNS interventions, by taking advantage of the predictive abilities of person-specific.

A realistic volumetric description of the electrically stimulated cochlea forms an integral part of modern-day CI research. These descriptions can potentially assist a non-invasive investigation into the electrical situation of a stimulated cochlea or can be used in model-based visualisations, model-predicted mappings and model-based diagnostics (Hanekom and Hanekom, 2016). Consequently, this study aims to provide a model refinement software tool which can be used to increase the geometric accuracy of models generated by the automated method. The modelling component of this study will expand the automated approach, which could (i) reduce the time required to construct a user-specific model using

the manual method alone, while (ii) increasing the overall accuracy of a model relative to one generated by the automated method alone. Furthermore, the modelling component will include an investigation into variants of the same model, which could improve the techniques used in future modelling work.

1.5 RESEARCH OUTPUTS

Two journal articles from work presented in this dissertation are in preparation for submission to accredited international journals.

- *Highly detailed automatically generated user-specific CI models for clinical application.*
- *Apical reference stimulation: A possible solution to facial nerve stimulation.*

1.6 DISSERTATION OVERVIEW

Chapter 2 presents a literature review of aspects related to FNS. The epidemiology of FNS is discussed, including the underlying mechanisms thought to be primarily responsible for this complication. A description of conventional methods and their known shortcomings is also provided. Chapter 3 contains a description of the proposed software refinement tool, encompassed by proposed variants of the 3D model, which will be investigated. The method used to create the FN geometry is also discussed, followed by descriptions of the proposed intervention and the experimental setup. Chapter 4 illustrates the results related to the accuracy of landmark data, T-level predictions for geometric variations and experimental results. Chapter 5 presents a general discussion of the results. Chapter 6 provides a summary of the findings.

CHAPTER 2 LITERATURE STUDY

2.1 CHAPTER OVERVIEW

This chapter aims to provide an overview of the literature that constitutes the framework for the present study. In Section 2.2 an introduction to FNS is presented, which includes a brief overview of possible causes, proposed factors which increase the risk of FNS and conventional intervention strategies. In Section 2.3 the epidemiology of FNS is presented. In Sections 2.4 factors which increase the risk of FNS is reviewed. In Section 2.5 a discussion on present solutions is provided. In Section 2.6 a summary is presented which concludes the chapter.

2.2 INTRODUCTION

The first attempt to elicit auditory percepts through electrical stimulation goes as far back as 1790, when Alessandro Volta placed two rods into his ears and connected it to 50 V electrochemical cells, thereby delivering an electric shock into his ear canals. The electricity caused him to perceive a loud “bam” and then the sound of boiling soup. Due to the somewhat unpleasant sensation in his brain, the scientist immediately terminated the experiment and did not repeat it (Wilson and Dorman, 2008). Just over two centuries later, hundreds of thousands of people have received commercially available CIs, with an estimated 57,000 implants being sold in 2016 alone (Technavio, 2016). CIs are the accepted

treatment for severe to profound sensorineural hearing loss, and the growth of the CI market is evidence of its success (Hanekom and Hanekom, 2016).

As with the majority of medical treatments, various shortcomings and complications still exist. One of the most common side-effects of CIs is FNS. Just as Alessandro Volta inadvertently stimulated more than just his AN through his experiment, similarly CIs may also unintentionally affect nerves other than the AN. FNS occurs when electric current intended to stimulate the AN, spread beyond the cochlea to the nearby FN, causing facial muscles to contract involuntarily (Berrettini et al., 2011). FNS can be severe and uncomfortable and can limit the CI dynamic range, which can often reduce speech perception benefits (Seyyedi et al., 2013). The presence of FNS is specific to the CI user and may be severe, mild or absent, or may be absent on one side and present on the other in bilateral implantees.

Various predisposing factors of FNS have been suggested, which include otosclerosis, cochlear ossification (post-meningitis, otosyphilis), temporal bone fracture, closed head injury, osteoporosis, hydrops and cochlear malformation. (Ahn et al., 2009, Berrettini et al., 2011, Bigelow et al., 1998, Cushing et al., 2006, Kelsall et al., 1997, Muckle and Levine, 1994, Rotteveel et al., 2004). Implant design, stimulus parameters and local tissue impedances are also considered to influence the incidence of FNS (Niparko et al., 1991).

The following attempts have been made to address FNS: lowering stimulation levels, disabling offending electrodes, advanced stimulation techniques, botulinum toxin treatment and even the surgical explanation of a specific implant, or reimplantation with a different device (Ahn et al., 2009, Alharbi et al., 2012, Berrettini et al., 2011, Langman et al., 1995). Interventions often cause undesirable effects on hearing and speech understanding and could negatively impact an individual's quality of life or may result in unwanted surgery, which might not alleviate all FNS symptoms.

2.3 EPIDEMIOLOGY

FNS was initially reported in a study conducted in 1988, in which 152 surgeons were questioned regarding general complications in CIs (Cohen et al., 1988). Out of 459 cases, FNS was reported in only four (0.9%) persons. Since then, several reports regarding FNS have been published. The same group of researchers expanded their sample size to 4969 and found that 101 (2.03%) of implantees had complications associated with FNS (Hoffman and Cohen, 1995).

In 1991, another investigation into FNS took place at the VA Cooperative Study of Advanced Cochlear Implants. Out of 82 CI users, 12 (14.63%) demonstrated FNS within two years after implant activation. FNS resolved spontaneously in four of the 12 users. In the remaining users, electrodes had to be deactivated, or stimulation levels lowered (Niparko et al., 1991).

Stoddart and Cooper (1999) investigated CI complications in 100 adults implanted with a Nucleus multichannel device. Complications included poor sound quality, vibration, absence of auditory stimulation, small dynamic range, throat sensation, pain, FNS, poor loudness growth and dizziness. FNS was the predominant complication experienced by CI users. Mid-array electrodes were most frequently responsible for FNS. It was suggested that these electrodes were located closest to the FN and that any leakage current could cause FNS.

Berrettini et al. (2011) presented a retrospective review of 119 CI recipients implanted between 1999 and 2007 at the ENT Clinic of the University of Pisa. Eleven (9.2%) developed post-implantation FNS. Out of 11 users, four (36.4%) were reported to have cochlear abnormalities such as inner ear malformation, hypoplasia of the CN, and abnormalities due to otosclerosis and meningitis. In the group experiencing FNS, four (36.4%) experienced FNS directly after activation of the implant, one (9%) experienced FNS within a year after implantation and the remaining implantees, more than a year after implantation (Berrettini et al., 2011). Alharbi et al. (2012) also presented a 75-year old male who developed FNS

after four years of activation of his implant. The findings by Berrettini et al. (2011) and Alharbi et al. (2012) suggests that the onset of FNS is highly variable among different individuals.

At the Hospital of the University of Pennsylvania, a retrospective study was performed to determine the incidence of FNS in 58 CIs (54 persons) who received implants between 1980 and 1997 (Bigelow et al., 1998). FNS occurred in eight (13.8%) of the implanted cochleae. At the Denver Ear Institute, FNS was reported in 14 persons (7%) in a sample size of 200 implanted with the Nucleus 22-channel CI (Kelsall et al., 1997). Kempf et al. (1999) and Kelsall et al. (1997) reported FNS incidences of 3.0% and 1.0% in paediatric populations, respectively. The incidence of FNS in the paediatric population of CI users tends to be slightly lower, presumably due to a percentage of misdiagnosed cases (Berrettini et al., 2011). Cushing et al. (2006), however, suggested that an objective measure of FNS may illustrate an increased incidence of FNS in the paediatric population since they reported incidence rates ranging from 31% to 78%. More recent studies indicated FNS incidence rates of 12.3% (20 out of 163), 8.1% (12 out of 147) and 6.5% (39 out of 600) (Broomfield et al., 2000, Rayner et al., 2003, Smullen et al., 2005).

Ahn et al. (2009) conducted a study at the Asan Medical Center involving the use of the Nucleus 24-channel device. Out of 394 recipients, 23 (5.8%) experienced FNS. Their study aimed to determine the effect of the type of electrode on the incidence of FNS. The FNS incidence rate for straight electrode arrays was much higher than perimodiolar electrode arrays, with a 21.7% incidence using straight electrode arrays and 3.0% using perimodiolar electrode arrays (Ahn et al., 2009). These findings suggest that electrode design could influence the prevalence of FNS in the CI population.

In general, the incidence of FNS ranges from 0.9% to 14.6% across all studies, which represent a remarkable portion of the CI population (Berrettini et al., 2011). These findings illustrate the necessity of further investigations into FNS.

2.4 FACTORS WHICH INFLUENCE THE INCIDENCE OF FNS

Factors which appear to cause FNS are either related to changes in the bone encapsulating the cochlea or to malformations which affect stimulation current distributions through the tissue surrounding the cochlea. The most common of these factors are discussed below.

2.4.1 Otosclerosis

Otosclerosis is a progressive otic capsule disease which affects the middle and inner ear in humans (Cureoglu et al., 2010). In some cases of severe otosclerosis, a person can experience hearing loss due to abnormal growth of bone tissue at the stapes footplate. The stapes is one of the three bones, which make up the ossicles. In normal-hearing individuals, the stapes is usually attached to the oval window, through which vibrations are transferred and propagated throughout the cochlea. A fixed stapes may cause conductive hearing loss since abnormal bone growth prevents sound vibrations from passing through the ossicles (Cureoglu et al., 2010). Fixed stapes occur in 12.3% of otosclerotic persons (Sargent, 2001). Bone conduction (BC) hearing aids can benefit individuals suffering from conductive hearing loss since it often delivers an increased functional gain and hearing performance (Tsang et al., 2013). In severe cases of cochlear otosclerosis, atrophy of the spiral ligament and stria vascularis often hinders recycling ions by reducing the endocochlear potential, resulting in cochlear hair cell dysfunction (Cureoglu et al., 2010). Hair cell dysfunction results in hearing impairment, which cannot be treated with a BC hearing aid, often requiring cochlear implantation.

FNS during intracochlear electrical stimulation has widely been associated with otosclerosis (Seyyedi et al., 2013). Bigelow et al. (1998) reported an FNS incidence of 75% in otosclerotic individuals. Otosclerosis can cause the otic capsule to demineralise, reducing bone impedance between the cochlea and FN canal (Ramsden et al., 2007). Reduced bone impedance may shunt current from the electrode toward the FN (Seyyedi et al., 2013). Figure 2.1 illustrates otosclerosis which affected the bony tissue between the FN canal and the upper

basal turn of the cochlea (UBTC). Figure 2.1 (a) and (b) illustrate normal bone in which the individual did not experience FNS, while Figure 2.1 (c) and (d) illustrate otosclerotic bone material, which resulted in FNS. Alterations in bony material may cause micro-channels, which allow stimulation current to reach the FN.

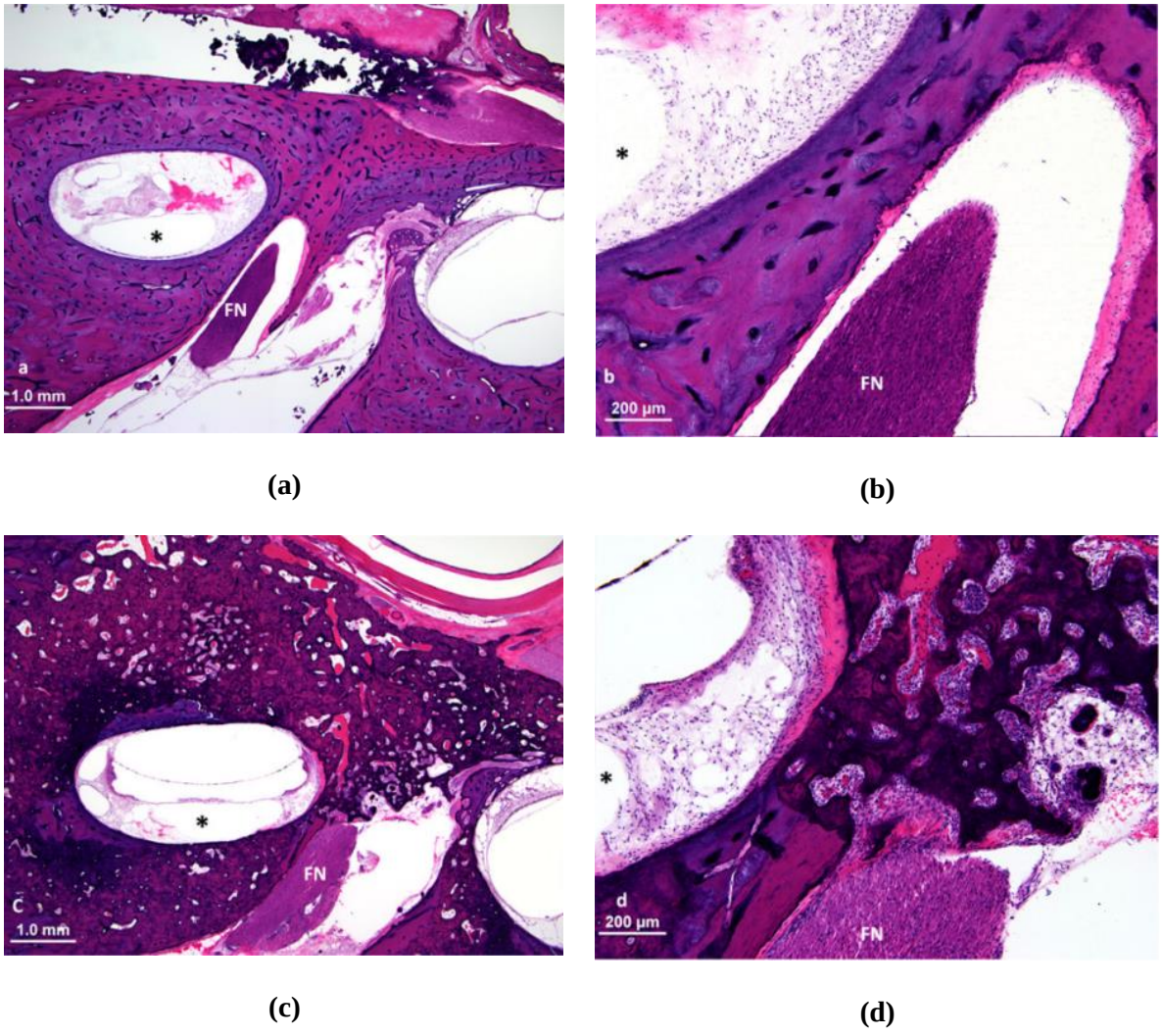

(a) **(b)**

(c) **(d)**

Figure 2.1. Images showing demineralised bone existing between the UBTC and the FN. Figure (a) and (b) illustrate the images of a normal bone and (c) and (d) illustrate images of otosclerotic bone. Figures (b) and (d) are enlarged images of figures (a) and (c), respectively. Taken from Seyyedi et al. (2013), with permission.

2.4.2 Meningitis

Meningitis is a disease which inflames the meninges of the human body (Short, 2016). It is rare but can be fatal if left untreated. Bacterial, viral or fungal infections may be predisposing factors of meningitis. Chronic headaches, sensorineural deafness, cortical blindness, learning and behavioural difficulties, cerebral palsy and epilepsy are common symptoms of meningitis. Meningitis can cause cochlear fibrosis (thickening and scarring of connective tissue) or labyrinthine ossification (LO) (Novak et al., 1990, Steenerson et al., 1990). LO is the pathologic formation of new bone within the lumen of the otic capsule and is a common cause of profound deafness and loss of vestibular function (Steenerson et al., 1990, Yeung et al., 2017). LO occurs in almost 80% of persons deafened by meningitis (Steenerson et al., 1990). Gross et al. (2017) presented a CI user who developed meningitis at the age of 21 months. Bilateral FNS eventually occurred during electrical stimulation, presumably as a result of the effects of meningitis. Mancini et al. (2008) suggested that meningitis is a predisposing factor to FNS due to a change in bone impedance caused by LO or cochlear fibrosis.

2.4.3 Inner ear malformation

Inner ear abnormalities are present in a considerable portion of congenital deaf persons (McClay et al., 2002). The use of CIs to treat congenital profound hearing loss have recently become more common (Mylanus et al., 2004). Inner ear malformations seem to increase the risk for FNS after cochlear implantation (Papsin, 2005). Cushing et al. (2006) reported an FNS incidence of 78% in CI users with malformed cochleae. The incidence of FNS is often higher in malformed cochleae, presumably due to a decreased distance between the FN and the cochlear wall (Ahn et al., 2009).

Common cavity deformity is an abnormality in which the vestibule and cochlea are not separated and, consequently, form a common cystic cavity (Ruckenstein, 2012). This abnormality is the second most common inner ear malformation (Jackler et al., 1987a).

Numerous studies have indicated that common cavity deformity carries an increased risk for FNS during electrical stimulation (Beltrame et al., 2000, Jackler et al., 1987b, Papsin, 2005, Tucci et al., 1995). FN anomalies are often caused by common cavity (Ruckenstein, 2012). FNS related to common cavity might be due to an aberrant course of the FN, dehiscence over the nerve, or proximity between the FN and electrode array (Mylanus et al., 2004).

2.4.4 Temporal bone fracture

Fracture of the temporal bone usually occurs as a result of blunt head injury. Temporal bone fractures are mostly associated with motor vehicle accidents, falls, and gunshot wounds (Patel and Groppo, 2010). Various studies suggest that temporal bone fractures increase the risk of FNS in CI users (Berrettini et al., 2011, Camilleri et al., 1999, Cushing et al., 2006, Espahbodi et al., 2015, Graham et al., 2000, Seyyedi et al., 2013). Espahbodi et al. (2015) reported FNS in 10% of implanted persons in the setting of a prior temporal bone fracture. It has been suggested that electric current may spread through low impedance pathways caused by incomplete or delayed healing of fracture lines in the temporal bone (Espahbodi et al., 2015). Espahbodi et al. (2015) suggested that FNS following temporal bone fractures can be reduced or eliminated by augmented CI fitting parameters (Espahbodi et al., 2015).

Camilleri et al. (1999) presented a study in which seven persons with profound hearing impairment following temporal bone fractures, received CIs. The Nucleus 22-channel and Ineraid devices were used. Two users (28.6%) experienced FNS, which could not be eliminated by augmenting CI fitting strategies. Both underwent explantation of the device and implantation into the contralateral cochlea (Camilleri et al., 1999). Maas et al. (1996) presented a person who experienced total deafness due to a temporal bone fracture after which he received an implant in the left cochlea. The person developed severe FNS, and the device was explanted and reimplanted into the right cochlea whereafter FNS was minimal.

2.4.5 Width of the bony cochlear nerve canal (BCNC)

The BCNC is the short canal between the base of the cochlea and the fundus of the internal auditory canal (Stjernholm and Muren, 2002). Figure 2.2 illustrates a CT scan indicating the BCNC, marked with a black line. Rah et al. (2016) suggested that a relationship exists between FNS and the width of the BCNC. The width of the BCNC has been thought to have a direct influence on hearing T- and C-levels since a narrow BCNC usually indicates a narrow CN, which typically requires high stimulation currents to create an adequate hearing sensation. It is suggested that high T- and C-levels increase the risk of FNS since increased stimulation currents can spread beyond the cochlea and inadvertently stimulate the nearby FN. Rah et al. (2016) presented 64 paediatric implantees, of which 32 experienced FNS. The objective was to evaluate whether a relationship exists between a narrow BCNC and the prevalence of FNS. The width of the BCNC in the FNS group was measured to be 1.09 ± 0.52 mm while the control group measured a general wider BCNC of 1.99 ± 0.61 mm. Therefore, it has been suggested that a narrow BCNC could increase the risk of FNS in CI users.

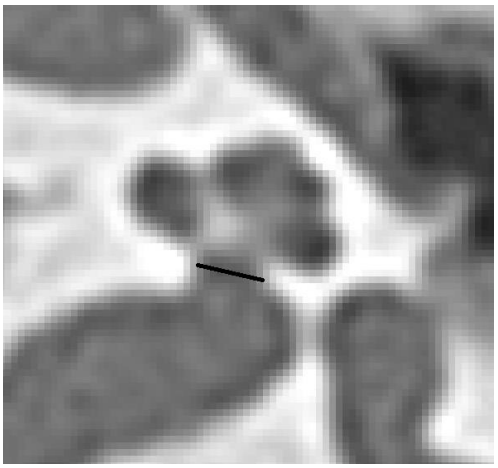

Figure 2.2. CT scan of a cochlea indicating the width of the BCNC with a black line.

2.5 PRESENT FNS INTERVENTIONS

Various attempts have been made to address FNS. The common objective of interventions is to reduce electrical current densities at the FN. High interindividual variability exists among CI users regarding the effectiveness of interventions since an intervention which may be effective for one individual will not necessarily alleviate symptoms in another. The most common interventions are presented below.

2.5.1 Reducing electrode stimulation level

FNS can often be treated by reducing stimulation levels of individual electrodes (Bigelow et al., 1998). If the maximum stimulation level of offending electrodes is reduced to below the T-level of the FN, but above the T-level of the AN, the user can still potentially benefit from the implant without experiencing the effects of FNS. Bigelow et al. (1998) presented a CI user implanted with a 3M single-channel device who developed FNS eight years after implantation. Symptoms were initially alleviated by reducing the clipping level, but FNS progressively recurred after which the clipping level was further reduced. The effect which reduced stimulation levels had on sound perception was not reported. The same user eventually had to undergo an explanation of the 3M single-channel device due to implant failure. The device was replaced with a CLARION 16-channel device in the same ear due to infectious problems in the contralateral ear. FNS occurred immediately at the onset of implant activation, mainly from the fourth electrode. Within two months, FNS progressed and involved channels two to eight. The stimulation levels of the CLARION device were reduced to below the FN T-level and, consequently, FNS was alleviated. The study suggests that hearing was not affected by reduced stimulation levels for the CLARION device.

Reducing stimulation levels was also reported by Espahbodi et al. (2015), which presented a 30-year-old male who had a bilateral temporal bone fracture after falling from a rooftop. The injury caused hearing loss in both ears. Bilateral implantation of perimodiolar implants was performed. At the onset of device activation, FNS was absent though eventually, the

user reported muscle contraction on the left side of his face and throat. It was confirmed that stimulation on electrodes 15 to 19 resulted in FNS. After decreasing C-levels, FNS was mitigated. Subsequently, FNS recurred, and it was determined that electrode 19 was the cause of FNS. After deactivation of electrode 19, FNS was once again alleviated. A follow-up audiometric test revealed hearing sensitivity in the normal to mild loss hearing range, with HINT (hearing in noise test) sentences scores of 97% for the right ear, 98% for the left ear and 99% bilaterally.

Berrettini et al. (2011) also presented 11 CI users experiencing FNS. Six users reported alleviated FNS symptoms after stimulation levels were reduced, without any deterioration in speech perception. In the remaining five users, selected electrodes had to be deactivated, and stimulation levels reduced to alleviate symptoms, which led to deteriorated speech perception. Ahn et al. (2009) also reported deteriorated speech perception due to low stimulation levels and deactivated electrodes. Graham et al. (2000) further suggested that there might be a sensitising effect when stimulation levels are reduced since FNS can eventually recur even when the stimulation level is reduced to levels well below those which previously did not stimulate the FN. Therefore, reducing stimulation levels can be beneficial for users experiencing FNS, but might not alleviate symptoms for all users, and FNS might progressively recur. Furthermore, reducing stimulation levels can result in low loudness levels, which might not be adequate for speech perception.

2.5.2 Deactivating offending electrodes

Graham et al. (2000) suggested that switching off individual electrodes responsible for stimulating the FN can be beneficial for selected users. In the 11 users presented by Berrettini et al. (2011), five (45.5%) users illustrated no improvement when stimulation levels were reduced. FNS was only mitigated after deactivating selected electrodes. The deactivation of selected electrodes often results in a deterioration in speech perception (Battmer et al., 2006, Polak et al., 2006). Ahn et al. (2009) suggested that as more electrodes are deactivated, less benefit from the implant may be expected. Polak et al. (2006) presented a CI user who

experienced severe FNS. The progressiveness of FNS necessitated the gradual deactivation of several electrodes, but this also negatively affected speech perception, which resulted in a 0% score in a CUNY sentence test. Reimplantation was required since programming strategies resulted in unacceptable speech perception. Interestingly, Graham et al. (2000) reported that deactivated electrodes could be switched on again after a while since the sensitising ability of excitable nerve often causes T-levels to return to normal when stimulation is temporarily halted. However, T-levels are likely to decrease after reactivation of deactivated electrodes, making this approach unviable.

2.5.3 Implantation into scala vestibuli

Since the onset of cochlear implantation, the scala tympani has widely been used for implantation because of the proximity to the middle ear, accessibility, and remoteness from the cochlear duct (Steenerson et al., 1990). However, it is also known that the distance between the scala tympani and FN is consistently less than the distance between the scala vestibuli and the FN (Bigelow et al., 1998). Due to the scala vestibuli being located further away from the FN, it can be a desirable option for implantation, especially if the risk for FNS is high (Polak et al., 2006). Furthermore, implanting into the scala vestibuli might result in an easier electrode insertion since the scala vestibuli cross-section may be greater than the scala tympanic cross-section (Steenerson et al., 1990). Steenerson et al. (1990) also suggested that the scala vestibuli may at times be used for implantation following meningitis since cochlear fibrosis and ossification usually starts at the entrance of the cochlear aqueduct into the scala tympani. Bigelow et al. (1998) presented an individual who experienced FNS despite a scala vestibuli insertion, illustrating that implantation into the scala vestibuli does not eliminate the risk of FNS.

2.5.4 Protecting facial nerve through surgery

The risk of FNS can be reduced by making use of sophisticated surgery techniques. Ruiz et al. (2006) presented a 20-year-old female with a malformed cochlea caused by otosclerosis,

who was implanted with a Nucleus-24 Contour implant after becoming deaf. Only 16 electrodes were fully inserted into the cochlea. Otosclerosis destroyed the FN aqueduct, which drastically increased the risk for FNS. During implantation, surgeons extracted the incus bone and placed it between the FN and the implanted electrode array. Post-surgery tests indicated that no FNS was present, suggesting that this technique could be an excellent way to protect the FN from electrical stimulation in CIs. The individual exhibited excellent long-term post-surgery results with no FNS reported.

2.5.5 Electrode array design

Straight or pre-curved electrode arrays are typically used during cochlear implantation (Boyer et al., 2015). The straight electrode array retains its straight course when no forces are exerted on it, and will typically take the curve of the cochlea once inserted, resting along the lateral wall of the cochlea (Boyer et al., 2015). The pre-curved or perimodiolar electrode array has a pre-manufactured curve, designed to rest close to the modiolus (Doshi et al., 2015). Figure 2.3 (a) and (b) illustrate the straight and perimodiolar electrode arrays, respectively.

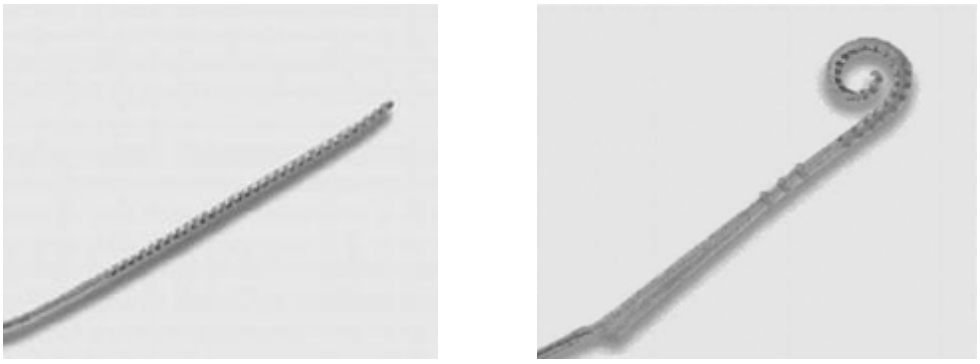

(a) **(b)**

Figure 2.3. Straight electrode array in Figure (a) compared to a perimodiolar electrode array in Figure (b). Taken from Battmer et al. (2006), with permission.

Studies have indicated that the incidence of FNS is much lower when a perimodiolar electrode array is used, compared to a straight electrode array, in users with anomalous cochleae (Ahn et al., 2009, Battmer et al., 2006, Marshall et al., 2005, Matterson et al., 2007, Semaan et al., 2012). Furthermore, Seeber and Bruce (2016) reported that electrode placement close to the modiolus could potentially decrease auditory T-levels, which could improve implant battery life. Battmer et al. (2006) presented four CI users implanted with straight electrode arrays, which progressively developed FNS. The straight electrode arrays were replaced with perimodiolar electrode arrays with modiolar facing contacts, whereafter FNS was eliminated in all four cases. It is suggested that a perimodiolar electrode array reduces current at the lateral wall of the cochlea due to an improvement in the localisation of the electrical stimulation (Battmer et al., 2006, Berrettini et al., 2011). This hypothesis does not always hold true since limited benefit has been observed in selected CI users (Ahn et al., 2009, Rotteveel et al., 2004).

2.5.6 Increasing pulse width

Increasing the pulse width has also been suggested as an FNS intervention. Assuming that similar loudness levels can be achieved when the charge remains the same, decreased stimulation levels can be used to elicit a comparable response (Battmer et al., 2006). Decreased stimulation levels can reduce the spread of electrical current at the FN.

Alharbi et al. (2012) presented a case report in which the pulse width was increased, and the stimulation mode changed, to reduce FNS symptoms. A pulse width of 75 μs and a stimulation rate of 900 Hz were used. However, a deterioration in hearing and speech understanding was observed after these modifications. Kelsall et al. (1997) reported that increasing the pulse width can reduce FNS symptoms, but that longer pulse widths places considerable limitations on map program options and can, therefore, limit the benefit in mitigating FNS symptoms.

2.5.7 Triphasic Pulse Stimulation

Various studies have indicated that triphasic stimulation, instead of conventional biphasic stimulation, can be used to address FNS (Abdelhamed, 2019, Bahmer et al., 2017, Bahmer and Baumann, 2016, Schatzer et al., 2014). A triphasic pulse consists of three pulses, two with the same polarity and one with the opposite polarity. Bahmer and Baumann (2016) used surface electromyography (SEMG) to quantitatively measure muscle contractions related to FNS for both triphasic and biphasic stimulation. The amplitude of the EMG signals for triphasic stimulation, in general, was lower compared to biphasic stimulation, suggesting that FNS was successfully reduced with triphasic stimulation. However, T- and C-levels also increased with triphasic stimulation. This observation suggests that higher current levels are required to reach T- and C-levels for triphasic stimulation, compared to biphasic stimulation, but that FNS symptoms can be reduced when using triphasic stimulation. A follow-up study produced similar results as the initial study (Bahmer et al., 2017). Additional findings associated with triphasic stimulation indicated that cathodic-first triphasic stimulation had a more favourable effect on the reduction of FNS compared to anodic-first triphasic stimulation.

2.5.8 Botulinum toxin

When a CI user experiences severe FNS, and modifying CI fitting parameters demonstrate little or no improvement, botulinum toxin injections can be used as a treatment since it induces temporary facial muscle paralysis (Langman et al., 1995, Trentman et al., 2015). Botulinum toxin treatment interferes with neural transmissions by blocking the release of acetylcholine, which is the principal neurotransmitter at the neuromuscular junction (Nigam and Nigam, 2010). Langman et al. (1995) presented a case report of a CI user who experienced FNS on 15 of 22 electrodes, of which all 15 had to be deactivated. After receiving botulinum toxin treatment, the number of deactivated electrodes was reduced to eight. An increase in the dynamics range was reported from four electrodes, which were active prior to the treatment. These improvements considerably increased sound quality and

speech understanding.

Sprouting of nerve terminals and formation of new synaptic contacts usually cause a recovery of nerve functions within two to three months after treatment, making botulinum toxin a temporary solution and, consequently, necessitate frequent botulinum toxin injections (Nigam and Nigam, 2010). It also introduces a risk to develop unwanted muscle complications and the treatment has financial implications, which should be considered (Trentman et al., 2015).

Gross et al. (2017) presented an individual who received botulinum toxin treatment due to FNS. Although the treatment proved to inhibit FNS symptoms, invisible involuntary muscle contractions were reported by the user. Furthermore, Gross et al. (2017) reported that a user's inability to use facial expressions is another undesired effect of botulinum toxin treatment which should be considered.

2.5.9 Explantation or reimplantation

In some cases of severe FNS, when modified CI fitting parameters illustrate little benefit, explantation or reimplantation of the device may be required (Camilleri et al., 1999, Cushing et al., 2006). A user can be reimplanted with a different device in the same cochlea, or the same implant can be explanted from one cochlea and implanted into the contralateral cochlea in the case of unilateral implantees (Battmer et al., 2006). During reimplantation, a straight electrode array is usually replaced with a perimodiolar electrode array to reduce the amount of current spread at the FN. However, a perimodiolar electrode array is often undesired since a lateral wall electrode array is recommended for hearing preservation (O'Connell et al., 2017). Furthermore, histological examinations of intracochlear structures revealed that a degree of damage is usually inflicted during surgery (Martins et al., 2015). Intracochlear damage as a result of surgery can induce residual acoustic hearing loss, which is a further undesired result in terms of hearing preservation (Miranda et al., 2014). Therefore, explantation and reimplantation are typically seen as a last resort and should be avoided.

A different electrode type might not always be required since the device can often be explanted from the side responsible for FNS, and implanted into the contralateral cochlea. Maas et al. (1996) presented a bilateral deaf individual who was implanted on the left side, after which FNS progressively developed. Since the device itself was still functional, it was removed from the left side and reimplanted into the right ear. Reduced FNS was reported on the right side with acceptable speech discrimination.

If FNS persists and the CI illustrate inadequate speech perception benefits, the device is often explanted, and the person becomes a non-user (Theunisse et al., 2018).

2.6 CHAPTER SUMMARY

This chapter provides an overview of the body of knowledge relating to FNS. Firstly, an introduction to the complication was presented, followed by examples and incidence rates. Secondly, the predisposing factors which seem to increase the likelihood of FNS were summarised. The chapter ended with a summary of present FNS interventions. The effectiveness of treatments and techniques relating to FNS, including the side-effects and effect on speech perception, were reported. From this literature review, it is evident that the majority of interventions may be inadequate in terms of eliminating all FNS symptoms while maintaining acceptable speech perception. Further investigation into the exact mechanisms which cause FNS, and potential alternatives to present intervention strategies, is thus required.

CHAPTER 3 METHODS

3.1 CHAPTER OVERVIEW

In Section 3.2 the 3D modelling workflows, developed by Malherbe et al. (2016) and Crous et al. (2018), are summarised and a refinement tool is proposed, which aims to increase the accuracy of the model geometry and, consequently, the predictions made by the model. In Section 3.3 three geometric modifications are described to determine the degree to which these variations affect predicted T-levels. In Section 3.4 the methodology used to generate and incorporate the FN geometry into the cochlear model is presented. In Section 3.5 a custom stimulation mode is proposed to serve as an alternative to conventional monopolar (MP) stimulation. In Section 3.6 a description of the experimental setup to evaluate this intervention in a clinical environment is included, which include software design, hardware setup and EMG electrode placement. In Section 3.7 a summary is presented which concludes the chapter.

3.2 DEVELOPMENT OF THE COCHLEAR AND ELECTRODE GEOMETRIES

A person-specific 3D volume conduction model which include the cochlea, electrode array and FN, can be beneficial when investigating different FNS interventions since it would eliminate the need to perform extensive clinical tests, which are typically required to probe different setups and stimulation modes. Determining the mechanisms of the specific presentation of FNS in a user might not be accessible through standard clinical procedures as it requires an understanding of stimulation current paths through the unique cochlea and temporal bone structures of the user. An accurate person-specific model is thus required to

allow interventions to be predicted. Firstly, two existing 3D modelling workflows are discussed in this section: the manual method and the automated method. A refinement tool is proposed, hereafter referred to as the adapted automated method (AAM), which attempts to improve the accuracy of the automated method geometries.

3.2.1 Manual method

Malherbe et al. (2016) introduced a manual workflow to create 3D volume conduction models of the cochlea and electrode array. In summation, CT scan data taken from the head of an implantee are used to create a person-specific 3D volume conduction model by manually identifying landmarks on the scans. Using image processing software (ImageJ[1]), the cochlea is isolated in the CT scan stack, and rotated to Cochlear View, as outlined by Xu et al. (2000). The CT scan data are enhanced to increase image quality and visibility, especially that of the cochlear wall and electrode array. The CT scan data are radially sliced at 1° intervals using an estimate of the location of the modiolus as the centre point and aligning the first slice with the opening of the round window.

The investigator manually digitises the course of the cochlea and electrode array by estimating the position of the most lateral point on the cochlear wall and the electrode centre on every slice. The measurements are represented in cylindrical coordinates using θ as the rotational angle, and ρ- and z-values as the horizontal and vertical distance, respectively. The ρ-values, i.e. the spiral radii of the measured lateral boundary spiral, are compared with 11 template spirals. Each template spiral is scaled, rotated and translated iteratively to find the best fit (Procrustes fit), by using an error calculation between measured ρ-values and template ρ-values. The ρ-values of the best fitting spiral template are used in combination with the measured z-values of the lateral boundary to create a 3D spiral defining the course of the most lateral point of the cochlear wall, hereafter referred to as the new lateral boundary spiral.

[1] https://imagej.nih.gov/ij/

A 3D template containing the cochlear structures is remapped to align with the course of the new lateral boundary spiral. Should the cochlear structures intersect the modiolus due to the course of the new lateral boundary spiral, the ρ-values of the template are scaled, resulting in a narrow cochlear duct which does not intersect the modiolus. Similarly, if intersections occur between adjacent sections of the cochlear duct, z- and ρ-values are scaled until all intersections have been eliminated. The electrode array centre, which is estimated on the CT images, is used to determine the position and course of the electrode array geometry in the final model. The narrowest width of the BCNC is also measured on the CT data and is used to create the geometry of the AN stem coming out of the cochlea. The geometry of the AN stem width is set to the same width as the BCNC. The electrode array centre, which is estimated on the CT images, is used to determine the position and course of the electrode array geometry in the final model. Based on these measurements, a final 3D model is created which mimics the characteristics of a unique cochlea.

3.2.2 Automated method

Crous et al. (2018) developed a workflow in which the landmark detection process is automated, hereafter referred to as the automated method. The automated method is similar to the manual method but differs in the way landmarks are digitised on CT images, and the number of landmarks used to define the characteristics of the cochlear wall. A knowledge-based landmark detection algorithm is used to automate the digitisation of data points. This technique requires the investigator to select three points on the cross-section of the cochlear duct (the superior, inferior and lateral points) at four angles (0°, 90°, 180° and 270°). The position of the cochlea on the CT scan data is determined by identifying the mean apical point of the cochlear spiral, and the location of the inlet to the BCNC, since all cochlear duct and electrode array data points will be located between these two landmarks. The mean apical point is determined by estimating the apical point for all radial slices and taking the average of these coordinates. The algorithm digitises landmarks on the superior, inferior and

lateral spirals of the cochlear wall, guided by reference data. An average is taken of 15 previously measured cochleae, which is used as the reference data.

The electrode artefacts on the CT data are used to determine the path of the electrode array. Multilevel clustering-based thresholding is used to isolate the point with the highest absorption rate, which is used to define the electrode spiral. These points are smoothed and are used as the trajectory of the cylinder representing the electrode array geometry in the final model.

When all the necessary spiral and electrode landmarks are digitised, the spiral data are interpolated to compensate for values which could not be extracted by the extraction algorithm, after which a smoothing function is applied to ensure smooth trajectories. The loft-feature in COMSOL[1] is used to create the final model.

3.2.3 Adapted automated method

Both the manual and automated method aim to create person-specific models using landmarks from an implantee's CT data. Coupling these volume conduction models to a neural model enables the investigator to make auditory T-level predictions. The models from both methods, however, predict T-levels which do not accurately correspond with clinically measured T-levels. Discrepancies could be due to a variety of reasons, but it has been suggested that cochlear morphology and the fibre location relative to the electrode array, plays a vital role in neural excitation predictions (Badenhorst et al., 2017, Malherbe et al., 2016). It is, therefore, essential to ensure morphologic accuracy before making T-level predictions.

When the cochlear duct is created during the manual method, it only incorporates the lateral boundary spiral to define the characteristics of the duct and does not utilise the superior and

[1] https://www.comsol.com/

inferior boundary spirals. Consequently, the height and width of the cochlear duct are only dependant on the scaled cochlear structure template. Template matching of the ρ-values of the lateral spiral during the manual workflow might further introduce discrepancies due to the extensive anatomic variations which the human cochlea exhibits (Erixon et al., 2009). Furthermore, the manual method proves to be tedious since the landmark detection process requires extensive involvement by the investigator.

The automated method attempts to address some of the issues mentioned. The cochlear structure template is scaled in width and height to fit between the lateral, superior and inferior spirals identified on the cochlear duct, making it slightly more accurate than the manual method. The detection algorithm furthermore reduces the time to create a model since much of the landmark detection process is automated.

An issue often encountered with the automated method is inaccurately detected landmarks. Discrepancies are due to low-resolution CT scans and the electrode artefact, which can obscure the cochlear wall, often influencing the detection of landmarks. These incorrectly detected landmarks might influence predicted T-levels and can cause geometric errors, especially when sections of the cochlear duct incorrectly intersect the modiolus or when improperly scaled boundaries intersect with adjacent boundaries.

Due to the scaling of the cochlear structure template, the automated method can furthermore generate cochlear geometries, which do not resemble the typical form of structures as seen on detailed anatomical images. In some instances, poorly shaped geometries introduce geometry and meshing errors when a finite element model is constructed. It is also possible that inaccuracies are introduced during the spiral smoothing process. Low-resolution CT images often cause landmarks, which describe a cochlear spiral, to be contaminated by measurement noise since the location of the detected landmark can change substantially between consecutive slices. A spline smoothing function is applied during the automated method to eliminate measurement noise. In some instances, the smoothing function incorrectly modifies accurately detected landmarks. This is especially evident in regions in which the rate of change of digitised points is high, such as the basal turn, which is distally

coiled from the round window, causing a sharp turn towards the modiolus (Shin et al., 2013). Pietsch et al. (2017) also mentions that a sharp vertical rise in the course of the spiral is sometimes evident in the human cochlea, approximately where the first turn reaches the second turn, around 450°-500°.

Figure 3.1 shows a graphical representation of the automatically generated structures registered onto a midmodiolar CT image of the cochlea. It illustrates some of the discrepancies mentioned. The CN and scala tympani structures are slightly deformed, especially at the lower middle turn. It is also clear that the cochlear duct and electrode array at the basal turn of the cochlea misalign with the cochlear duct and electrode artefact visible on the CT image.

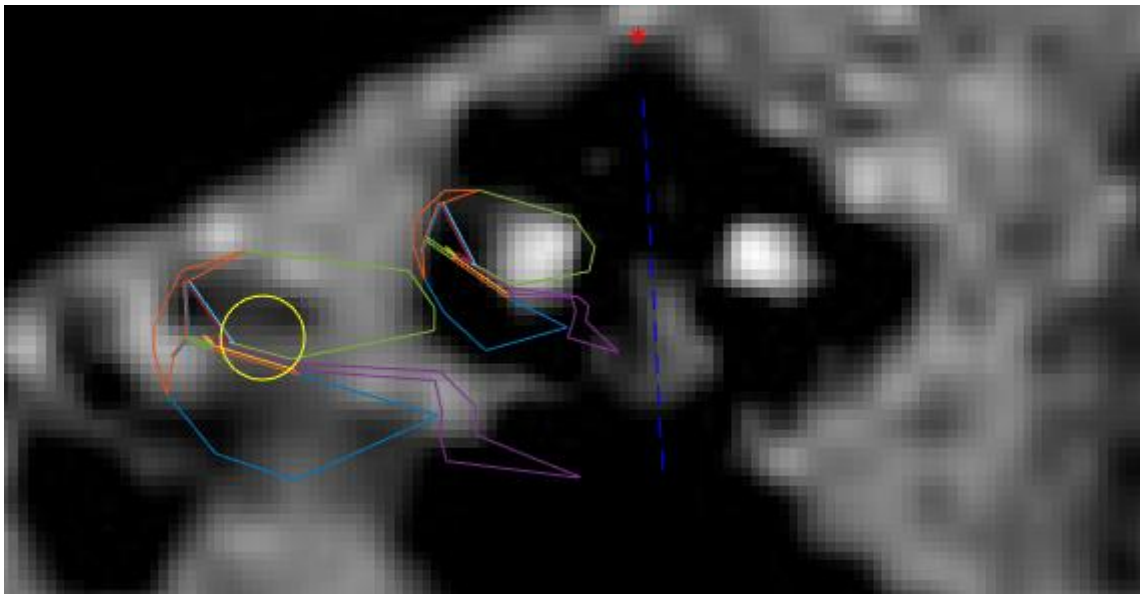

Figure 3.1. Registered cochlear structures and electrode array, which were generated by the automated method. The structures in the cochlear duct for the lower basal and lower middle turns are illustrated. The modiolus and mean apical point are indicated with a dashed line and asterisk, respectively. Note the misalignment between the modelled lower basal geometry and electrode array, and the location of these elements on the CT image.

To improve the correspondence between CT scan data and model geometries, the AAM was introduced. The objective of the AAM is to utilise the spiral trajectories generated by the automated method and to register the cochlear and electrode array structures onto CT images, as illustrated in Figure 3.1. Through inspection, the investigator can determine whether cochlear and electrode array structures align with landmarks visible on CT images. When discrepancies exist, the investigator can effortlessly make adjustments through the AAM. Furthermore, the AAM grants the investigator the freedom to modify model trajectories to simulate different scenarios, which would otherwise not have been incorporated by the manual or automated methods. An example is when the electrode array partly exits the wall of the basal turn of the cochlea (Ho et al., 2007). This scenario is visible on CT scans and would otherwise not have been incorporated by the manual and automated methods since these workflows often extend the cochlear wall boundary until the cochlear duct encapsulates the electrode array geometry.

The AAM is facilitated by a graphic user interface (GUI) with built-in functionality to modify and correct discrepancies. Adjustments can be made to the cochlear duct position, position and shape of the cochlear structures, electrode position, and electrode insertion-depth. Therefore, the AAM allows for the rapid generation of person-specific models by taking advantage of the labour-saving ability of the automated method, and further increase geometry accuracy using the AAM. This approach enables the investigator to create accurate person-specific cochlear models, effortlessly. The development of the AAM was divided into subsections, all of which are discussed below.

3.2.3.1 Data initialisation

Since the AAM uses the model which is generated by the automated method, proper program initialisation is required to allow an accurate presentation of cochlear structures and the electrode array. Once the automated workflow has completed, all variables in the workspace are saved to a MATLAB variable file. The AAM uses this MATLAB variable file to initialise all variables and structures in the GUI. The MATLAB file contains, amongst other things, the Cartesian coordinates of the spiralling trajectories of the cochlear structures, electrode

centre points, electrode radii, and the location of the modiolus in the CT image stack. Upon execution of the GUI, the investigator is required to specify the location of the MATLAB variable file and a folder containing all relevant CT images, which is used to initialise the AAM.

The automated method generates 41 spirals which define the cochlear structures. Each spiral line consists of 440 points, making a 720° turn. Figure 3.2 illustrates a set of 41 points at an angular distance of 0°. The AAM linearly interpolates the 440 spiral points to create 721 points to enable the registration of the cochlear structures onto every CT image at 1° intervals. The electrode array spiral is interpolated in the same fashion, but the number of interpolated points is dependent on the electrode insertion-depth.

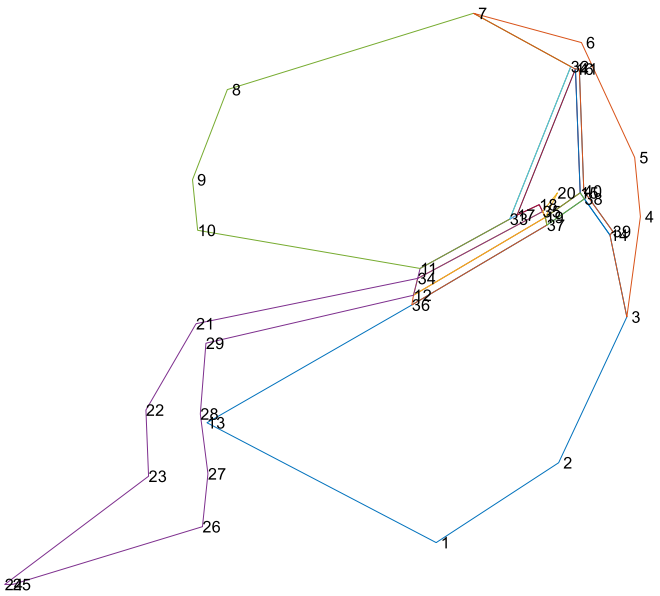

Figure 3.2. Cochlear structures defined by 41 points generated during the automated method. Each point represents a spiralling trajectory, and the combination of all spiralling trajectories define the 3D geometry of the cochlear model.

The AAM was initially developed to use a perfect circle to represent the shape of the electrode array on CT images. A circle representation of the cross-section of the electrode array would have been valid if an assumption was made that the electrode array, which is

visible on CT images, is perfectly perpendicular to all radial slices. Furthermore, an electrode array entering a CT image at an angle other than 90° would cause an oval shape when presented on a 2D plane. Using a circle instead of an oval resulted in differences between the visual representation in the GUI and the final 3D electrode array geometry. To ensure an accurate electrode array representation, the AAM creates circles in 3D space on the electrode spiral, to form a cylindrical structure representing the electrode array. The AAM interpolates all cylindrical data points for z- and ρ-values at 1° intervals. When the AAM registers the electrode array on the scan, it uses the interpolated values and not a perfect circle. This approach correctly illustrates the noncircular shape of the electrode array at cross-sections where the electrode array is not perfectly perpendicular to the CT image.

Figure 3.1 illustrates the cochlear structures, electrode array, most apical point and modiolus line after the initialisation process. Only the lower basal and lower middle turns of the cochlear duct were made visible to simplify the adaption process. It is essential to be able to visualise both the lower basal and lower middle turns to ensure that no intersections between adjacent sections of the cochlear duct occur during the adaption process.

3.2.3.2 Initial geometry modifications

Figure 3.1 illustrates the erroneous shapes representing some cochlear structures. Erroneous cochlear shapes necessitated an investigation into possible geometry modifications during the initialisation process, which could be applied to multiple spiral trajectories to reduce the overall time it would take the investigator to make the required adjustments. When modifications are made during the initialisation process, the entire spiral is modified by performing the same operations at all points on the trajectory.

The CN, as seen in the lower middle turn of the cochlear duct, illustrates a shape which might not accurately represent the typical form of the CN since an erroneous narrowing at the inlet to the duct is present, almost causing an intersection of the CN boundaries. Should the CN boundaries intersect, geometric errors can occur when the final model is created. The space between the CN and the scala tympani, and the space between the CN and scala

vestibuli are also relatively large compared to high-resolution anatomical images of the cochlea (Agrawal et al., 2018). The size of this open space is especially important since the electrical properties of bone tissue are assigned to all the regions which are not encapsulated by one of the cochlear structures. The osseous spiral lamina is a thin bony shelf, which partly divides the scala tympani and scala vestibuli (Agrawal et al., 2018). The automated workflow creates a sizeable open space, in comparison to microanatomy data, resulting in a thick osseous spiral lamina.

To improve these aspects, the AAM modifies the geometries of the CN, scala tympani and scala vestibuli during the initialisation process. Figure 3.2 shows the representation of the cochlear structures defined by spirals numbered from 1 to 41. The AAM modifies the CN by calculating the Euclidean distance between spirals 34 and 12 and consequently using this distance to adjust spirals 21 and 29. The Euclidean distance between spirals 21 and 29 is modified so that it is 1.5 times wider than the distance between spirals 34 and 12. The increased width ensures that the nerve width increases towards the region of the spiral ganglion. The Euclidean distance between spirals 24 and 25, which represents the width of the CN closest to the modiolus, is also increased. The space between these spirals are set to be 1.5 times the width between spirals 21 and 29, and are positioned to create an angle of 45° with the horizontal plane. Should the investigator modify the position of the cochlear duct during the adaption process, the spacing between spirals 24 and 25, and the 45° angle between them, prevent geometric errors from occurring, which are typically caused by intersecting boundaries after spirals are modified. The modifications of spirals 24 and 25 ensure that proper nerve spacing is maintained at the modiolus during the adaption process.

Once these spirals are adjusted, the rest of the CN geometry in the region of the spiral ganglion also needs to be modified to ensure a proper shape. During the modification process, adjustments are made to spirals 22 and 23 to form a straight line between spirals 21 and 24. Similarly, spirals 26, 27 and 28 are adjusted to create a straight line between spirals 29 and 25. After that, spirals 22, 23, 26, 27 and 28 are moved vertically to create a CN widening. The widening of this area mimics the characteristics of the spiral ganglion as seen on images of the anatomy of the cochlea (Gray, 1918).

The next step was to modify the shape of the scala tympani and scala vestibuli to address the improper width of the osseous spiral lamina. This modification procedure decreases the width between spirals 10 and 21, and the width between spirals 13 and 29, thereby decreasing the open space between the scala tympani and vestibuli geometries, and the CN geometry. The Euclidean distance between spirals 10 and 21 is set to be the same as between spirals 11 and 34. The Euclidean distance between spirals 13 and 29 is set to be the same as between spirals 12 and 36.

Moving spiral 13 closer to the CN geometry resulted in an erroneous geometry representing the scala tympani. Consequently, spiral 42 was added to the scala tympani geometry to ensure a smooth shape. Figure 3.3 illustrates the cochlear structures and electrode array representation after it was modified during the initialisation process. White circles show the spirals that were modified or added.

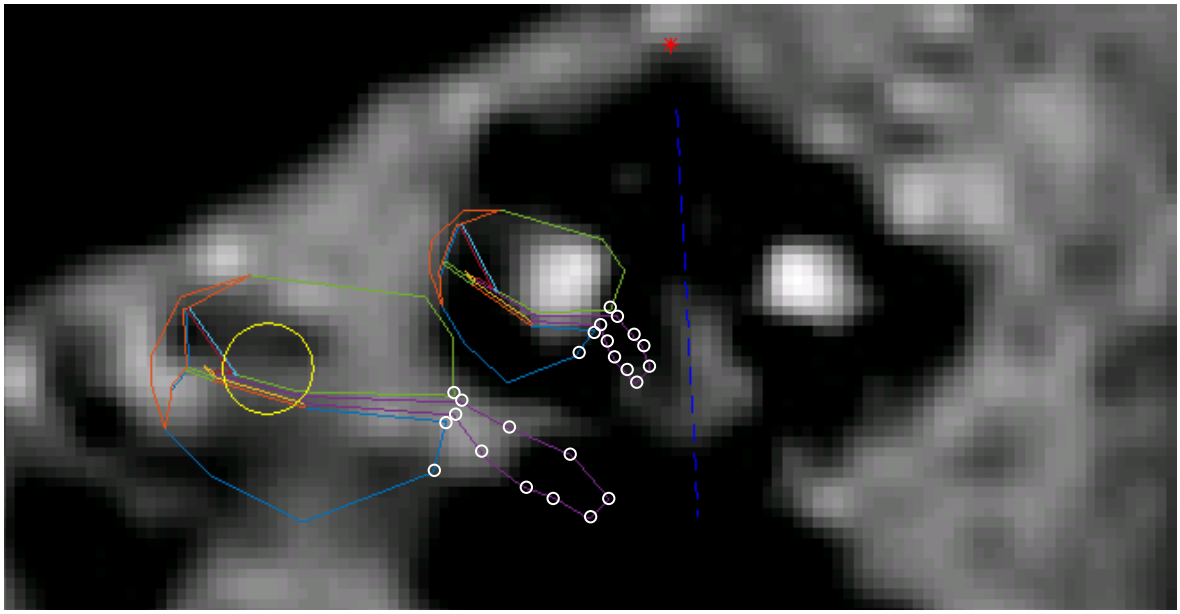

Figure 3.3. Cochlear structures after initialisation. Modifications were made to the CN (purple), the scala tympani (blue), and the scala vestibuli (green). The red asterisk shows the mean apical point which was used as the origin of all coordinates. The modiolus line is illustrated as a blue dashed line. White circles were placed on the spirals which were modified or added during the initialisation process. The yellow circle represents the electrode array.

3.2.3.3 Electrode course correction

In Figure 3.3, a misalignment between the electrode array representation and the electrode artefact is evident at the lower basal turn. At the lower middle turn, an electrode representation is not present despite the fact that a clear artefact is visible on the CT image. This may indicate that the electrode insertion-depth is incorrect. These discrepancies can be attributed to an incorrectly detected electrode array course, or electrode data which were influenced by the smoothing process. Therefore, an electrode course correction algorithm was developed to increase the accuracy of the modelled electrode array and insertion-depth without extensive involvement from the investigator. The algorithm starts by prompting the investigator to identify the location of the electrode array on the first slice where the electrode artefact is visible, which is usually at the round window or the 0° radial slice. The investigator can select any region on the artefact since the weighted centroid is used to determine the centre point of the electrode artefact. Secondly, the investigator is prompted to enter the angular distance at which the electrode artefact terminates on the radially sliced CT scan stack, which can be determined when browsing through the slices. The algorithm uses this manually identified angular distance as a stopping condition for the course correction algorithm.

After receiving input from the investigator, the algorithm creates a search field in which the weighted centroid is calculated. For consecutive slices, the weighted centroid position found on the previous slice is used to position the new search field. The weighted centroid uses the location and intensity of pixels to determine the point which constitutes the highest absorption rate in that region. All weighted centroid points are stored and, consequently, the accuracy of the electrode array course is improved. By specifying the end of the electrode array, the algorithm can effectively modify the electrode insertion-depth since it searches for the next electrode artefact until it reaches the specified angular distance, thereby allowing the investigator to increase or decrease the electrode insertion-depth, as needed. It may be beneficial to modify the insertion-depth of the modelled electrode since a number of advantages of deeply inserted long electrodes have been reported (Hochmair et al., 2015), which could further be investigated through models.

The correction procedure proved to be useful in increasing the accuracy of the course of the electrode array, but low-resolution CT images caused notable measurement noise in electrode location data since the calculated electrode centre between two consecutive slices can be erratic. Therefore, a digital filter was used to smooth the electrode spiral. A careful choice of the filter was made since selected filters would cause the spiral to deviate from the actual course of the electrode array, rendering the electrode course correction process futile. A moving average filter with a window size of 50 was used, which was suitable for maintaining the integrity of the electrode spiral while creating a realistically smooth course of the electrode array.

3.2.3.4 CT image offset

The automated method, and consequently the AAM, only utilises the first 181 radially sliced CT images since this includes all available CT data. When presenting CT images in the GUI, the AAM mirrors the CT images horizontally when inspecting cochlear structures beyond 180°. Horizontal mirroring of a 2D image makes use of the centre of the image as the point of rotation. The problem, however, is that the axis used as the centre of the radial slices is not necessarily located at the centre of the 2D image since the cochlea is often isolated after the CT stack was radially sliced. This mismatch causes a horizontal offset in the image when it is mirrored. Therefore, Intensity-Based Image Registration was used to calculate the offset between the mirrored version of the 0° slice and the 180° slice. The AAM uses this calculation to rectify the offset error observed between the 180° and 360°, and 540° and 720° slices. Figure 3.4 shows an example of the image offset error that occurred, and the correction thereof, using an Intensity-Based Image Registration procedure.

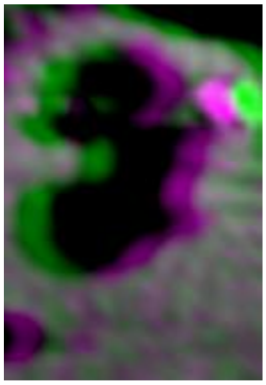

Figure 3.4. Example of the offset error which occurred between the 0° slice and the horizontally mirrored 180° slice. Intensity-Based Image Registration was used to calculate the offset, which was used to correct the offset when the AAM presents CT data between 180° and 360°, and between 540° and 720°.

3.2.3.5 Modification process

The automated method creates spiral trajectories for the cochlear structures and electrode array. The AAM aims to provide a software refinement tool, which can be used to efficiently and effortlessly modify sections of the cochlear duct, cochlear structures or electrode array generated by the automated method, by taking advantage of the interactive ability of the GUI. A number of functions were developed for this purpose.

After the initialisation process, 43 spiral trajectories define the cochlear structures and electrode array. In some instances, it might be necessary to modify the position of a section of one of the spirals if a more desirable course can be determined from the radial slices. Modifying a single spiral is especially applicable if, for example, the electrode array position needs to be adapted, since it consists of only one spiral trajectory. A button was added to the GUI which prompts the investigator to specify the spiral number which needs to be adapted. If the specified spiral number is valid, an asterisk will appear at the present location on the present slice. The investigator can then drag the asterisk using the pointer to a more desirable position, whereafter a double click on the new asterisk position would indicate that a final

position was selected. Consequently, the spiral is modified, and the adapted geometry is reconstructed onto the CT image.

Adapting a point on the spiral without adapting the adjacent sections can cause an irregularity in the trajectory. To prevent irregularities, the adjacent sections of the spiral should be modified to ensure that the spiral trajectory maintains a smooth and realistic shape. Therefore, the difference between the original point and the newly selected point is calculated, and the offset is used to modify the adjacent sections on the spiral. A decreasing offset value is added to adjacent points to ensure that the modified section merges smoothly with the original spiral. In other words, a range of offset values is added to the specified section of the spiral, decreasing outwards to merge with the original spiral. A non-linear decreasing offset was used since a linearly decreasing offset usually causes sharp edges where the original and the modified sections of the spiral merge. A polynomial function was used for this purpose since the start and end of the function can be manipulated to have a prolonged rate of change. The only requirements for this curve were that it should be limited between 0 and 1, and it should have a slope nearing zero at the start and end of the curve, thereby ensuring smooth transitions between the modified and original sections. Equation (3.1) represents a fourth-order polynomial function which meets these requirements.

$$y(x) = 8.98 \times 10^{-6}x^4 - 8.23 \times 10^{-4}x^3 + 4.17 \times 10^{-4}x + 0.97 \qquad (3.1)$$

This equation was derived using the polyfit-function in MATLAB. By inspection, an appropriate curve was defined by specifying data points which satisfy these requirements. A polynomial fit to these data points was performed to derive (3.1). The polynomial curve was evaluated for x-values ranging from 1 to 60. The resulting array was multiplied with the offset value to create a non-linear decreasing array, which has the form of the curve defined by the polynomial in (3.1) and which is scaled relative to the offset value. This array was used to modified 60 points before and after the modified point.

In addition to the modification of one spiral, the AAM also allows changing multiple spirals with a single operation. For this purpose, the investigator is prompted to modify 4 points on the cochlear duct in the same fashion as a single point. Firstly, the most lateral spiral on the cochlear duct, represented by point 5, is adapted. This process causes an entire shift of all points, moved by the same amount as point 5, excluding spirals 24 and 25. The cochlear structures can be moved in any direction to fit the cochlear duct visible on the CT image. Secondly, the most superior spiral, represented by point 7, is adapted. With this adaption, only the upper section of the cochlear duct is moved while the rest of the spirals are kept in position. Thus, this modification allows the investigator to change the shape and size of the scala vestibuli, scala media and spiral ligament. Thirdly, the most inferior spiral, represented by point 1, is adapted. This modification causes the lower section of the cochlear duct to move while the rest of the spirals are kept in position, which allows the investigator to change the shape and size of the scala tympani. Finally, the middle of the cochlear duct is modified by moving point 34, located approximately in the centre of the cochlear duct. This modification adapts all data points in the centre of the duct while keeping the spirals on the cochlear wall fixed.

The multiple point adaption procedure enables the investigator to modify the size and shape of the scala tympani, scala vestibuli, scala media and spiral ligament. Only these large cochlear structures are modified since minimal detail regarding the small cochlear structures is typically visible on CT images. Even though limited detail of the large cochlear structures exists, estimates of these shapes and sizes can be made when considering the position of the electrode artefact relative to the duct, the shape and size of the cochlear duct and available pre-and post-operative information.

In some instances, the automated method generated cochlear structures, which misaligned with the cochlear duct at multiple angular positions, when registered onto the CT images. Adapting the duct on a wide range of spiral data, using the multiple point adaption process, proved to be tedious since only a section of data can be modified at a time. In an attempt to provide an expeditious way to set the course of the cochlear duct, a method was implemented which enabled the investigator to move all points of the cochlear duct at intervals of 45°.

The pointer is used to move all cochlear structures simultaneously, by clicking and holding any part on the duct and moving it to a more desirable position. Buttons are displayed at the bottom of the GUI, enabling the investigator to browse through the CT scans at intervals of 45°. An interpolation process is performed which connects all adjusted ducts to create a smooth spiral geometry. Figure 3.5 illustrates the cochlear and electrode array structures after selected spirals have been adjusted. The mean apical point and modiolus line is also marked using an asterisk and dashed line, respectively.

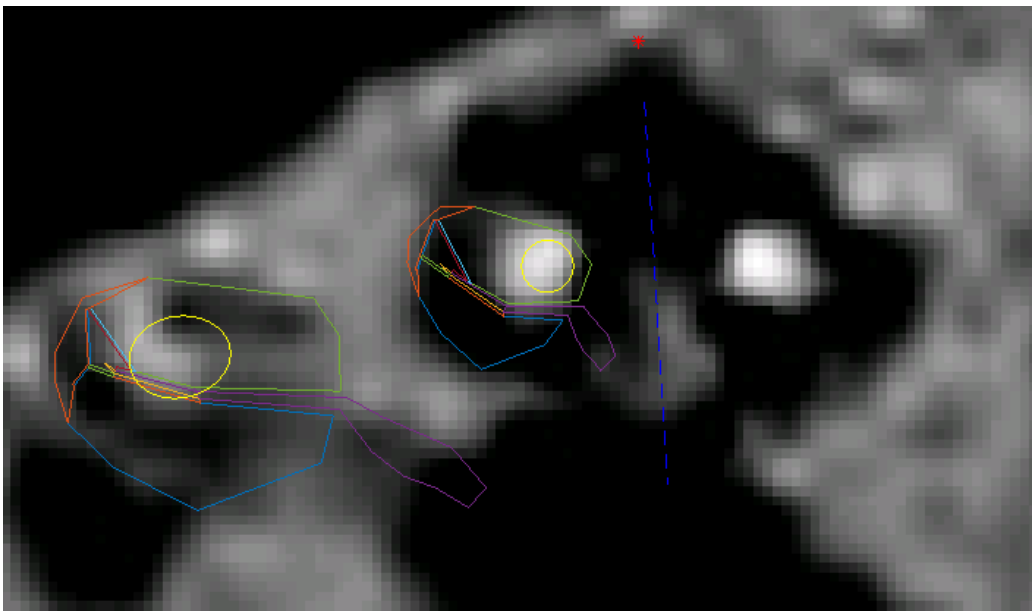

Figure 3.5. Cochlear structures and electrode array after the modification process. Multiple points were adapted to improve the correspondence between the cochlear structures and the cochlear duct visible on the CT image. Note the improvement in the accuracy of the electrode array and the cochlear duct, in comparison to Figure 3.1.

Yoo et al. (2000) suggested that the helico-spiral is a suitable approximation for the typical cochlear curve. In addition to the modification functionalities, an option was added to display the course of a helico-spiral approximation. Yoo et al. (2000) defines a helico-spiral approximation in cylindrical coordinates as

$$\rho = ae^{b\theta} \tag{3.2}$$

and

$$z = ce^{d\theta} \tag{3.3}$$

where a = 1.14987, b = 0.0754585, c = 3.23203 and d = -0.126636. The helico-spiral approximation is created and moved, whereafter it is resampled at 1° intervals to be able to display its course on each slice, starting at a location specified by the investigator. The investigator can choose to display the spiral or to hide it. The primary objective of displaying the helico-spiral approximation is to indicate the course of a typical cochlear spiral, which could assist the investigator in modifying the course of the cochlear duct if CT images are not sufficiently clear.

3.2.3.6 Geometry creation

Once all adjustments have been made, a save-button on the GUI can be used to export the modified trajectories into a separate MATLAB variable file. A button to create the geometries was added and can be used to initiate the creation of the final COMSOL model, which uses the saved trajectories to create the cochlear structures and electrode array. During the COMSOL model creation, various elements are automatically added and assigned to facilitate the modelling process. The following automated procedures are executed during model creation:

- The cochlear geometries are created and combined into a single model.
- A Stationary Study object is added to the model. This is a COMSOL object used to simulate steady-state behaviour.
- Material properties are defined and assigned to the cochlear geometries.
- The correct number of Point Current Source objects are created for the corresponding number of active electrodes which are fully inserted into the cochlea. This number is automatically determined after the geometry is created. The Point Current Source

object is a COMSOL component used to simulate current injections at the electrode array contact points.

- The correct number of Parametric Sweep parameters are included, which correspond with the number of Point Current Source objects. Each parametric sweep parameter is assigned to a Point Current Source. The Parametric Sweep object is a COMSOL component used to create a separate simulation for every active electrode.
- A sphere is included in the model which encapsulates the cochlea, simulating the otic capsule. The electrical properties of bone tissue are assigned to the sphere.

Once the final model is created, it can be solved to get the potential distribution throughout all geometries. This result is stored in the COMSOL model file. Once the model has been solved, the investigator can use the GUI to predict T-levels since a neural model was integrated into the GUI. A Hodgkin and Huxley based human compartmental deterministic ANF model proposed by Badenhorst et al. (2017) were used to determine FN and AN T-levels. A button was added for this purpose. The saved data are used to calculate the location of the nodes on the nerve geometry, which is specified by the neural model. The software extracts voltages from the solved COMSOL model at the specific nodes. The extracted voltages serve as input to the neural model and can predict T-levels based on the extracted voltages for every active electrode.

3.2.4 Analytical cochlear model

The modelling methods discussed to this point use a full 3D CT scan stack of the cochlea, from which the boundary of the cochlear duct and position of the electrode array can be identified at multiple angular distances. For one of the individuals who took part in this study, the full CT scan stack was not immediately available. Only selected pre- and postoperative views of images were available, mostly already in Cochlear View. These images were not sufficient to be used in the conventional modelling workflow since there were not enough CT data to measure the course of the required spirals. Pietsch et al. (2017) proposed a 3D analytical cochlear model in which only four measurements from CT scans

are required. All measurements are taken from Cochlear View (Xu et al., 2000). Pietsch et al. (2017) report that the proposed model fits analysed data from anatomical scans with high precision, making it suitable to be used in an instance where limited CT data are available. By using this model, the lateral, superior and inferior spirals were derived, and a 3D model was created.

In addition to the four measurements specified by Pietsch et al. (2017), the width of the BCNC could also be determined from the available scans. The width of the BCNC was used to create the CN geometry. Figure 3.6 (a) and (b) show preoperative scans in Cochlear View and illustrate the four measurements, as described by Pietsch et al. (2017). Figure 3.7 illustrates the way in which the BCNC was measured for the same participant.

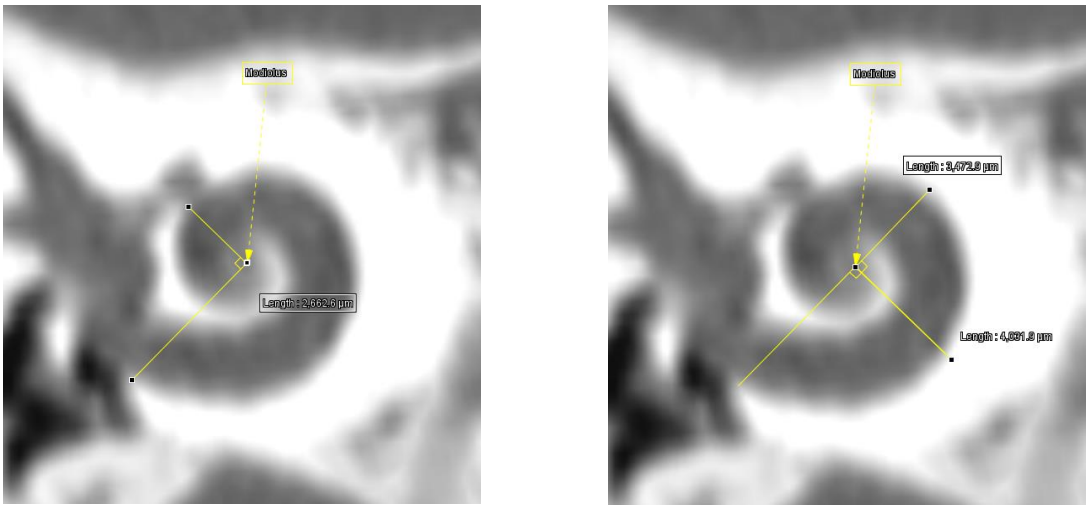

(a) **(b)**

Figure 3.6. Four measurements taken from preoperative scans in Cochlear View as specified by Pietsch et al. (2017).

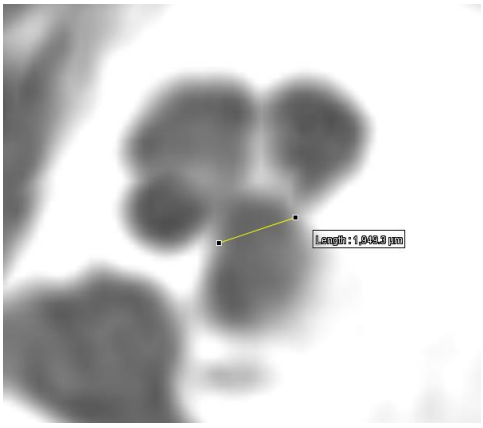

Figure 3.7. The measurement of the width of the BCNC for the specific user.

Table 3.1 provides a summary of the measured parameters.

Table 3.1. Measured parameters used in the analytical cochlear model.

Parameter	Value (mm)
A_a	5.38
B_a	4.03
A_b	3.47
B_b	2.66
BCNC	1.95

Pietsch et al. (2017) reported a typical B-ratio $\left(\frac{B_a}{B_a+B_b}\right)$ of 0.42 ± 0.04. From the measurements in Table 3.1, the B-ratio was calculated to be 0.60. The calculated B-ratio is larger than the reported value, but not improbable due to the high interindividual cochlear variability. Some cases reported by Pietsch et al. (2017) illustrated a B-ratio nearing a value of 0.6. A value for the A-ratio $\left(\frac{A_a}{A_a+A_b}\right)$ was not reported, but was calculated to be 0.61 for the measurements in Table 3.1. The measurement of 1.95 mm for the BCNC corresponds with the value of 1.98 ± 0.41 mm reported by Ocak et al. (2018). The lateral, superior and inferior spirals from the output of the analytical model were used to scale the cochlear structure template, which was used to create the final COMSOL model. Limited electrode

array data were available from the available CT images, but through inspection, it was determined that a scala tympanic insertion was most probable, with an approximate insertion-depth of 360°. The electrode array course was therefore guided by the boundaries of the scala tympani, fitting the electrode array evenly into this geometry for an angular distance of 360°.

3.3 GEOMETRIC VARIATIONS

Variations in volume conduction models are likely to affect predicted T-levels. The question, however, is whether small geometric variations would have a notable effect on neural excitation predictions. Predicted T-levels for three different variations in models were determined to estimate the influence of geometric variations. These variations are presented below.

3.3.1 Presence of the organ of Corti

The organ of Corti (OC) is the sensory epithelium of the cochlear duct. It contains hair cells which convert mechanical energy, caused by sound waves entering the cochlea, into nerve impulses (Fritzsch et al., 2011). In the volume descriptions used in this study, the OC geometry is represented as a small triangular prism adjacent to the basilar membrane geometry and surrounded by the scala media geometry. The OC typically has a higher impedance compared to surrounding structures. Since the COMSOL model only simulates electrical hearing and not normal hearing, the relevance of the OC comes into question. When a CI delivers an electrical stimulus, the underlining nerve cells are excited and not necessarily the hair cells inside of the OC. Even though the presence of the OC might introduce a slight change in impedance pathways, the effect might be negligible due to its small size. Including the OC into the model often introduces unwanted geometric, meshing and computational complexities. Omitting the OC geometry without having an adverse effect on neural predictions, could reduce modelling complexity, which could decrease the computational cost involved. Therefore, two simulations were created to investigate this

hypothesis; one simulation with the OC included, and one excluding the OC. Predicted T-levels for the two simulations were compared to each other to determine how it affects the outcome.

3.3.2 CN shape

Kalkman et al. (2014) reported that conductivities for bone and the modiolus had a considerable influence on intrascalar potentials. They reported that the modiolus had an approximate bone-nerve ratio of 35:65. The modelling methods discussed in the present study do not generate a separate geometry for the modiolus. Instead, the CN geometry partly occupies the cavity of the modiolus. Figure 3.8 (a) shows the midmodiolar cross-section of a person-specific model generated by the manual method. A cavity is visible in the upper region of the modiolus. The electrical property of temporal bone is assigned to this region since it is not incorporated by one of the cochlear structures. Sharp corners where the spiral ganglion and central CN geometry merge are also evident. A cross-sectional micro-CT scan of the human cochlea is shown in Figure 3.8 (b) as a comparison. Little bony material in the region of the modiolus is visible on the scan.

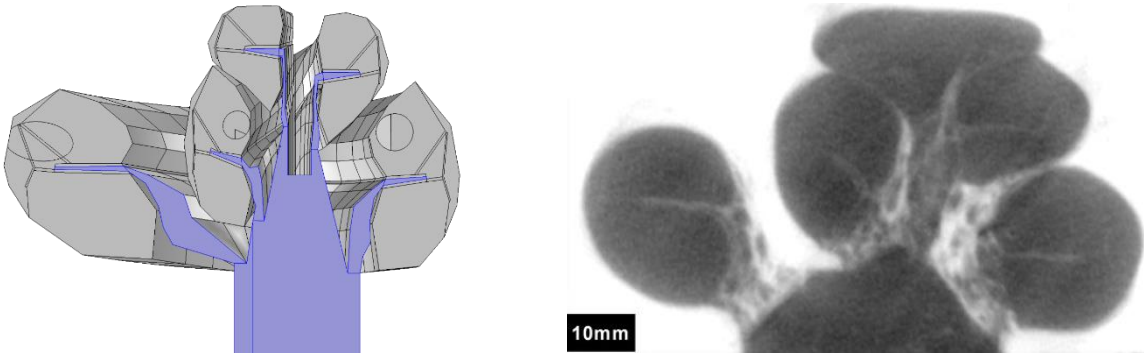

(a) **(b)**

Figure 3.8. Figure (a) shows a midmodiolar 2D slice of a 3D constructed model using the manual method. Figure (b) shows a midmodiolar micro-CT image of the human cochlea, which was taken from Elfarnawany et al. (2017), with permission.

A modified version of the CN was created to determine how this affects T-level predictions. In the proposed geometry, the bony cavity on the modiolus is slightly reduced by increasing the CN height. This modification also removes some of the sharp corners to make a smooth connection between the spiral ganglion and the central CN. The proposed geometry was created by utilising the loft-feature in COMSOL. Figure 3.9 illustrates the modified CN geometry. Two simulations were created to determine the effects that the proposed geometry have on predicted T-levels; one with the original CN geometry, and one with the modified CN geometry. Predicted T-levels for the two simulations were compared to determine how it affects the outcome.

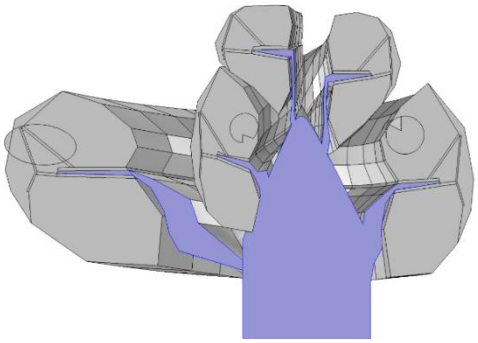

Figure 3.9. The modified CN geometry.

3.3.3 The granularity of cochlear geometries

Both the manual and the automated method use different approaches to create the cochlear geometries. The manual method creates quadrangular surfaces in a 3D space, which are knit together to form an enclosed area which is converted to a solid. The automated method, on the other hand, constructs a sequence of equally spaced cross-sectional polygons and uses the loft-feature to create a solid object. The loft-function creates smooth geometries by inserting extra data points between adjacent polygon faces to fit the general projection of the cochlear curve. Consequently, the technique used during the manual method results in

faceted cochlear geometries, while the technique used during the automated method results in smooth cochlear geometries.

Extra data points, introduced when using the loft-feature, cause a drastic increase in model detail, which furthermore introduces undesired computational cost, and often introduce geometric and meshing errors. Due to the somewhat unpredictable placement of extra data points when the loft-feature is used, it can cause cochlear geometries to intersect with adjacent geometries, introducing problems when geometries are meshed or when materials are assigned, due to small geometric pieces which are separated from the cochlear volumes when the final geometry is created. Though it is possible to simulate the lofted geometries, the question remains whether this increased complexity would have a remarkable effect on predicted T-levels. Figure 3.10 (a) illustrates a model created during the automated method, and (b) illustrates a model using the same trajectories, but created using a similar approach as in the manual method. The electrode array geometry was kept the same for the two models.

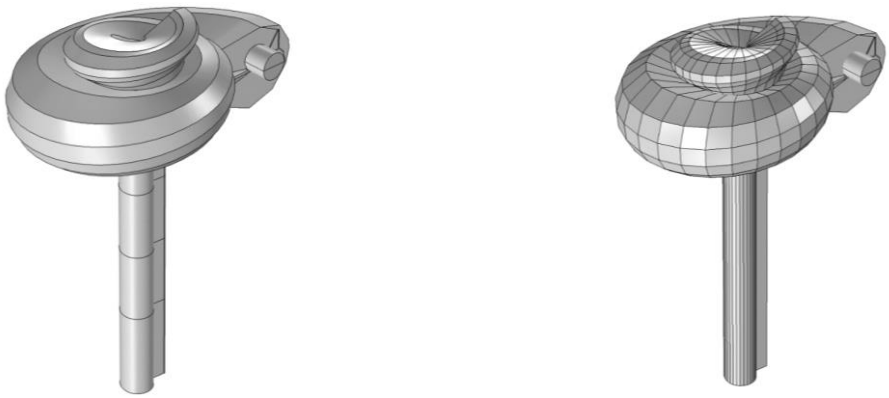

(a) **(b)**

Figure 3.10. Illustration of the cochlear geometries generated using the (a) loft-feature and (b) quadrangular surfaces.

3.4 CREATING THE FACIAL NERVE GEOMETRY

Incorporating the FN geometry into a model of the electrically stimulated cochlea is critical to an investigation into possible interventions to FNS. Electrical potential distributions can be extracted from this geometry and used in a neural model to make predictions about neural excitations in the FN (Gross et al., 2017). Gross et al. (2017) proposed a method to incorporate a person-specific FN geometry into a model of the cochlea. The method constructs the FN geometry by using measurements from CT images. It uses the length, width, and angle of the labyrinthine, tympanic and mastoid segments of the FN branch to create this geometry.

The labyrinthine segment is located between the geniculate ganglion (GG) and the meatal foramen (EF) (Shin et al., 2014). The length of the labyrinthine segment (LLS) was measured from the axial view (referred to as the "superior view" by Shin et al. (2014)) as shown in Figure 3.11.

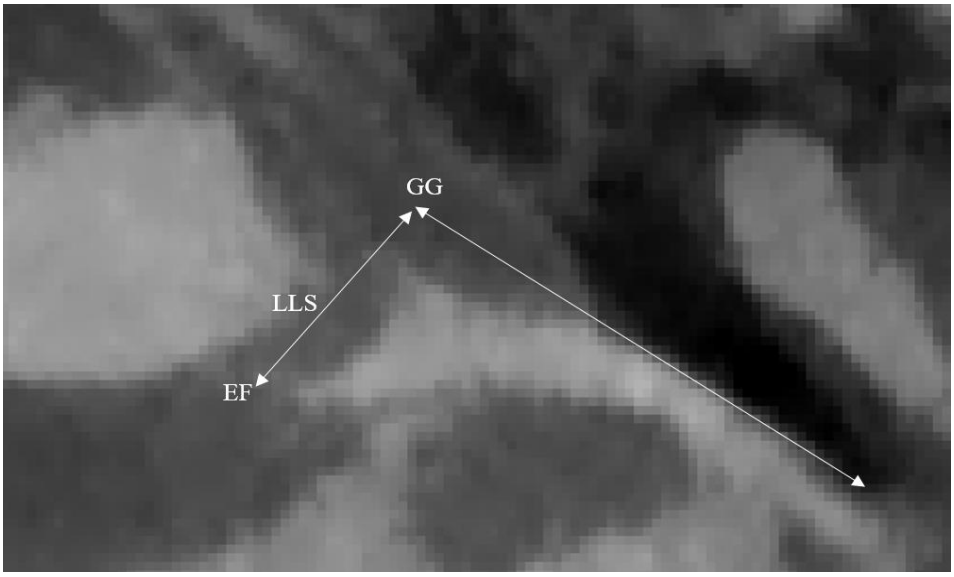

Figure 3.11. The LLS is shown on the figure and was measured between the midpoint of EF and the midpoint of the GG.

The labyrinthine segment follows a curvilinear course (Shin et al., 2014). Thus, a proper approximation of the LLS would be to use a curved line, as shown in Figure 3.12. For this study, a straight-line measurement was used to approximate the LLS. However, it is essential to consider the curvilinear course of the labyrinthine segment when measuring the angle between the labyrinthine and the tympanic segments (ALT), since a straight-line approximation would result in an increased angle, compared to reported values. Figure 3.12 shows the measurement of the ALT.

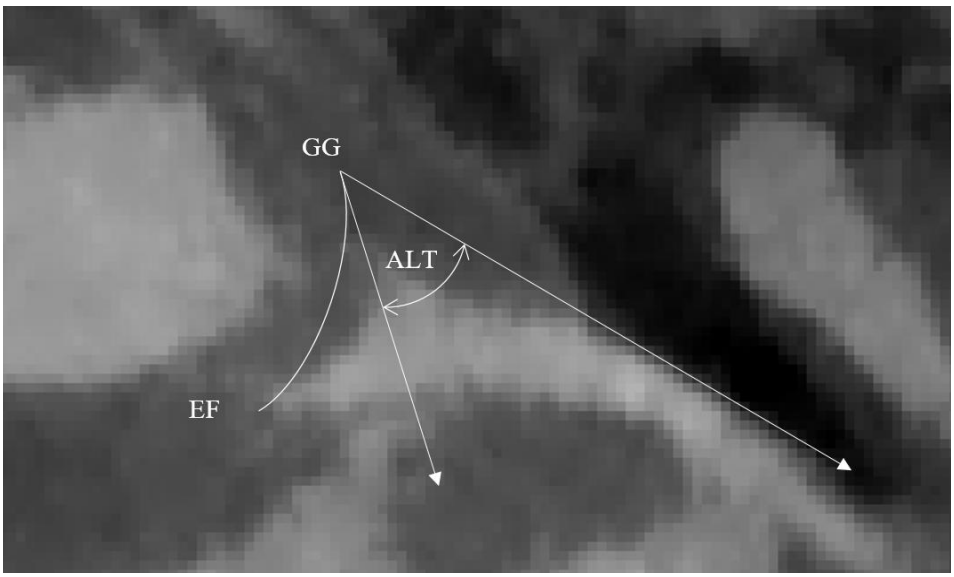

Figure 3.12. Illustration of the measurement of the ALT.

Figure 3.13 illustrates the width measurements of the labyrinthine segment. The first measurement (WL1) was taken immediately lateral to the EF, and the second measurement (WL2) was taken midway on the labyrinthine segment. Both measurements were taken perpendicular to the bony wall of the labyrinthine segment canal.

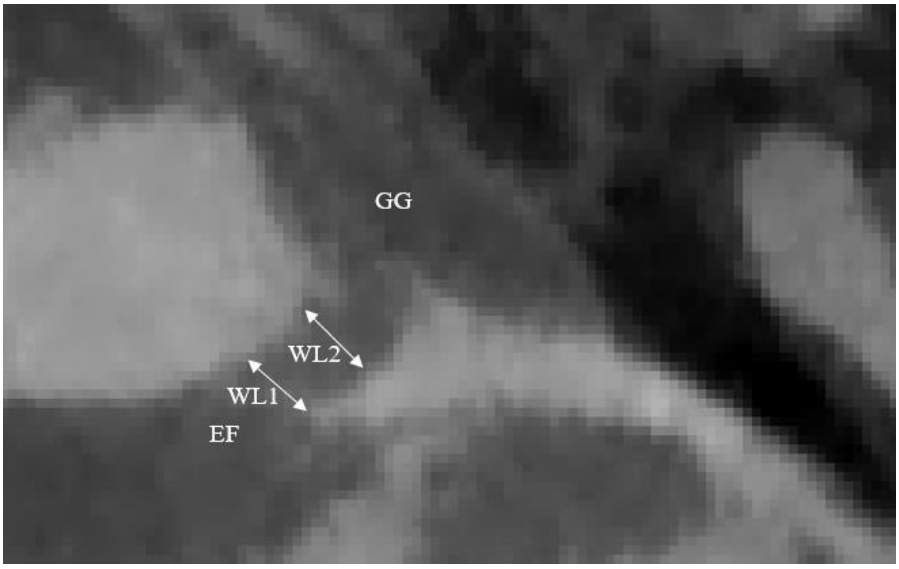

Figure 3.13. Locations of the width measurements of the labyrinthine segments, WL1 and WL2.

The length of the tympanic segment (LTS), the length of the mastoid segment (LMS) and the angle between the tympanic and mastoid segment (ATM) were measured from Cochlear View (referred to as "anterolateral view" by Shin et al. (2014)). The LTS was taken as the straight-line distance from the midpoint of the GG to the midpoint of the second genu (SG) as shown in Figure 3.14. The LMS was taken from the midpoint of the SG to the stylomastoid foramen (SMF). Figure 3.14 also illustrates the ATM measurement between the straight lines of the LTS and LMS.

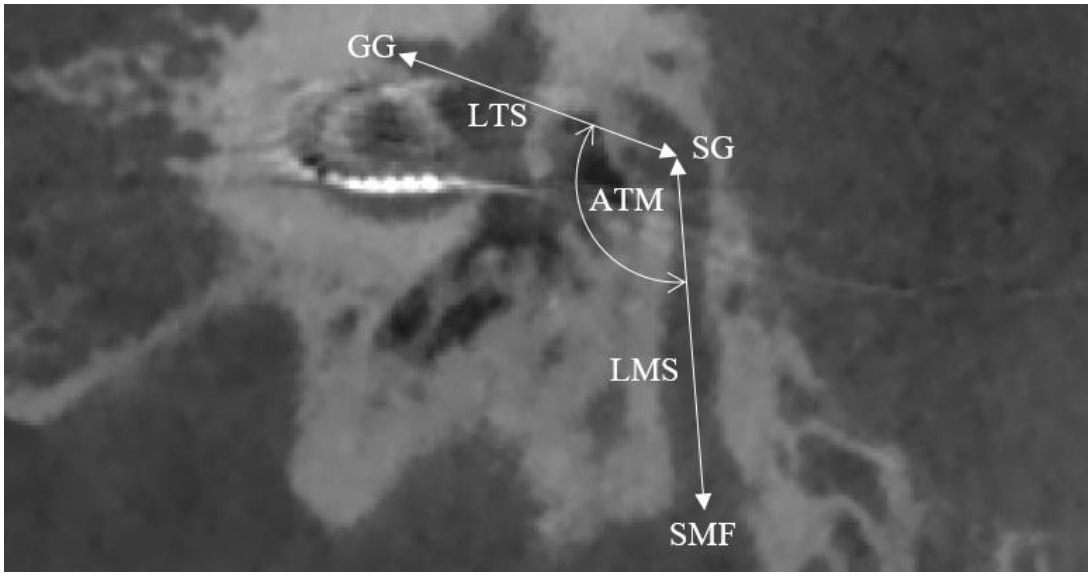

Figure 3.14. CT scan indicating the way in which the LTS, LMS and ATM were measured.

Figure 3.15 illustrates the method used to measure the three tympanic segment widths (WT1, WT2 and WT3) and mastoid segment widths (WM1, WM2 and WM3). WT1 was measured immediately posterior to the GG, WT3 was measured immediately anterior to the SG, and WT2 was measured midway on the LTS. WM1 was measured immediately inferior to the SG, WM3 immediately superior to the SMF, while WM2 was measured midway on the LMS.

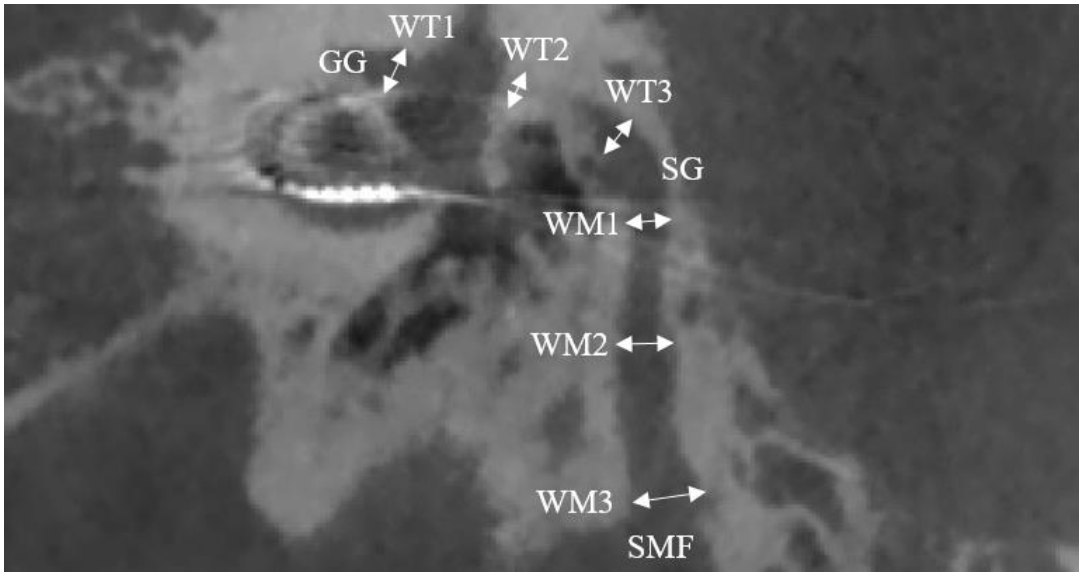

Figure 3.15. CT scan illustrating the way in which the three widths were measured for each of the tympanic and mastoid segments.

By using these measurements, the FN geometry was created using software developed by Gross et al. (2017), whereafter it was imported into the final COMSOL model. The FN geometry was positioned in the model using the location of the GG relative to the modiolus, which is visible on the CT scan in Cochlear View. Figure 3.16 illustrates the final FN geometry relative to the cochlea in the COMSOL model. FNFs were placed on the outer surface of the FN geometry, as indicated in Figure 3.16.

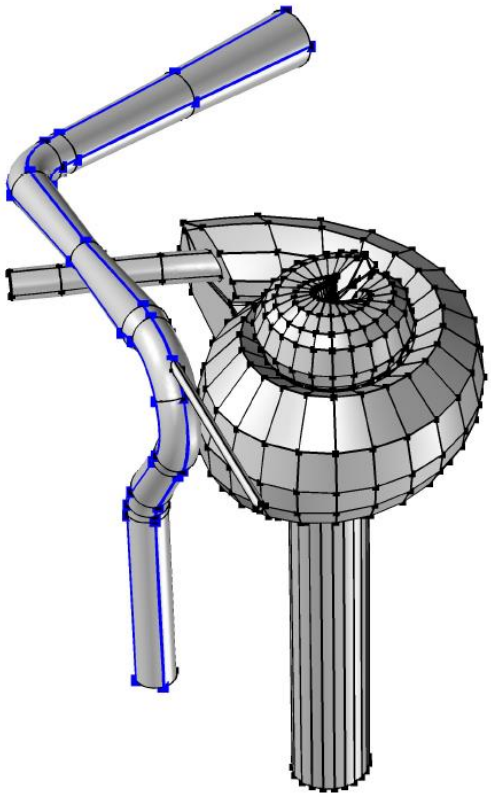

Figure 3.16. An example of the final FN COMSOL geometry imported into the model. The location of the FNFs are indicated with blue lines on the FN geometry.

3.5 MODEL-BASED INTERVENTION

One of the most common stimulation modes used in commercial CI strategies is MP stimulation (Klawitter et al., 2018). In MP stimulation, one of the intracochlear electrodes (ICEs) acts as the active electrode while one or more extracochlear electrodes (ECEs) acts as the reference electrode. In Cochlear Nucleus[1] implants, two electrodes typically exist exterior to the cochlea: a ball electrode, usually placed under the temporalis muscle, and a plate electrode on the internal package of the implant. In MP1 stimulation, current exists between the designated active ICE and the ball electrode, and in MP2 stimulation, current

[1] https://www.cochlear.com/intl/home

exists between the active ICE and the plate electrode. For MP1+2 stimulation, the current is sourced from the active ICE to both ECEs. The default stimulation mode used in Cochlear Nucleus implants is MP1+2 mode since it is generally associated with low T- and C-levels, reducing total implant energy requirements.

In bipolar (BP) stimulation, two ICEs are set as the active and reference electrodes. An ICE directly adjacent to the active electrode can be set to act as a reference electrode (BP stimulation) or can have N electrodes between the active electrode and reference electrode (BP+N stimulation). BP stimulation mode often reduces FNS due to electrical current being limited to inside the cochlea, but frequently increases hearing T- and C-levels.

In this study, a custom BP stimulation mode is proposed. This custom BP stimulation mode constitutes an active ICE, with the reference electrode assigned to be the most apical ICE. This stimulation mode, hereafter referred to as the apical reference (AR) stimulation mode, will be compared to conventional MP stimulation to determine the effects of different stimulation modes on EMG data, auditory T-levels and dynamic range. Model predictions and clinical experiments will be used to investigate AR stimulation, of which the results are presented in the following chapter.

3.6 EXPERIMENTAL DESIGN

The AR stimulation mode aims to limit the amount of current reaching the FN. So far, a description of the model, which can be used to simulate the proposed stimulation mode, was provided. In addition to the model-based investigation, the stimulation mode was furthermore assessed in an experiment. The goal of the experiment was to determine how the AR stimulation mode affects auditory T- and C-levels while simultaneously capturing EMG data, since the electrical artefact is often detectable in the tissue surrounding the implant. A well-controlled setup was required to deliver the stimulus and capture EMG signals, concurrently. A data logger was used to captured EMG signals during stimulation and a speech processor (SP) unit was used to deliver stimuli to a participant. A software tool

was developed to control and synchronise the SP unit and data logger, and to serve as an interface between the participant and the hardware.

3.6.1 The stimulus

During the experiments, stimuli were delivered using the L34 SP developed by Cochlear Limited. The SP unit of the CI user was replaced with the L34 SP to deliver customised stimuli. The L34 SP connects to the Freedom Programming Pod, also developed by Cochlear Limited, which connects to a computer through a USB port.

Supporting software interfaces for the L34 SP are provided by Cochlear Limited in different programming languages. The MATLAB interface, also known as the Nucleus MATLAB Toolbox (NMT), only allows stimulation in an MP configuration, making it unsuitable for the present study. For this reason, the Python interface libraries were used instead, since it also allows for BP stimulation. These libraries were developed in Python version 2.3, while the GUI and data logger control software were developed in the latest version of Python. Python version 2.3 libraries were executed using the latest version of Python, by sending shell commands to the Windows kernel. These libraries require six stimulation parameters, which are summarised in Table 3.2.

Table 3.2. L34 parameters.

Parameter	Description
Active electrode	The anodic electrode.
Reference electrode	The cathodic electrode.
Current level	The amplitude of the stimulus (CU).
Phase width	The duration of the stimulus pulse (μs).
Phase gap	The duration of the gap between pulses (μs).
Period	The time between the onset of consecutive stimuli (μs).

The active and reference electrodes can be configured as an ICE, which is a positive integer in the range 1-22, or an ECE, which is a negative integer (-1, -2 and -3). MP1, MP2 and MP1+2 modes are specified when setting the reference electrode to -1, -2 and -3, respectively. The AR stimulation mode would always have a reference electrode value of 22 since this refers to the most apical ICE.

The stimulation level is specified as current units (CUs) and is a positive integer in the range 0-255, which can be converted to dB (relative to 1 μA) using (3.4) and (3.5).

$$I(\mu A) = 17.5 \times 100^{\frac{CU}{255}} \tag{3.4}$$

$$I(dB) = 20 \log_{10} I(\mu A) \tag{3.5}$$

The phase gap and period were set to 20 μs and 10000 μs, respectively, and were kept the same throughout the experiments. A period of 10000 μs was chosen to ensure that all muscle activity ends before the next pulse is delivered (Bahmer and Baumann, 2016). One hundred pulses were delivered at a time, resulting in a total stimulus duration of 1 s.

3.6.2 The EMG

Two SX230-FW EMG amplifiers from Biometrics Ltd.[1] were used to measure facial muscle activity and electrical artefacts, and the PicoLog1216[2] data logger was used to capture the EMG signals. The SX230-FW EMG amplifiers use a bipolar configuration, i.e. every device has two measuring electrodes while a third electrode is used as a reference electrode. The EMG amplifier has a gain of 1000. It has a high-pass cut-off frequency of 20 Hz, and a low-

[1] http://www.biometricsltd.com/surface-emg-sensor.htm

[2] https://www.picotech.com/download/manuals/pl1000-en-2.pdf

pass cut-off frequency of 450 Hz. The EMG amplifiers have a positive power supply pin, a negative power supply pin (or ground) and an EMG signal output.

The EMG amplifiers were used to record two signals during experiments consisting of one electrode pair per signal, with a mutual reference electrode. This configuration resulted in five EMG electrodes in total. One pair of recording electrodes were placed in the vicinity of the eye, and the other pair of recording electrodes in the vicinity of the mouth since muscle contractions often occur in the region of the orbicularis oculi and oris muscles on the same side as the CI (Bahmer et al., 2017). The reference electrode acts as ground to the differential input of the preamplifier and is typically placed on an electrically inactive region of the body (Luca, 2002, Zahak, 2012). The reference electrode can be placed on the participant's forehead in facial EMG (Van Boxtel, 2010), but can also be placed in any area with a bony prominence and far away from the EMG detecting surfaces such as the os coxa, clavicle or wrist (Luca, 2002, Wang et al., 2013, Zahak, 2012). The reference electrode was placed on the clavicle for these experiments since this resulted in the least amount of noise during initial testing.

The EMG amplifiers require a single-sided supply voltage between 3.5 V and 5.5 V. Therefore, a 5 V rechargeable battery (cell phone power bank) was used to supply power to the EMG amplifiers to ensure electrical safety from mains electricity. Furthermore, the participant was optically isolated from mains electricity, using an optocoupler.

Since the EMG amplifiers have a high-pass cut-off frequency at 450 Hz, a minimum sampling rate of 900 Hz was required to satisfy the Nyquist Theorem. The data logger can capture data at a maximum sampling speed of 1 MS/s. This speed can only be achieved when one channel is used, and when a maximum of 8192 samples are taken at a time. Under any other condition, the maximum sampling rate is 100 kHz, shared across all channels. For two channels, this equates to a sampling rate of 50 kHz per channel for a sampling duration larger than 8.192 ms. This speed is still fast enough to satisfy the Nyquist Theorem conditions for an EMG signal. Two sampling rates were used during the experiment: 50 kHz (slow sampling) using two channels, and 1 MHz (fast sampling) using one channel. Slow sampling

was used to capture data for a stimulation sequence on both channels simultaneously. The sampling duration was set to 1.5 s to capture the entire 1 s stimulation sequence. The sampling and stimulation processes were placed on different computer threads to ensure concurrent execution. Sampling and stimulation could not be synchronised with high precision by the software. Therefore, an increased sampling duration was used, compared to the stimulus duration, to ensure that the entire stimulus sequence is captured.

Fast sampling was used to capture the details of the electrical artefact if one was present. The fast sampling duration was 8.192 ms and was triggered when the measured signal increased above a specific threshold value. Fast sampling was only implemented on the channel where the EMG electrodes were within the shortest distance from the implant itself since the artefact would theoretically be the largest at this position due to a reduced impedance between the stimulating electrode and the measuring electrode.

3.6.3 Experimental GUI

The experimental procedure was divided into three phases: a level adjustment phase, a hearing T-level phase and a level-dependent response phase. A GUI was developed, which was used to manage these phases and control all hardware and software processes. Figure 3.17 illustrates the main screen of the GUI. The investigator starts by specifying an active electrode, a reference electrode and the pulse width. Three buttons on the GUI enables the investigator to initiate each of the experimental phases. The parameters for the experiment must be set before initiating phases.

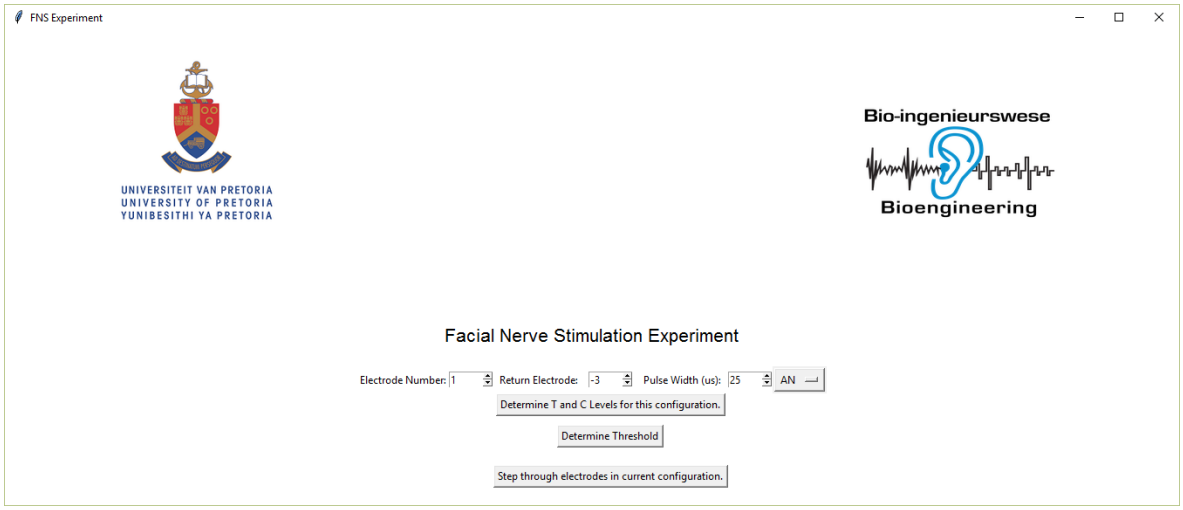

Figure 3.17. The main screen of the experimental software tool. From this screen, the investigator specifies the active and reference electrodes, the pulse width, and the phase of the experiment.

3.6.3.1 Level adjustments

In the first phase, the participant was tasked with adjusting their hearing T- and C-levels. The window shown in Figure 3.18 was presented on a separate computer screen in front of the participant. From this screen, subjective adjustments can be made to the T- and C-levels by using the corresponding slider.

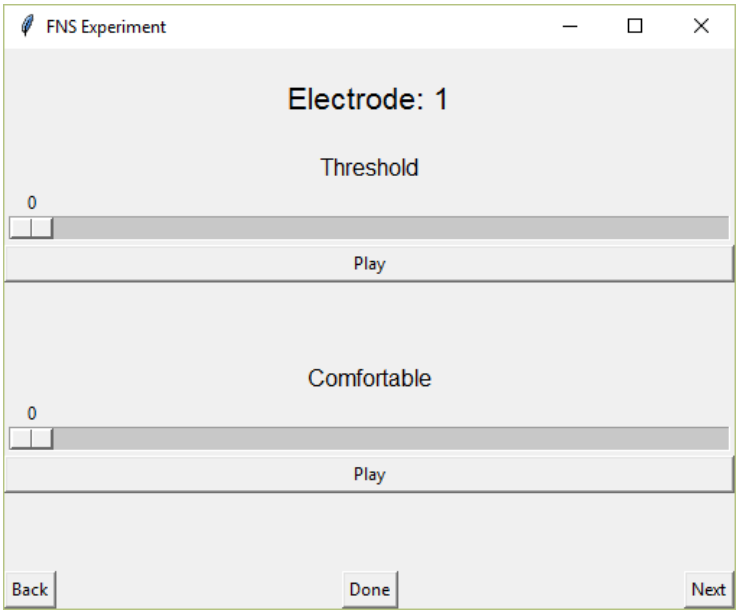

Figure 3.18. Participant T- and C-level adjustment interface. The participant must adjust the slider and then press the "Play" button for the stimuli to be delivered. On every delivery, EMG data were recorded.

A participant can adjust the slide bar and can press the "Play" button to deliver the stimulus at that specific level. Once satisfied with the T- and C-levels for a specific electrode, the T- and C-levels for the next electrode can be configured by pressing the "Next" button, which advances to the next active electrode of which the number is displayed in the caption of the screen. The pulse width, return electrode and phase gap are kept the same during the level adjustment phase. Once T- and C-levels for all active electrodes are set, the "Done" button is used to store the user-specified T- and C-values.

The T-levels specified by the participant are not the final T-levels since a more exact method for determining the T-levels is used in the second phase of the experimental process. For every stimulus which was delivered during the level adjustment phase, EMG data were recorded.

3.6.3.2 Psychoacoustic T-level

In the second phase of the experimental procedure, more exact hearing T-levels were determined using a psychoacoustic experimental procedure. The two-interval forced-choice (2IFC) method was used, as described by Gelfand (2017). For this process, two circles are displayed, as shown in Figure 3.19. The left circle turns green for two seconds, whereafter the right circle turns green for two seconds. One of the two intervals is randomly selected by software, and the stimulus is delivered only during the selected interval, i.e. when the specific circle is green. The participant is tasked with selecting the interval in which the stimulus was perceived by clicking on the corresponding circle. The starting stimulation level is calculated as the mean of the user-specified T- and C-levels from the previous experimental phase. Since this level would always be above the actual T-level, the participant will always perceive the first stimulus, which is vital for correct T-level convergence.

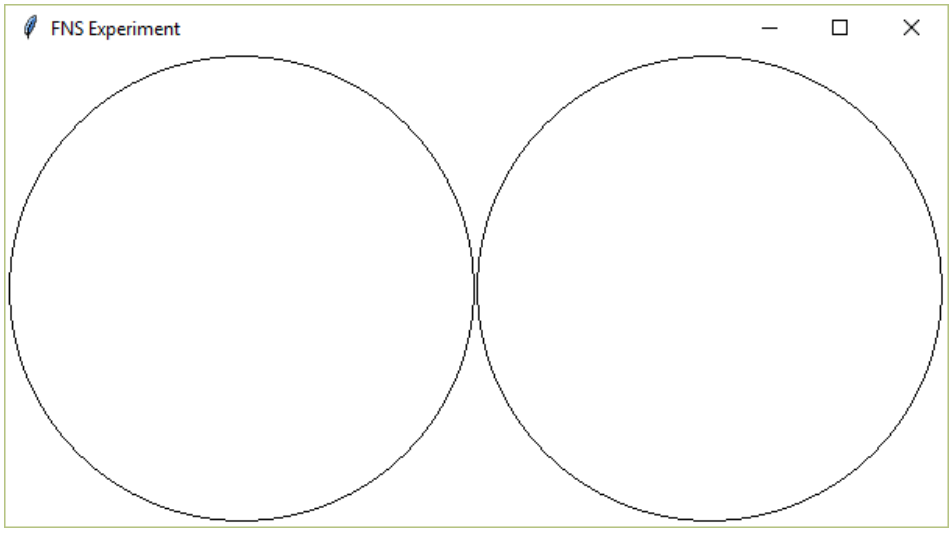

Figure 3.19. 2IFC interface. Each circle will turn green for two seconds, in which one interval is chosen at random to deliver the stimulus.

The 2IFC method uses the parameter estimation by sequential testing (PEST) procedure (Gelfand, 2017). This procedure causes the step size to change based on the accuracy of the answers provided. This technique improves precision and uses the minimal number of trails to converge to the correct T-level. Once the T-level is determined, the process repeats by

starting again at a level above T-level. This process repeats three times whereafter an average T-level value is calculated. During every stimulus which is delivered, EMG data are captured.

3.6.3.3 Level-dependent response

After the first and second phase of the experiment, EMG data often exclude recordings at selected stimulation levels throughout the dynamic range. In the final phase, the aim was to ensure that EMG data were recorded over the entire dynamic range. This process begins by displaying the window shown in Figure 3.20 to the investigator. The investigator can select specific electrodes which will be used in this process. The T-level value which is used to activate fast sampling, can be specified on this screen next to the electrode number. The process starts by stimulating at C-level and then stepping down in steps of 3 CUs. EMG data are recorded on every stimulus for both slow and fast sampling. The stimulation level is decreased in steps of 3 CUs until the stimulus is just below the T-level, which was determined in the second phase of the experimental process.

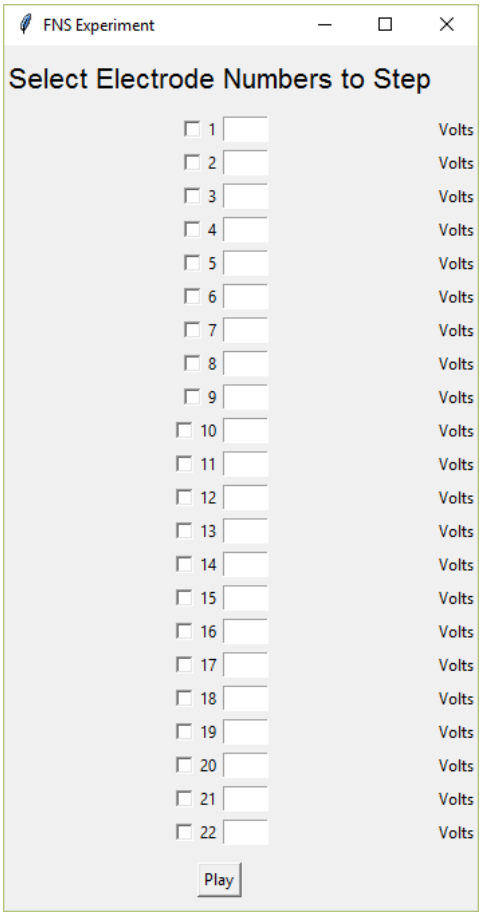

Figure 3.20. Level-dependant responses screen. The investigator can select electrodes and specify T-levels which are used to initiate fast sampling if the recorded voltage elevates above the T-level.

3.7 CHAPTER SUMMARY

In this chapter, an overview of the methods used in this study was discussed. Two general themes were discussed: the modelling process which was followed and the clinical experimental procedure.

In Section 3.2, two existing modelling workflows were discussed and a refinement tool described, which attempts to increase the accuracy of the final model generated by the automated method. In Section 3.3, different geometric variations are described. Section 3.4 describes the method used to generate and include the FN geometry in the model. In Section

3.5, a brief description of the intervention which was investigated in the present study is provided. Section 3.6 describes all hardware and software involved in the experiments performed.

CHAPTER 4 RESULTS

4.1 CHAPTER OVERVIEW

This chapter presents all results gained from this study. In Section 4.2 the spirals from the AAM and automated method are compared to measurements made by an experienced anatomist. In Section 4.3 the accuracy of the analytical cochlear model is evaluated. In Section 4.4 predicted T-levels for different geometric variations are presented. In Section 4.5 T-level predictions for two FNS interventions are shown to establish their effectiveness. In Section 4.6 the results from clinical tests are presented to illustrate the effect of the AR stimulation mode on EMG recordings and auditory T- and C-levels. In Section 4.7 a summary is presented which concludes the chapter.

4.2 EVALUATION OF THE AAM

The AAM attempts to improve the accuracy of the model, which was generated using the automated method. Trajectories from both the AAM and the automated method were compared to measurements made by an experienced anatomist. The comparison was made using the cylindrical coordinate system, in terms of ρ and z, which translates to the horizontal and vertical distances on the radial slices, respectively. The measured ρ- and z-values were smoothed by performing a polynomial fit to the raw data.

4.2.1 Polynomial fitting of raw data

The raw data were measured at 5° intervals for a specific cochlea, but measurement noise on the spirals necessitated a smoothing procedure. Pietsch et al. (2017) suggested that measured ρ- and z-values can be approximated with a third- and fourth-order polynomial curve, respectively. Figure 4.1 illustrates an example of a third- and fourth-order polynomial fit to the ρ- and z-values of the lateral spiral. Note the slight dissimilarities between the polynomial approximations and the measured data. An example of this is evident in the first 200° of the z-values, in which the approximation seems to follow an incorrect trend.

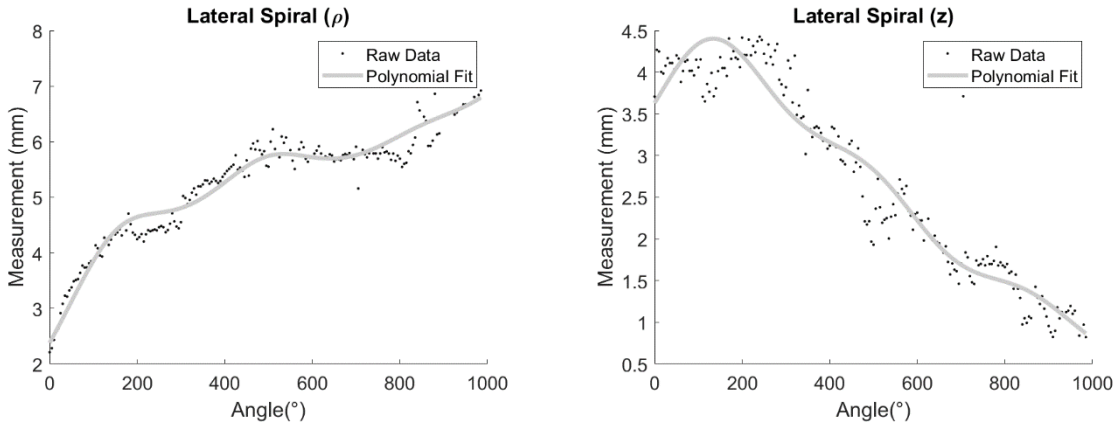

(a) **(b)**

Figure 4.1. Polynomial fitted ρ- and z-values for measurements of the lateral spiral. Figure (a) illustrates the ρ-values fitted with a third-order polynomial and Figure (b) the z-values fitted with a fourth-order polynomial. Slight dissimilarities exist between the polynomial approximations and the measured data.

Figure 4.2 (a) and (b) illustrate a third- and fourth-order polynomial fit approximation for the ρ- and z-values of the electrode array. Similar to the lateral spiral, dissimilarities can be observed between measurements and the approximations. For example, the ρ-values of the polynomial approximation deviates notably from the measured data in the first 150° and the last 100°.

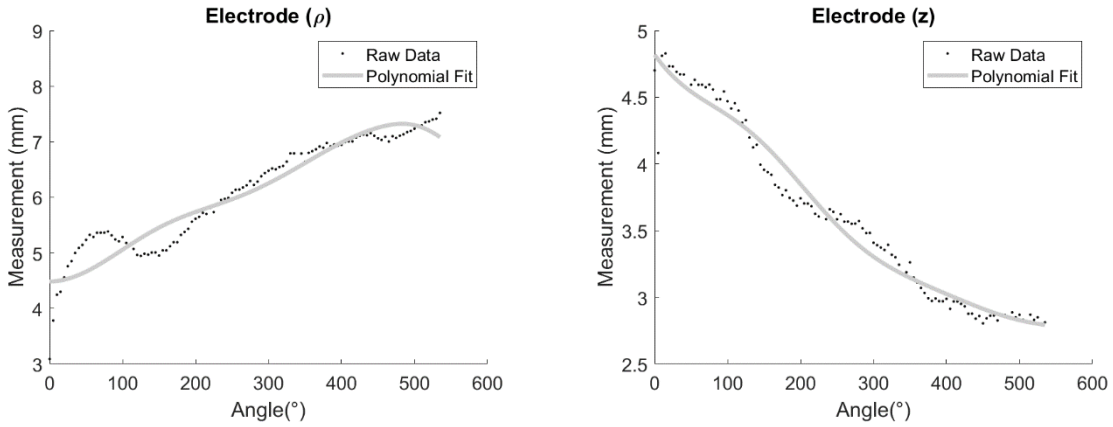

(a) **(b)**

Figure 4.2. Polynomial fitted ρ- and z-values for measurements of the electrode array. Figure (a) illustrates the ρ-values fitted with a third-order polynomial and (b) the z-values fitted with a fourth-order polynomial. Dissimilarities are evident in both approximations, with the ρ-values deviating especially in the first 150° and the last 100°

In an attempt to improve the correspondence between the measured data and the approximated spirals, the polynomial order used for both the ρ- and z-values was increased. Figure 4.3 illustrates the sixth-order polynomial approximations for both the ρ- and z-values for the same data as in Figure 4.1. The sixth-order polynomial approximations demonstrate an improved fit to the measured ρ- and z-values.

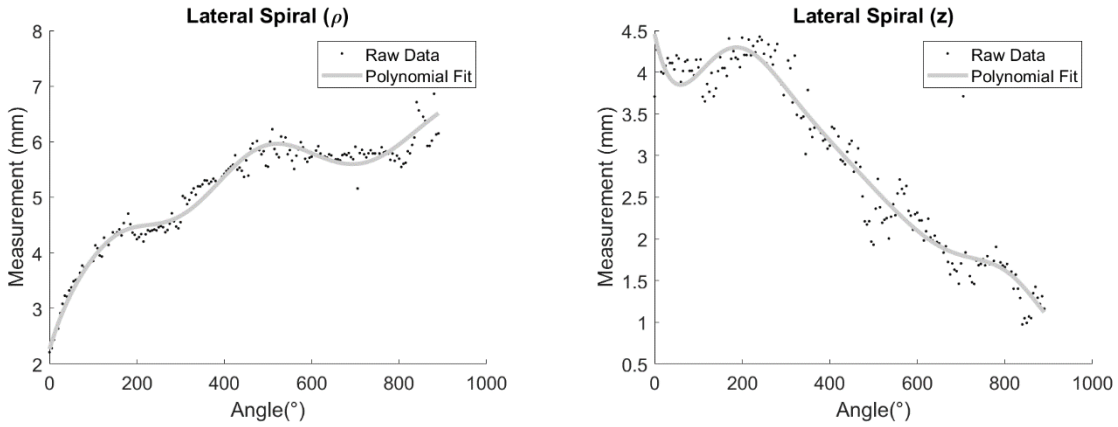

(a) **(b)**

Figure 4.3. Polynomial fitted ρ- and z-values for measurements of the lateral spiral. Figure (a) illustrates the ρ-values and (b) the z-values, both fitted with a sixth-order polynomial. These polynomial approximations illustrate improved accuracy compared to lower order polynomial approximations for the lateral spiral.

Figure 4.4 illustrates the sixth-order polynomial approximations of the electrode data, which also show an improved correspondence with the measured ρ- and z-values.

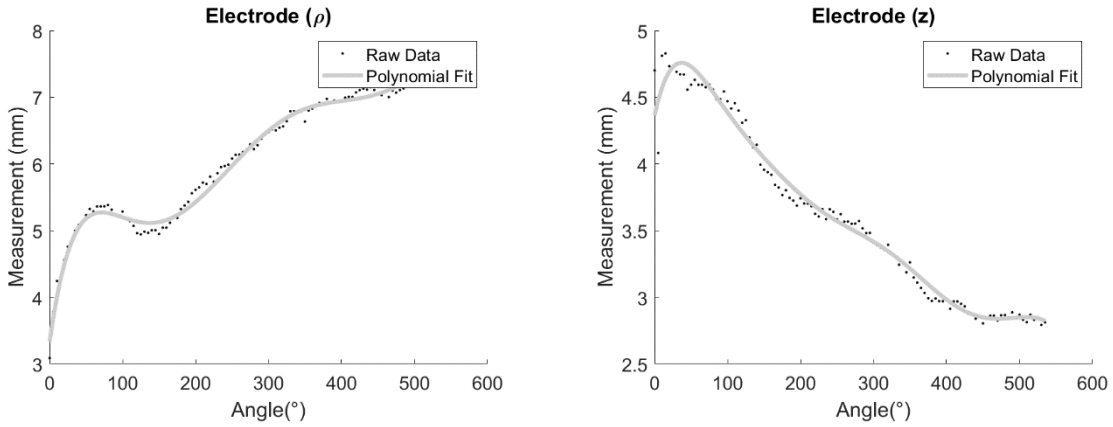

(a) **(b)**

Figure 4.4. Polynomial fitted ρ- and z-values for measurements of the electrode array. Figure (a) illustrates the ρ-values and (b) the z-values both fitted with a sixth-order polynomial. These polynomial approximations illustrate improved accuracy compared to lower order polynomial approximations for the electrode array.

It is evident that higher-order polynomials produce a closer fit to the subtle deviations in the trajectories of the landmarks, than the lower-order polynomials. Therefore, the sixth-order approximations of measured data were used for all comparisons that followed due to an improved correspondence between raw data and polynomial approximations.

4.2.2 Comparisons between the AAM and automated method

Figure 4.5 shows two examples in which the automated method generated spirals, which deviated from the measured trajectories. After the adaption process using the AAM, the accuracy of these spirals was increased, as illustrated in Figure 4.5.

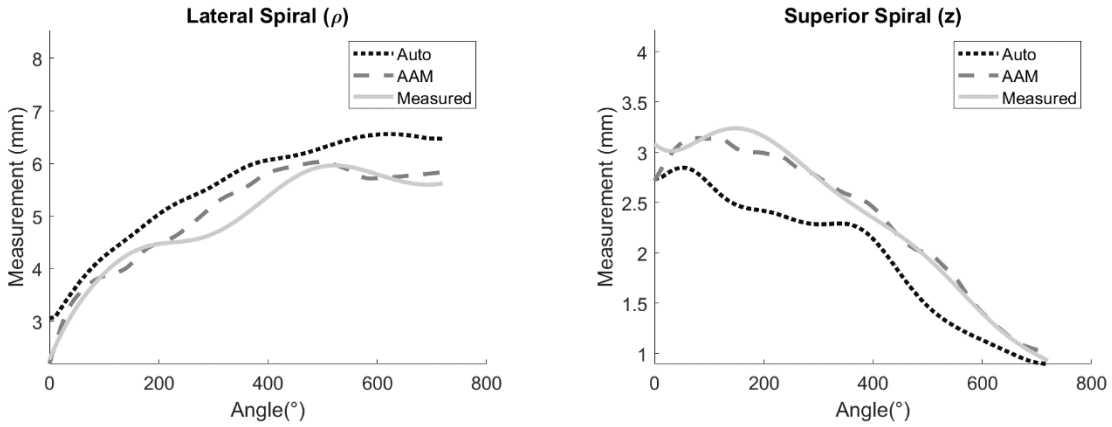

(a) **(b)**

Figure 4.5. Comparisons between the automated method, AAM and measured data. Figure (a) illustrates the ρ-values of the lateral spiral and Figure (b) illustrates the z-values of the superior spiral.

Figure 4.6 shows a comparison between the measured spiral, the automated trajectory and the AAM trajectory of the electrode array. For both the ρ- and z-values, the AAM illustrates an improved fit to the measured trajectory, compared to the automated method.

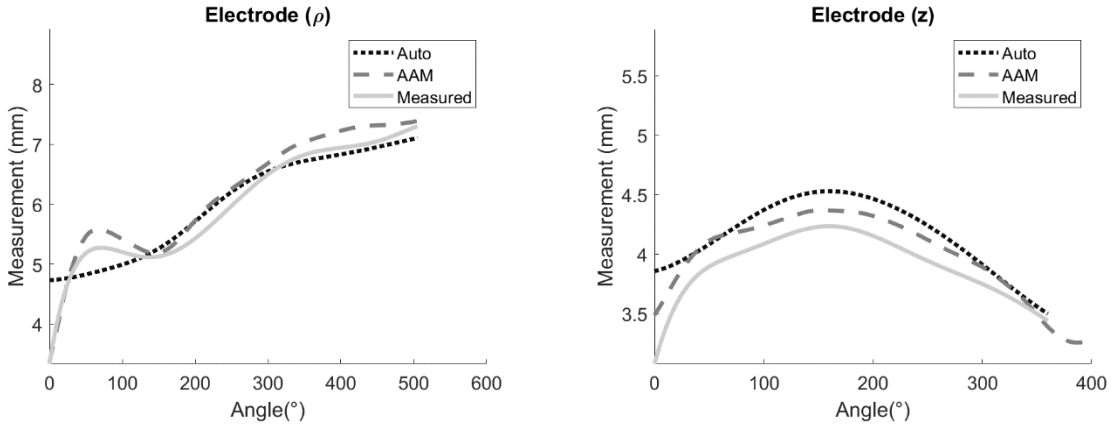

(a) **(b)**

Figure 4.6. Comparisons between the automated method, AAM and measured data for the electrode array. Figure (a) and (b) illustrate the ρ- and z-values of the electrode array.

4.3 EVALUATION OF ANALYTICAL COCHLEAR MODEL

Pietsch et al. (2017) suggested that an analytical cochlear model can predict the course of the cochlea, based on four measurements taken from Cochlear View. For one of the participants in the present study, only limited CT scan data were initially available, for which the analytical approach was used to create a 3D model.

In due course, the full CT scan stack was received from the radiologist. An experienced anatomist was tasked with identifying landmarks on the cochlear duct and electrode array using the full CT scan stack, whereafter the data were approximated with sixth-order polynomial curves. Figure 4.7 shows a comparison between the measured spirals and the analytical model in terms of the ρ- and z-values. The correspondence between the measured ρ- and z-values, and the ρ- and z-values generated by the analytical model is acceptable, with minor deviations at selected angular distances.

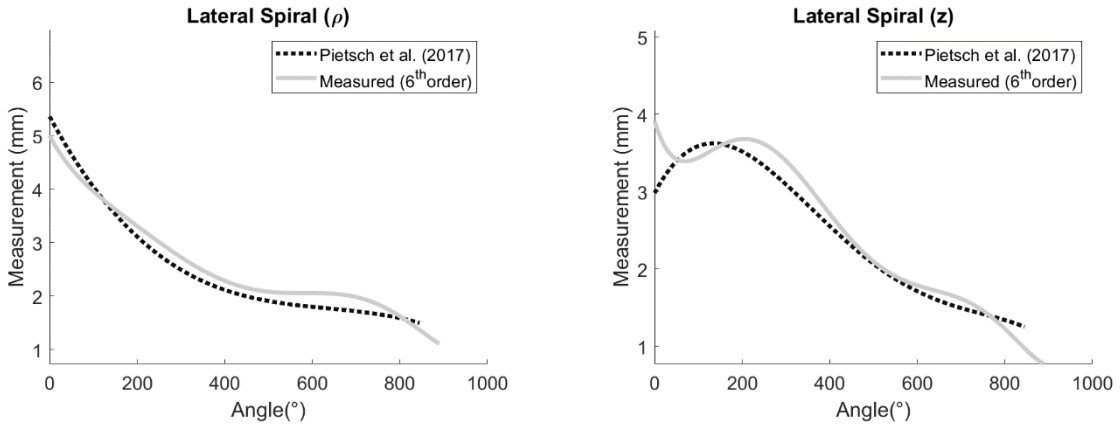

(a) **(b)**

Figure 4.7. A comparison between the predicted lateral spirals generated by the analytical model and the measured spirals. Figure (a) illustrates the ρ-values of the analytical model compared to the sixth-order polynomial approximation of the measured data. Figure (b) illustrates the z-values of the analytical model compared to the sixth-order polynomial approximation of the measured data.

4.4 GEOMETRIC VARIATION

The effects of three different modifications to the volume conduction models were considered: the presence of the OC geometry, the shape of the CN geometry, and the granularity of cochlear geometries. In Section 3.3.1, the exclusion of the OC was discussed in which it was suggested that the small volume representing the OC are likely to have little effect on predicted T-levels. Excluding the OC can reduce modelling complexity. Furthermore, the modifications that were made to improve the geometry of the CN were discussed in Section 3.3.2, in which the original and modified CN geometries are presented in Figure 3.8 and Figure 3.9, respectively. The possible effect that the granularity of the cochlear geometries has on predicted T-levels was discussed in Section 3.3.3, with an example of smooth and faceted geometries presented in Figure 3.10. The results from these variations are presented below.

4.4.1 Excluding the OC

A person-specific model was used to determine the effects of the presence of the OC geometry on neural excitation predictions. Figure 4.8 shows the predicted T-levels for models which include and exclude the OC. Both models predict similar T-levels, illustrating that the absence of the OC does not have an adverse effect on predicted T-levels.

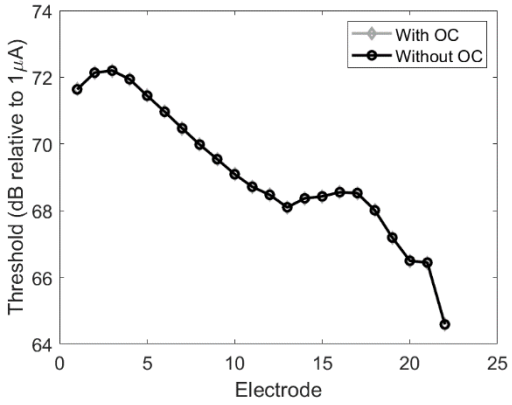

Figure 4.8. Predicted T-levels for a person-specific model, with and without the OC geometry. MP1+2 stimulation mode was used with a pulse width of 25 μs.

4.4.2 CN shape

Two simulations were created to assess the effects that the proposed CN geometry modification has on predicted T-levels. The same model trajectories were used to compare the original CN geometry, the modified CN geometry and map T-levels. Figure 4.9 shows a comparison between the two simulations. It is evident that for the majority of active electrodes, similar T-levels were predicted with the exception of a number of basal and apical electrodes.

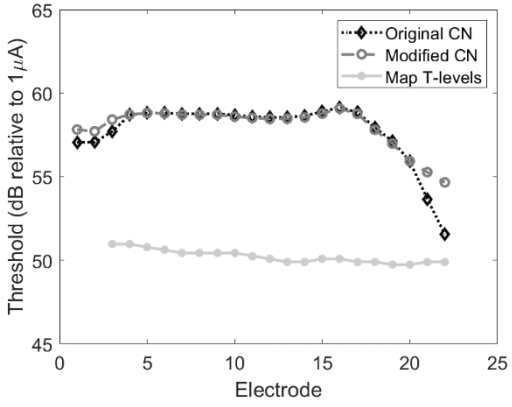

Figure 4.9. Predicted T-levels for the original and modified CN geometries. MP1+2 stimulation mode was used with a pulse width of 25 μs. The map T-levels are also presented as a comparison.

4.4.3 The granularity of cochlear geometries

Two simulations were created to evaluate the effects that granularity has on predicted T-levels. The same model trajectories were used for both simulations. Figure 4.10 shows predicted T-levels for smooth and faceted geometries, presented with the map T-levels. Predicted T-levels for smooth and faceted geometries are remarkably similar, with minor differences evident on selected electrodes.

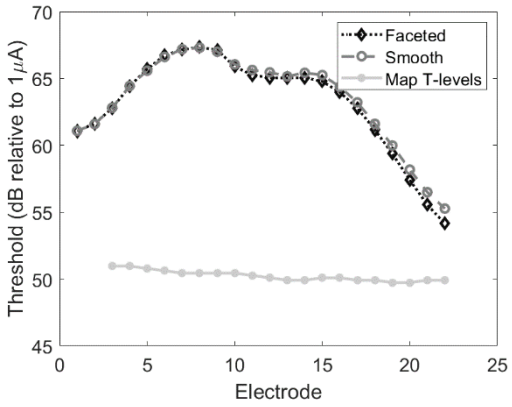

Figure 4.10. Predicted T-levels for the smooth and faceted cochlear geometries. MP1+2 stimulation mode was used with a pulse width of 25 μs. The map T-levels are also presented as a comparison.

4.5 MODEL-PREDICTION OF INTERVENTIONS

The effects that stimulus pulse width and the AR stimulation mode has on predicted FNF and ANF T-levels were investigated. These predictions are presented below. For all subsequent simulations the OC was excluded, and the original CN geometry was used. Furthermore, all models were created using faceted geometries.

4.5.1 Pulse width

Various studies have suggested that the effects of FNS can be reduced by increasing the pulse width of the stimulus, and in so doing, decrease the amplitude of the stimulus (Alharbi et al., 2012, Battmer et al., 2006). This hypothesis was tested during simulation to determine whether models can predict this phenomenon. Figure 4.11 (a) and (b) illustrate predicted T-levels for FNFs and ANFs during MP1+2 stimulation, stimulated with pulse widths of 25 μs and 300 μs, respectively. From Figure 4.11 it is evident that the predicted ANF and FNF T-levels are at similar levels for a pulse width of 25 μs, but that a pulse width of 300 μs elevated all FNF T-levels above ANF T-levels.

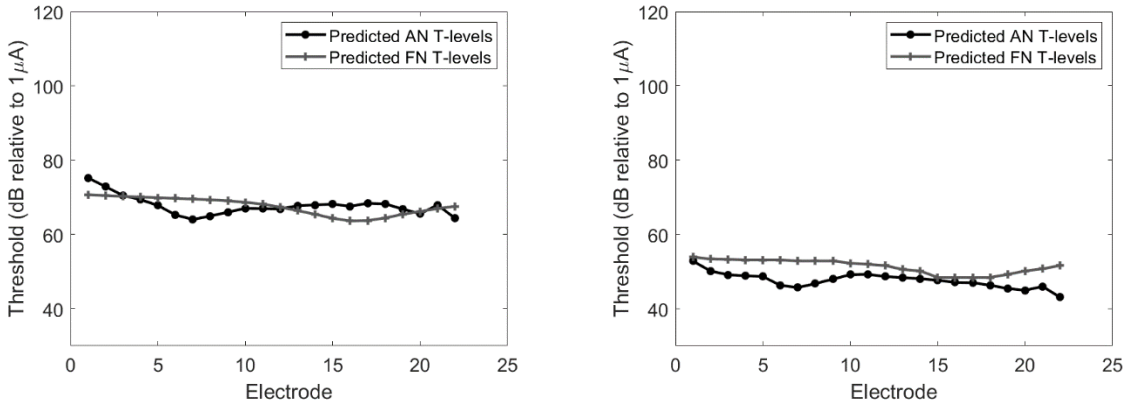

(a) **(b)**

Figure 4.11. Predicted ANF and FNF T-levels for the MP1+2 stimulation mode. A pulse width of 25 μs was used in (a) and 300 μs in (b).

4.5.2 AR stimulation

Figure 4.12 (a) and (b) illustrate predicted T-levels for FNFs and ANFs during AR stimulation, stimulated with a pulse width of 25 μs and 300 μs, respectively. For a 25 μs pulse width, a noticeable increase in the difference between ANF and FNF T-levels can be observed, compared to the predicted T-levels for the same pulse width and with the MP1+2 stimulation mode. For the 300 μs pulse width, this difference increased even more. Note the

local maxima and minima for the FNF T-levels during AR stimulation, which are influenced by the location of the active electrode relative to the FN geometry.

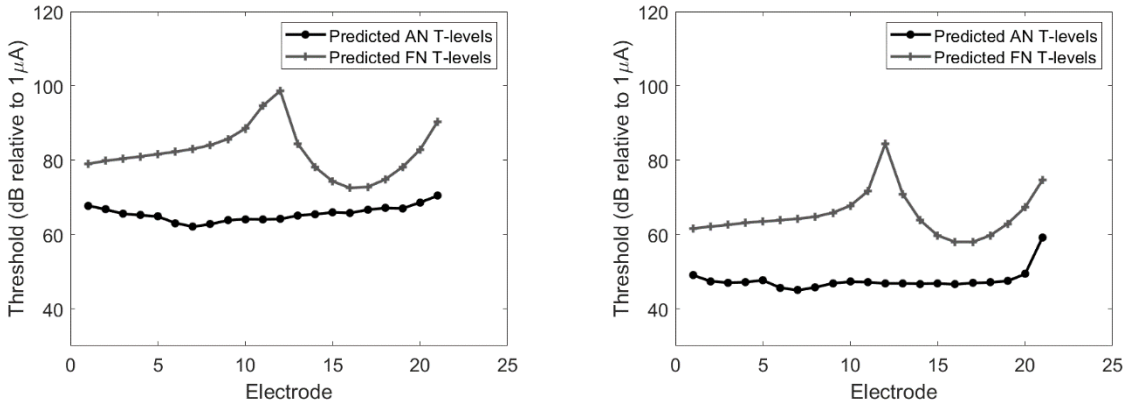

(a) **(b)**

Figure 4.12**.** ANF and FNF T-levels for AR stimulation**.** A pulse width of 25 μs was used in (a) and 300 μs in (b).

4.6 CLINICAL RESULTS

One of the objectives of the clinical experiments performed in this study was to determine the effect that the AR stimulation mode has on hearing T- and C-levels and EMG recordings. For this purpose, two participants were used. The first participant was used in a pilot study. The person did not experience FNS, but the opportunity was used to determine whether the experimental setup was appropriate for determining accurate T- and C-levels and to evaluate the effect of the AR stimulation mode on psychoacoustic levels. Furthermore, the study was used to verify that the electrical artefact caused by the implant can successfully be captured using the EMG devices and datalogger. In a successive study, a participant was used who experienced severe FNS. From the results in the pilot study, minor changes to the experimental setup were made in the successive study.

The clinical results are separated into three sections. The first section contains the EMG data captured from both the pilot and successive studies. The second section contains auditory T- and C-levels from the pilot study. The third section contains auditory T- and C-levels from the successive study.

4.6.1 EMG Data

Two concurrent EMG recordings were made during every stimulus. EMG data were captured in the vicinity of the eye, henceforth referred to as EMG1, and in the vicinity of the mouth, henceforth referred to as EMG2.

During the pilot study, EMG data initially did not contain any observable electrical artefact. The absence of the electrical artefact in the EMG data was unexpected since it has been reported that the electrical artefact can be captured by SEMG (Bahmer and Baumann, 2016). It was later determined that the low-pass cut-off frequency of the SX230-FW EMG amplifiers is only 450 Hz and thus attenuated the majority of the artefact for short pulse widths due to the high-frequency contents of the signal. Though distorted, the artefact caused by wide pulse stimuli was observed on EMG recordings due to the increased energy existing at low frequencies.

Consequently, wide pulse widths were used for all EMG recordings since the electrical artefact was required to evaluate the amount of current existing in the tissue surrounding the cochlea. Figure 4.13 shows recordings for EMG1 and EMG2 in which a 400 μs pulse width was used. The artefact caused by the implant is visible in the EMG recording, with EMG1 illustrating a larger artefact compared to EMG2.

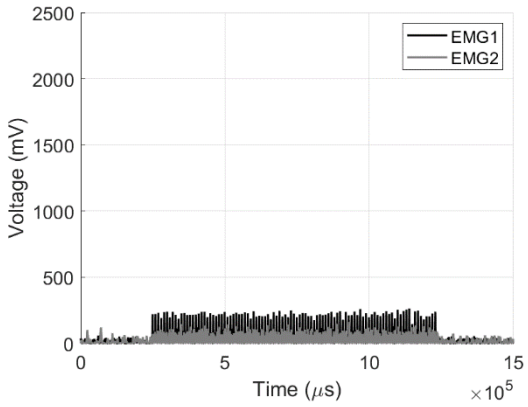

Figure 4.13. An example of EMG data captured during MP1+2 stimulation. Two channels were recorded, EMG1 and EMG2. The pulse width was 400 μs. EMG1 was recorded in the vicinity of the eye, and EMG2 in the vicinity of the mouth.

Figure 4.14 (a) shows a magnified section of the EMG noise in the absence of a stimulus. Figure 4.14 (b) shows a magnified EMG recording illustrating the artefact recorded during stimulation, with active electrode eight in an MP1+2 configuration. A pulse width of 400 μs and a stimulation level of 42.9 dB was used. Note how the spontaneous EMG activity, which is evident in (a), disappears during stimulation in (b), most likely due to the signal being truncated as a result of the EMG amplifiers, which use a single-sided power supply.

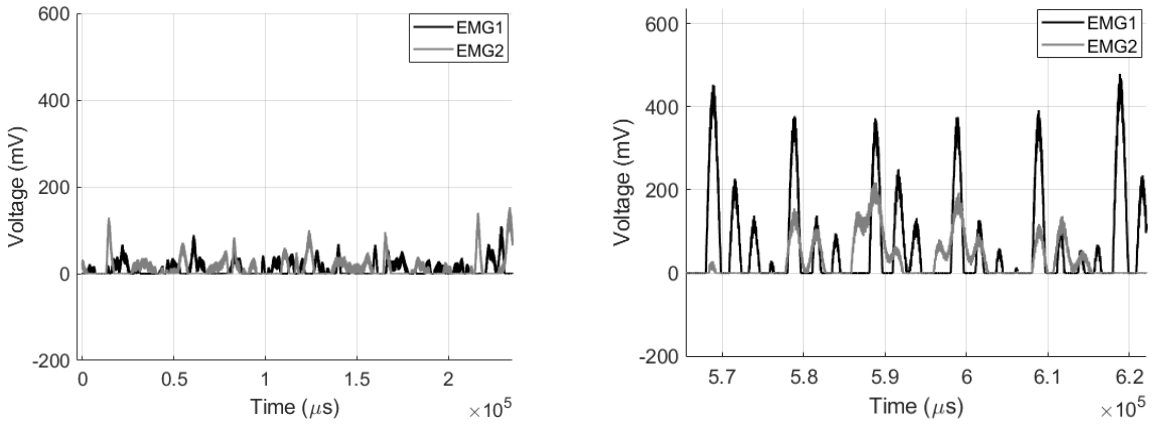

Figure 4.14. Magnified EMG signals. Figure (a) shows EMG noise in the absence of a stimulus and (b) shows the EMG recording made during stimulation, showing the electrical artefact. In Figure (b), electrode eight was used to stimulate in an MP1+2 configuration with a pulse width of 400 µs.

The EMG signal energy was used to compare AR and MP1+2 stimulation. The energy of the EMG signal was calculated for data between 0.5 s and 1 s. This timeframe was used since the stimulus and the start of the EMG recording could not be synchronised with high precision using computer threads, thereby requiring using an extract from the EMG recording. Using EMG data outside this timeframe might include data in the energy calculation in which no stimulus was present, which could influence the results.

The energy was calculated for a range of stimulations. The energy level for one stimulation sequence was calculated using (4.1).

$$E = \sum_{n} |V[n]|^2 \tag{4.1}$$

The calculated energy levels were used to plot stimulus intensity-dependent energy curves. If duplicate data were available for a specific stimulation level, the average energy was calculated. For each active electrode, both MP1+2 and AR stimulation were used. The

notation of the AR stimulation is BP+*N*, in which *N* is an integer chosen in order for the reference electrode to be assigned to the most apical electrode.

Figure 4.15 illustrates stimulus intensity-dependent energy curves for data captured during the pilot study. Figure 4.15 (a), (b) and (c) presents a comparison between MP1+2 and the AR stimulation mode for active electrodes 2, 10 and 16, respectively. These graphs illustrate an increase in energy levels as stimulation levels are raised during MP1+2 stimulation but show no apparent increase for the AR stimulation mode.

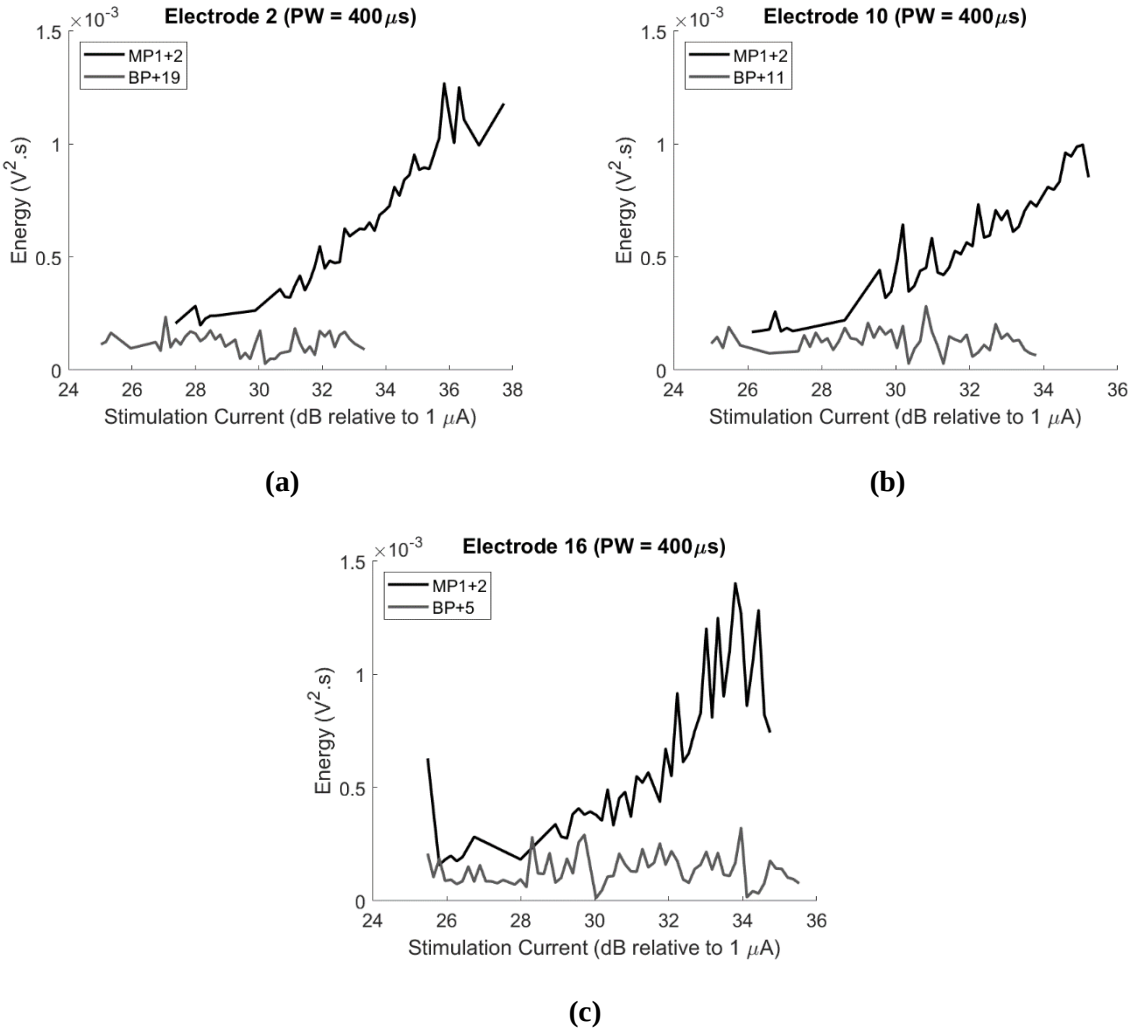

Figure 4.15. Stimulus intensity-dependent energy levels for different active electrodes and stimulation modes captured during the pilot study. A pulse width of 400 μs was used for all stimuli. Active electrodes 2, 10 and 16 were used in (a), (b) and (c), respectively.

Figure 4.16 shows the stimulus intensity-dependent energy curves from EMG data which were recorded during the successive study. Data were captured for active electrodes 3, 5 and 8, illustrated in Figure 4.16 (a), (b) and (c), respectively. A similar result to that in the pilot study was observed, with the MP1+2 stimulation mode illustrating increases in energy levels for increased stimulation levels. Moreover, the stimulus intensity-dependent energy curves for the successive study illustrate a lower variability, compared to the intensity-dependent energy curves in the pilot study.

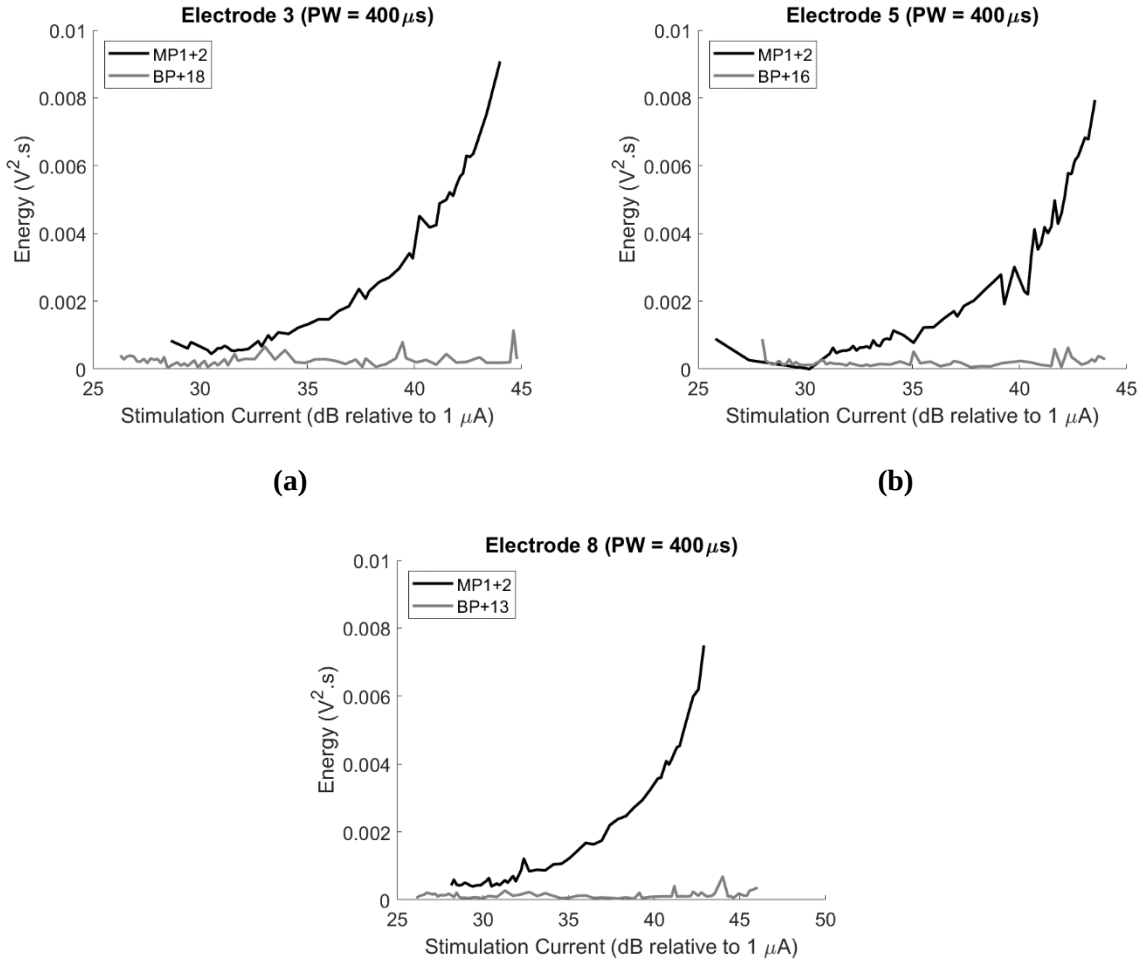

Figure 4.16. Stimulus intensity-dependent energy levels for different active electrodes and stimulation modes captured during the successive study. A pulse width of 400 μs was used for all stimuli. Active electrodes 3, 5 and 8 were used in (a), (b) and (c) respectively.

4.6.2 Successive study subjective report

Bahmer and Baumann (2016) hypothesised that a reduction in the electrical artefact could reduce FNS symptoms. Therefore, the electrical artefact visible in EMG data was used as an objective measure for the presence of FNS. However, subjective feedback was also recorded during the successive study to determine whether a relationship exists between the subjective

reports of FNS and the energy levels of the EMG data. Table 4.1 presents a summary of the subjective feedback recorded during the experiments. From Table 4.1, it is evident that the participant did not perceive FNS during AR stimulation, but that FNS was present for MP1+2 stimulation.

Table 4.1. Subjective feedback from the participant in the successive study.

Electrode number	Pulse width	MP1+2	AR stimulation
3	25 μs	FNS at high current levels.	No FNS up to C-level.
	400 μs	Severe FNS at high current levels.	No FNS up to C-level.
5	25 μs	FNS at high current levels. Muscle contraction was observable on the left of the chin while stimulating the right cochlea.	No FNS up to C-level.
	300 μs	FNS at high current levels.	No FNS up to C-level. A full and loud sound reported.
	400 μs	FNS at high current levels.	No FNS up to C-level.
8	25 μs	FNS at high current levels.	No FNS up to C-level.
	400 μs	Moderate FNS at high current levels.	No FNS up to C-level.

The participants, in both the pilot and successive studies, reported full and loud sounds during AR stimulation at C-levels for the specific stimulating electrodes, presumably due to an increased population of neural fibres being stimulated.

4.6.3 Pilot study hearing results

After successful implantation of a CI, an audiologist usually determines T- and C-levels for a specific user, which are used to configure settings for optimal CI performance. The T- and C-levels determined by the audiologist were compared to T- and C-levels determined in the psychoacoustic tests conducted in this study. This comparison was made to ensure that the experimental process was appropriate and accurate to determine T- and C-levels. Stimuli were delivered in an MP1+2 configuration and with a pulse width of 25 μs to be able to compare the levels with values recorded by the audiologist. Table 4.2 shows a comparison between four electrodes, comparing the experimental T- and C-levels and the T- and C-levels determined by the audiologist.

Table 4.2. Measured T-levels compared to T-levels found by the audiologist for MP1+2 stimulation with a pulse width of 25 μs.

Electrode Number	Experimental T-level (dB)	Audiologist T-level (dB)	Experimental C-level (dB)	Audiologist C-level (dB)
5	46.19	45.41	52.15	49.01
10	49.49	47.92	54.66	52.94
15	47.45	48.23	53.57	52.94
20	46.19	46.82	51.68	51.21

Not all electrodes converged to a value close to the value recorded by the audiologist, with outlier T-level values evident for some electrodes. It was later determined that the cause of these outliers was due to the initial current step size being too large. For the 2IFC procedure, the initial step size is used to adjust the stimulation level. In some instances, the stimulation level was reduced to a level well below the actual T-level due to the initial step size being too large. Consequently, the participant would not perceive sounds after this occurrence. The stimulation level would then incorrectly converge to a value well below the actual T-level since the chance for the participant to choose the correct interval is 50%. These outlier T-

levels had to be discarded in the pilot study. In some instances, the stimulation level would increase again to a level above the actual T-level if the participant chose the incorrect interval. In most of these cases, the stimulation level would correctly converge to values close to the T-level recorded by the audiologist. In the successive study, the initial current step size was decreased to prevent underestimation of T-levels.

4.6.4 Successive study hearing results

In the successive study, the experimental process was performed for electrodes 3, 5 and 8. The pulse width and the stimulation mode were varied for different active electrodes. Figure 4.17 illustrates T- and C-levels for MP1+2 and AR stimulation. The results for both MP1+2 and AR stimulation are presented side-by-side to illustrate the effects that stimulation mode has on T- and C-levels for each configuration. In addition, predicted T-levels were included in the results as a comparison. For all configurations, AR stimulation produced higher C-levels and lower T-levels, compared to MP1+2 stimulation, illustrating an increased dynamic range for AR stimulation. Furthermore, predicted T-levels were significantly higher than the actual T-levels.

4.7 CHAPTER SUMMARY

In this chapter, the accuracy of the spirals generated by the AAM and automated method was evaluated against measurements made by an experienced anatomist. The accuracy of the analytical model was evaluated by comparing it to measured data. Furthermore, the predicted T-levels for variations in geometries were presented, followed by predicted T-levels determined by simulating different interventions. This chapter concludes with clinical results which include EMG data, a summary of subjective feedback from the participant in the successive study, and T- and C-levels from both the pilot and successive studies.

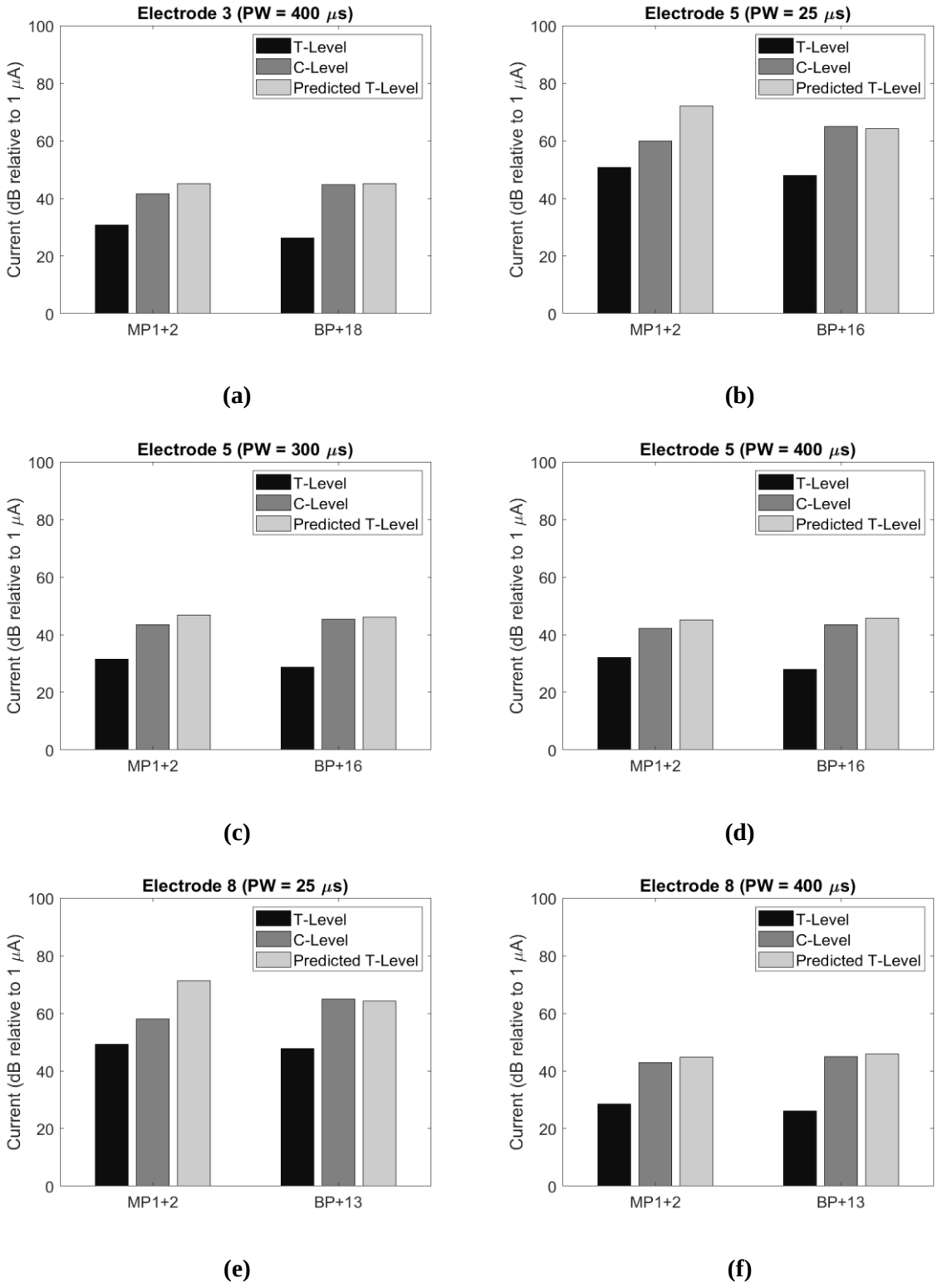

Figure 4.17. A comparison illustrating hearing T- and C-levels determined during psychoacoustic evaluation, for both MP1+2 and AR stimulation. Predicted T-levels are also illustrated.

CHAPTER 5 DISCUSSION

5.1 CHAPTER OVERVIEW

In this chapter, the results are interpreted in an attempt to provide answers to the research questions posed in Chapter 1. In Section 5.2 the accuracy of the models created using the AAM and the automated method is assessed. In Section 5.3 the accuracy of the analytical cochlear model is discussed. In Section 5.4 the effect of geometric variations on predicted T-levels is interpreted. In Section 5.5 model-based FNS interventions, which were investigated, are discussed and are rated according to their effectiveness in reducing FNS symptoms. In Section 5.6 the results from the clinical experiments are discussed. In Section 5.7 a summary is presented which concludes the chapter.

5.2 ACCURACY OF THE AAM

To determine whether the accuracy of models can be improved upon using the AAM, model trajectories were compared to measured trajectories. Due to measurement noise, the data were smoothed by fitting polynomial curves of different orders on it, after which these approximations were used to evaluate the accuracy of the automated method and the AAM. The fitting of polynomials to raw data and the comparison between the automated workflow and AAM are discussed below.

5.2.1 Polynomial fitting of raw data

Polynomials were used to approximate the true position and course of the cochlear duct and electrode array. Pietsch et al. (2017) suggested that a third-order polynomial can be used to approximate the ρ-values, and a fourth-order polynomial can be used to approximate the z-values of the cochlea. Figure 4.1 (a) and (b) present measured ρ- and z-values of the lateral spiral, approximated by using a third- and fourth-order polynomial fit, respectively. A mean absolute error (MAE) was calculated between the measured data and the polynomial approximation to establish the accuracy of the approximations to the measured points. The MAEs for the ρ- and z-values of the lateral spiral in Figure 4.1 were calculated to be 0.19 mm and 0.23 mm, respectively. Figure 4.3 illustrates the sixth-order polynomial fit for the lateral spiral for both the ρ- and z-values. The MAEs for the ρ- and z-values of the lateral spiral improved to 0.16 mm and 0.18 mm, respectively, illustrating an improved fit for a sixth-order polynomial approximation. The improved accuracy of the z-values is especially crucial since the cochlear height profile is often used to classify cochleae into separate groups according to different characteristics (Pietsch et al., 2017).

Figure 4.2 (a) and (b) show measured and approximated ρ- and z-values of the electrode array. The MAEs for the ρ- and z-values are 0.23 mm and 0.09 mm, respectively. Figure 4.4 illustrates the sixth-order polynomial approximations of the electrode array data. Using a sixth-order polynomial to approximate the electrode array data, resulted in improved MAEs of 0.07 mm and 0.06 mm for the ρ- and z-values.

While the third- and fourth-order approximations fit the cochlear spiral data to some degree, the electrode array approximation deviates from the measured data points. For both the lateral spiral and electrode array data, the sixth-order polynomial approximations tend to fit the measured data with higher accuracy, compared to the third- and fourth-order polynomials as suggested by Pietsch et al. (2017). Therefore, sixth-order polynomials were used to approximate all measured data in this study.

5.2.2 Comparison between AAM and automated method

A comparison was made between the automated method and the AAM, using the measured approximations as reference spirals. In Figure 4.5 (a), the ρ-values of the measured spiral, the automated method spiral and the AAM spiral are presented. The MAE, calculated between the spiral generated by the automated method and the measured spiral, is 0.62 mm. After adjustments using the AAM, the MAE of the ρ-values was reduced to 0.20 mm. The adapted spirals approximated the measured data with higher accuracy, compared to the automated method. Figure 4.5 (b) demonstrates a pronounced difference in z-values between the measured trajectories and the automated method trajectories, with an MAE of 0.39 mm. After adjustments using the AAM, the MAE was reduced to 0.07 mm, thereby illustrating improved accuracy.

Figure 4.6 (a) and (b) show examples of the ρ- and z-values of the electrode array. For the ρ-values, the MAE was calculated to be 0.20 mm for the automated method spiral, and 0.19 mm for the AAM spiral. Albeit similar MAEs for both methods, the spiral from the AAM illustrates a more realistic curve compared to the measured spiral, especially in the first 150°, while the automated method spiral deviates at this section. In Figure 4.6 (b) the AAM spiral illustrates an improved correspondence compared to the automated method spiral since the MAE improved from 0.26 mm to 0.16 mm.

Overall, the MAEs for the AAM ranged from 0.07 mm to 0.26 mm, with an average of 0.16 mm. The MAE for the automated method ranged from 0.20 mm to 0.62 mm, with an average of 0.37 mm. Noble et al. (2011) presented an automatic segmentation workflow in which a model was used with conventional CT scans for the segmentation of the cochlea. The mean and maximum surface errors were 0.21 mm and 0.80 mm. Reda et al. (2014) also illustrated that automatic segmentation of intracochlear anatomy in post-implantation CT images is possible, and reported mean and maximum segmentation errors of 0.22 mm and 0.73 mm. Compared to these reported errors, the AAM demonstrates acceptable accuracy.

5.3 EVALUATION OF THE ANALYTICAL COCHLEAR MODEL

Pietsch et al. (2017) proposed an analytical cochlear model, which can be used to predict the shape and course of the cochlear duct from four measurements. Due to limited CT scan data, this technique was used to derive the characteristics of the cochlear duct of one of the participants in this study. A full CT scan stack for the same person was received at a later stage, which was used to verify the accuracy of the analytical model. An experienced anatomist was tasked with identifying landmarks on the full CT scan stack, which were compared to the analytical model. Figure 4.7 (a) and (b) illustrate the ρ- and z-values generated by the analytical model, presented with the measured spiral as a comparison. The MAEs between the measured spirals and the analytical spirals were calculated to be 0.20 mm for the ρ-values and 0.16 mm for the z-values. Considering the errors reported by Noble et al. (2011) and Reda et al. (2014) for their automated workflows, the MAEs for the analytical model are relatively small. Furthermore, a desirable visual correspondence between the analytical and measured spirals exists. Therefore, the analytical model accurately predicts the individual 3D cochlear geometry from four clinical measurements. Based on these findings, this tool is recommended to predict the shape and course of the cochlear duct, if limited CT scan data are available.

5.4 GEOMETRIC VARIATIONS

This section aims to discuss how variations in models influence predicted T-levels. The effects of three different variations to a volume conduction model were explored, namely the presence of the OC, the shape of the CN and the granularity of cochlear geometries.

5.4.1 Excluding the OC

In Figure 4.8, predicted T-levels indicate that the exclusion of the OC did not have a considerable effect on predicted T-levels. An MAE of 0.0041 dB was calculated between predicted T-levels, indicating a negligible difference.

In the volume conduction models used in this study, the scala media geometry surrounds the OC geometry. Excluding the OC geometry from the model, causes the scala media geometry to fill the space of the OC. A typical value for the electrical conductivity of the scala media is 1.67 S/m and for the OC geometry 0.012 S/m (Malherbe et al., 2016). A substantial difference in conductivity is evident, however, due to the small volume that represents the OC geometry, little difference is observed in predictions. This corresponds with Malherbe et al. (2013), a study in which they assumed the effect of the OC to be negligible.

Including the OC in the model often introduces geometry and meshing errors. Using a fine mesh can resolve meshing errors in some instances, but in turn, increases the computational cost when solving a model. Based on these findings, the exclusion of the OC geometry from future models is recommended since it does not have a considerable effect on predicted T-levels and it introduces unwarranted modelling complications in the way that it was modelled in this study.

5.4.2 CN shape

The effects on T-levels caused by a modified CN geometry, was investigated. Figure 4.9 illustrates the difference in predicted T-levels between the model containing the original CN geometry and the model containing the modified CN geometry. Although similar T-levels can be observed for most electrodes, dissimilarities can be seen at the basal and apical electrodes. Dissimilarities exist at electrodes 1-3 (base) and electrodes 21-22 (apex). The maximum difference is 0.77 dB at the basal electrodes and 3.10 dB at the apical electrodes,

with the modified CN model predicting higher T-levels compared to the original CN model. The MAE between the two models in terms of predicted T-levels is 0.37 dB.

One possible explanation for dissimilarities is that the modified CN geometry typically occupies a greater volume at the base and apex compared to the original CN geometry, thereby reducing the amount of bone tissue. Bone material has a higher impedance compared to nerve material. By increasing the volume of the CN geometry at the apical and basal regions of the cochlea, the total impedance between the stimulating and reference electrodes is likely to decrease since electrical current will follow a path of least resistance from the ICEs towards the ECEs in MP1+2 stimulation. A low impedance pathway towards the ECEs could result in less current reaching the ANFs, which may increase predicted T-levels. This phenomenon also explains high T-levels for narrow BP stimulation (Zhu et al., 2012). During narrow BP stimulation, the active and reference electrodes have a low impedance pathway between them due to the short Euclidean distance. Reduced impedance often causes reduced current densities at the ANFs, thereby increasing T-levels.

Figure 4.9 shows that map T-levels are considerably lower than predicted T-levels. Overestimated T-levels is in accordance with Kalkman et al. (2016), who reported that model-predicted T-levels are still invariably higher than clinically measured T-levels. The reason for this remains unclear (Kalkman et al., 2016).

Equation (5.1) was used to evaluate the similarity in curve trends between predicted and map T-levels, as a function of the electrode number (e).

$$|D(e)| = |P'(e) - M'(e)| \tag{5.1}$$

Equation (5.1) uses the difference between the derivative of predicted T-levels, $P'(e)$, and the derivative of map T-levels, $M'(e)$, to calculate $|D(e)|$, the magnitude of the vector difference, which is an indication of trend dissimilarities. The unit of $|D(e)|$ is decibel per electrode (dB/e) since the rate of change, in decibels, between adjacent electrodes, is

calculated when the derivative is determined. Should the map and predicted T-levels follow the same trend, it would result in an answer of 0 dB/e. A large value would indicate substantial dissimilarities in the trend of the two curves.

A value of 15.80 dB/e was calculated between the map and predicted T-levels for the model containing the original CN geometry, while a value of 8.22 dB/e was calculated between the map and the model containing the modified CN, illustrating that the modified CN model has an improved trend.

Since the loft-function is used to create the CN geometry, numerous geometry and meshing errors are introduced, thereby increasing complexity and computational cost. However, the modified CN geometry affected apical and basal electrode T-levels. Although complexities are introduced when using the modified CN geometry, a more desirable trend can be observed for the modified CN. The modified CN geometry, therefore, seems to perform slightly better than the original CN geometry for predicting the trend of T-levels, while the original CN geometry performs slightly better than the original CN geometry for predicting absolute T-levels when considering the MAE.

5.4.3 The granularity of cochlear geometries

Figure 4.10 illustrates the difference in predicted T-levels between a smooth model and a faceted model. Predicted T-levels from both models are very similar, with a maximum deviation of 1.12 dB for the most apical electrode and an overall MAE of 0.33 dB. The model containing smooth geometries generally predicted slightly higher T-levels than the faceted model.

Smooth geometries drastically increase the complexity and computational cost of the overall model. Geometry and meshing errors frequently occur due to added data points produced by the loft-function, with some geometries unexpectedly intersecting adjacent geometries. In various cases, geometric errors can only be resolved by decreasing the size of the mesh,

primarily as a result of small geometric pieces, which are separated from the cochlear volumes when the final geometry is created.

In contrast, faceted geometries are created using quadrangular surfaces, knit together to form 3D geometries. Therefore, the boundaries of the cochlear structures are highly predictable. Consequently, this approach prevents unexpected intersections between adjacent geometries and generally do not require complicated meshes. Computational cost, geometric errors, and meshing errors decrease when using the faceted model.

From (5.1), a value of 19.96 dB/e was calculated between the map and predicted T-levels for the smooth model, while a value of 21.39 dB/e was calculated for the faceted model. Although the smooth model demonstrates a slightly improved trend compared to measured T-levels, the difference between the trends is negligible. Due to the predicted T-levels being very similar for the faceted and smooth geometries, and the smooth model demonstrating little improvement in terms of the trend of T-levels, the use of faceted geometries in volume conduction models is recommended, due to its simplicity during the modelling process.

5.5 MODEL INTERVENTIONS

Increasing the pulse width of the stimulus and, in so doing, decreasing the stimulation amplitude, is a technique often used to mitigate FNS symptoms due to the reduced spread of current at the FN (Alharbi et al., 2012, Battmer et al., 2006, Kelsall et al., 1997). The AR stimulation mode, discussed in Section 3.5, can also potentially reduce FNS symptoms since current is directed away from the FN and towards the apex of the cochlea. Both interventions were investigated by simulating the electrically stimulated cochlea for the different configurations. One way to evaluate the effectiveness of FNS interventions is to determine the relative difference between the FNF and ANF T-levels. Should FNF T-levels be much higher than the ANF T-levels, the individual should perceive sound without experiencing FNS. FNF T-levels, which are much higher than the ANF T-levels, could allow high stimulation levels before stimulating the FN, thereby increasing the usable dynamic range

of the implant. To quantify the performance of each intervention, a measure, the effective dynamic range ratio (EDRR), was devised and may be calculated using (5.2).

$$EDRR = \frac{\overline{FNF} - \overline{ANF}}{10_{dB}} \tag{5.2}$$

The average of ANF T-levels is subtracted from the average of FNF T-levels, and the answer is divided by 10 dB. A denominator of 10 dB was somewhat arbitrarily chosen as an acceptable dynamic range to refer to the difference between FNF and ANF T-levels. The typical dynamic range in CIs is 5-15 dB (Khater et al., 2015). An EDRR-value larger than 1 would indicate that the average of the FNF T-level is at least 10 dB higher than the average of the ANF T-levels, which is desirable since it would allow an acceptable dynamic range. A negative or near-zero EDRR-value would indicate that FNF T-levels are either below or close to the ANF T-levels, which is undesirable since little or no useable dynamic range would be available for speech perception.

Figure 4.11 (a) illustrates the predicted ANF and FNF T-levels for the MP1+2 stimulation mode, with a pulse width of 25 μs. The predicted T-level curves for the ANF and FNF are at a very similar level, with an EDRR of -0.011. For selected electrodes, FNF T-levels are lower than ANF T-levels. For these electrodes, the implication is that the user would perceive FNS before perceiving auditory sensations, which would be the case for electrodes 1-2 and 13-19, as evident in Figure 4.11 (a). These ICEs are located within proximity of the FN geometry, resulting in low impedance pathways between the active electrode and the FN geometry. Low impedance pathways cause decreased FNF T-levels since higher-intensity current levels stimulate the FN. Seyyedi et al. (2013) reported that electrodes responsible for FNS are typically located in the mid-array region of electrodes, ranging from 12 to 18. Berrettini et al. (2011) identified electrodes 16 to 18 and Iwasaki et al. (1998) identified electrodes 13 to 15. The offending electrodes reported in these studies correspond well with the electrodes identified in predictions.

Figure 4.11 (b) illustrates predicted T-levels for the same stimulation setup as in (a), but with a pulse width of 300 μs. As expected, predicted T-levels for both FNF and ANF are lower, compared to a pulse width of 25 μs, since wide pulse widths require stimuli with low amplitudes to achieve similar loudness levels (Battmer et al., 2006). FNF T-levels for all electrodes are above the ANF T-levels in this configuration, implying that the person would perceive sound on all electrodes before experiencing FNS. The difference between the ANF and FNF T-levels are more substantial than the difference illustrated in Figure 4.11 (a) since the EDRR increased from -0.011 for a 25 μs pulse width, to 0.379 for a 300 μs pulse width. This improvement corresponds with reported cases in which wide pulse widths reduced FNS symptoms (Alharbi et al., 2012, Battmer et al., 2006, Kelsall et al., 1997). Since the EDRR is less than 1, the improvement is still not sufficiently large to ensure adequate dynamic range for speech understanding. This is in accordance with Kelsall et al. (1997), who reported that wider pulse widths in persons with severe FNS are only of limited benefit.

Figure 4.12 shows predicted T-levels for the AR stimulation mode. Figure 4.12 (a) shows predicted T-levels for a 25 μs pulse width. All FNF T-levels are above ANF T-levels. This outcome suggests an increase in the difference between the ANF and FNF T-levels, with an EDRR of 1.67. The EDRR is much higher than both the 25 μs and 300 μs pulse widths used during MP1+2 stimulation. Therefore, the model suggests that AR stimulation can be more beneficial for CI users experiencing FNS, compared to MP1+2 stimulation, since the stimulation level can be increased to well above auditory T-levels before FNFs are excited. Models showed that AR stimulation with short pulse widths is, therefore, more effective in reducing FNS symptoms, compared to increasing pulse widths during MP1+2 stimulation. Since the EDRR is larger than 1, this intervention could potentially allow an adequate dynamic range for speech understanding.

Furthermore, Figure 4.12 (a) illustrates a local maximum in the FNF T-level curve at electrode 12, which is also the electrode furthest from the FN geometry. An increased distance implies that high impedance pathways exist between the stimulating electrode and the FN, resulting in reduced electrical current existing at the FN. Similarly, a local minimum is evident at electrode 16, which is located close to the FN, causing a reduction in T-levels.

The magnitude of the FNF T-levels seems to be more susceptible to the location of the stimulating electrode when the AR stimulation mode is used, compared to MP1+2 stimulation, since a high variability among FNF T-levels is observed in the predictions for AR stimulation.

The predicted ANF T-levels for AR stimulation are generally lower compared to T-levels for MP1+2 stimulation, for the same pulse width. On average, the AR stimulation T-levels are 1.82 dB lower than MP1+2 stimulation for a pulse width of 25 μs. This prediction corresponds well with the clinical ANF T-levels that were found in this study. Figure 4.17 shows reduced clinical T-levels for all AR stimulations, with an average difference of 2.98 dB. The average predicted difference in T-levels, between the AR and MP1+2 stimulation modes, is similar to the measured difference. Reduced T-levels for AR stimulation is presumably caused by low impedance pathways between the active and reference electrodes. ANFs, which are in this pathway, can be subjected to higher current densities, thereby explaining reduced T-levels.

Galvin and Fu (2005) investigated the effects of stimulation rate, mode and level on modulation detection by CI users. In their experiments, they determined T- and C-levels for two users in a narrow BP configuration (BP + 3) and a wide BP configuration (BP + 13), of which the latter is similar to the AR stimulation used in this study. For both participants, a wide BP configuration demonstrated an increase in dynamic range and a decrease in T-level. Pfingst et al. (2001) determined that results from speech performance tests were better for a wide BP configuration (BP + 6) than the narrow BP configuration. Pfingst et al. (1997) also suggested that the wide BP configuration resulted in the highest speech recognition scores, in comparison to conventional BP and common ground modes. The satisfactory performance of wide BP configurations supports the use of the AR stimulation mode since most electrodes on the array are located far from the most apical electrode.

Both wide pulse widths during MP1+2 stimulation, and the AR stimulation mode with short pulse widths, demonstrated benefits for users experiencing FNS. In addition, a combination of the two interventions was simulated. Figure 4.12 (b) presents predicted T-levels,

simulated for AR stimulation with a pulse width of 300 μs. For this configuration, the difference between ANF and FNF T-levels increased even further, with an EDRR of 1.77 between the ANF and FNF T-levels. Therefore, user-specific predictions show that this configuration would be most beneficial as an intervention for FNS for the participant in the study.

These results suggest that FNS interventions can be rated according to their effectiveness using model-predicted T-levels and the EDRR. The models illustrated that increased pulse widths could be beneficial for treating FNS, but that AR stimulation would be more beneficial, and that AR stimulation with a wide pulse width would be most beneficial.

5.6 CLINICAL RESULTS DISCUSSION

This section contains a discussion of the clinical results found in this study. Firstly, the experimental setup is evaluated, and the modifications to the experimental design are discussed. Thereafter, the findings in the EMG recordings and psychoacoustic tests are discussed.

5.6.1 Experimental setup

The pilot study was used to evaluate the validity of the experimental setup. From the pilot study, it was determined that two adjustments were required, namely the increase of the stimulation pulse width, and the decrease of the initial step size.

EMG recordings illustrated no observable artefact for stimuli with pulse widths of 25 μs. It was later determined that the 450 Hz low-pass cut-off frequency of the SX230-FW EMG amplifiers attenuated most of the electrical artefact due to the high-frequency contents present in the stimulus. During the pilot study, the pulse widths were gradually increased, after which the electrical artefact became evident. Wide pulse widths contain low-frequency components, which are not completely attenuated by the filter of the EMG device. Partially

attenuated artefacts were observed for wide pulse widths. To evaluate the amount of current, existing in the tissue surrounding the cochlea, the artefacts in the EMG recordings were evaluated. Therefore, wide pulse widths were used in the successive study.

In the pilot study, numerous auditory T-levels converged to values which did not correspond to T-levels recorded by the audiologist, while others converged correctly. For the 2IFC adaptive procedure, a correct or incorrect answer selected by the participant resulted in a reduction or an increase in stimulation level. On every reversal of the stimulation level direction, the step size was halved, as outlined by Gelfand (2017). Should the stimulation level be reduced to a value below the actual T-level, and the participant selects the incorrect interval, the stimulation level is increased to a level above or near the T-level, after which a sound will be perceived. However, if the participant coincidentally chooses the correct interval at an inaudible level, the stimulation is further reduced to a value well below the actual T-level. When this occurs, it becomes unlikely that the stimulation level would increase to a level above the actual T-level, especially when a large initial step size is used, and the stimulation step size is being reduced on every reversal. The probability that the participant would choose the correct interval for an inaudible stimulus is 50%. This prevented proper convergence to the correct T-level for some electrodes.

The initial step size of the level-adjustment process affected the extent of the change in stimulation level in the first few trails of the process. Therefore, a small initial step size was used in the successive study to ensure accurate T-level convergence every time. A small initial step size prevents the stimulation level from being underestimated. The step size is likely to influence the accuracy since Leek (2001) reported that various experimental variables, such as the step size, may influence the outcome of adaptive methods. Gelfand (2017) further describes a scenario in which a large step size may reduce the accuracy of an experiment since a step size which is too large, may place the highest inaudible presentation at levels with a 0% probability of response. However, Leek (2001) suggested that a large step size can be used, but that a statistical test should be performed to indicate whether performance at that level is better or worse than the targeted performance level (e.g., 75%

correct detections). Therefore, a series of stimuli should be presented at a specific level before the stimulation level is increased or decreased.

5.6.2 EMG Recordings

Bahmer and Baumann (2016) reported that muscle contractions often occur in the vicinity of the eye and mouth (orbicularis oculi and oris) during FNS. The results presented in Figure 4.13 showed that EMG1, which was recorded in the vicinity of the orbicularis oculi, contains larger artefacts compared to EMG2, which was recorded in the vicinity of the orbicularis oris. For EMG1, larger artefacts existed since the recording electrodes had a shorter distance to the stimulating ICEs.

Cushing et al. (2006) presented a study in which FNS in children were evaluated using EMG responses. Relative to the duration of the stimulus, they allowed a slightly increased recording time window. In the present study, a 1.5 s recording duration was used to capture the 1 s stimulus, since software synchronisation between the stimulus and start of the EMG recording could not be achieved with high precision. This is similar to the technique used by Cushing et al. (2006).

Figure 4.14 illustrates EMG signals captured during the successive study. Figure 4.14 (a) shows a section of an EMG recording in the absence of an electrical stimulus, illustrating the spontaneous activity of facial muscles. Figure 4.14 (b) shows a section of the EMG signal, captured while a stimulus was delivered and the electrical artefact was evident. The participant involved in the successive study had severe FNS and visual muscle contractions in the region of the chin during high stimulation levels, as described in Table 4.1. Despite visual evidence of muscle contractions, no FNS-related EMG signals could be distinguished between consecutive pulses as reported by Bahmer and Baumann (2016). One possible reason for this is that the EMG signals are truncated. The EMG amplifiers require a single-sided supply voltage, i.e. no negative part exists for the EMG data shown in Figure 4.14. When comparing Figure 4.14 (a) and (b), the spontaneous muscle activity seems to disappear

during stimulation since (b) mainly demonstrate the electrical artefacts and not any other observable muscle activity. A negative offset may be introduced during stimulation, which causes the EMG signal to shift out of the measuring range, thereby truncating values near and below zero. This offset could explain the absence of FNS-related muscle activity for the participant in the successive study.

The signal energy was evaluated for different active electrodes, stimulation modes and pulse widths. Figure 4.15 (a), (b) and (c) illustrate the stimulus intensity-dependent energy curves from the pilot study for electrodes 2, 10 and 16. For all graphs, high variability in the curves is evident, which is most likely caused by subtle movements by the participant, resulting in muscle activity unrelated to FNS. Figure 5.1 shows an example of EMG data containing movement artefacts. The movement artefacts are especially evident when comparing it to Figure 4.13, which shows an EMG recording in which little movement artefacts are present.

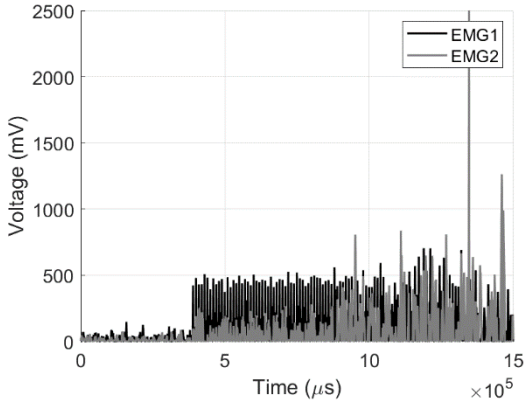

Figure 5.1. Example of EMG data containing movement artefacts. While the electrical artefact is visible in the first section of the recording, muscle activity, unrelated to FNS, can be seen in the second section, especially in EMG2.

Movement artefacts can be reduced by ensuring that the participant makes as few or no movements during EMG recordings, due to the high sensitivity of the EMG amplifiers. Furthermore, the EMG data, which contain movement artefacts, can be discarded if duplicate recordings exist for the specific stimulation level. Duplicate data were not available for the

pilot study and, consequently, high variability is evident in the intensity-dependent energy curves of the pilot study.

Despite high variability in intensity-dependent energy levels recorded during the pilot study, different trends are evident for MP1+2 and AR stimulations. MP1+2 stimulation shows a non-linear increase in the total energy for increasing stimulation intensities. For AR stimulation, energy levels remained constant for all stimulation intensities. This observation suggests that the electrical artefact was successfully reduced during AR stimulation. When the most apical electrode is configured to be the reference electrode, the electrical current that often exists between the active electrode and the ECEs in conventional MP1+2 stimulation, are directed to the apical point of the cochlea instead. The current, which usually exists in the surrounding tissue, is therefore reduced, consequently reducing the electrical artefact. Minimising extracochlear current, and therefore the electrical artefact, can be of benefit for CI users experiencing FNS since artefact reduction supports the idea of reducing FNS due to the reduced current reaching the FN (Bahmer and Baumann, 2016).

Figure 4.16 (a), (b) and (c) illustrate the energy levels for active electrodes 3, 5 and 8, respectively, recorded during the successive study. Duplicate EMG recordings were made during the successive study, whereafter most movement artefacts could be discarded without having a detrimental effect on the intensity-dependent energy curve. Discarding movement artefacts reduced irregularities in the curve, which is evident when the intensity-dependent energy curves from the pilot study are compared to the intensity-dependent energy curves from the successive study. The intensity-dependent energy curves in the successive study have a similar trend as the curves from the pilot study. MP1+2 showed a notable increase in energy levels, compared to AR stimulation, when stimulation intensities were increased. Both the pilot and successive studies, therefore, show that the AR stimulation mode successfully reduces the electrical artefact, and could reduce FNS symptoms.

During the experiments in the successive study, the subjective feedback provided by the participant was recorded and is presented in Table 4.1. When EMG energy levels were high due to MP1+2 stimulation, the participant reported FNS, and when low energy levels were

calculated for the AR stimulation, the participant reported no FNS. During MP1+2 stimulation, visual contractions in the region of the orbicularis oris were visible, which confirmed FNS. No visual indication of muscle contractions was visible for AR stimulation. This finding further supports the idea of reducing the electrical artefact to reduce FNS (Bahmer and Baumann, 2016).

5.6.3 Implant performance

Figure 4.17 shows that T- and C-levels are much lower for stimuli in which wide pulses were used, compared to short pulses. The reduction in T- and C-levels was caused by an increased charge introduced when using wide pulse widths, thus requiring lower stimulation amplitudes (Battmer et al., 2006).

In all cases, AR stimulation caused T-levels to decrease and C-levels to increase, thereby increasing the dynamic range. An increase in dynamic range is widely associated with an increase in implant performance (Khater et al., 2015). Conventional BP stimulation is known to result in higher T- and C-levels, presumably because of a smaller amount of neural tissue being stimulated (Zhu et al., 2012). Since AR stimulation mode directs the electrical current towards the apex, it could cause a larger population of neural fibres to be stimulated, resulting in decreased T-levels. The reason for the increase in C-levels might be because FNS is reduced, thereby allowing greater tolerance of higher stimulation levels. It might also be that the neural recruitment properties of the AR stimulation mode differ from that of MP1+2 stimulation mode. To determine the exact mechanism causing an increase in C-levels will require further investigation.

Predicted T-levels were much higher for all electrodes, in comparison to actual T-levels determined during experiments. Kalkman et al. (2016) suggested that models have an ongoing problem of being unable to reasonably predict realistic neural T- levels, which are invariably higher in the models than they are in clinical reality. Furthermore, not all predicted T-levels decreased for AR stimulation, as was evident for clinical T-levels. Further

improvements in volume conduction and neural models may be required to improve the accuracy of predictions.

Bahmer and Baumann (2016) reported that triphasic stimulation increases auditory T- and C-levels. AR stimulation, however, showed a general increase in C-levels and a decrease in T-levels, resulting in an increased dynamic range. Therefore, in terms of auditory T-levels, AR stimulation might be more beneficial compared to triphasic stimulation. Furthermore, reduced T-levels for AR stimulation might cause the implant to use less energy, resulting in increased battery life.

5.7 CHAPTER SUMMARY

In this chapter, the accuracy of the AAM was compared to the accuracy of the automated method. The AAM demonstrated cases in which an improvement in the accuracy of the model was observed. The analytical model, proposed by Pietsch et al. (2017), was also evaluated and illustrated acceptable performance compared to measured data. An investigation into geometric variations illustrated that the presence of the OC and the granularity of cochlear structures do not affect predictions by a substantial amount, but that the shape of the CN could influence predictions, especially at the apical and basal electrodes. Predictions regarding FNS interventions were discussed, and it was determined that AR stimulation with a wide pulse would be most effective in mitigating FNS symptoms in the specific individual. Reported cases of acceptable speech perception for wide BP stimulation furthermore supports the use of AR stimulations since the AR stimulation mode and a wide BP stimulation mode is similar. Furthermore, the clinical results were discussed. The experimental setup used in the pilot study was improved in the successive study and showed satisfactory results. Electrical artefacts were visible in EMG recordings and demonstrated a strong correspondence between the subjective feedback and the total energy calculated for the recorded EMG signals. AR stimulation resulted in lower energy levels, which suggest a reduction in FNS. Furthermore, the dynamic range increased, and T-levels decreased for AR stimulation during the successive study, illustrating an increase in implant performance.

CHAPTER 6 CONCLUSION

6.1 CHAPTER OVERVIEW

In Section 6.2 summaries of the answers to the research questions posed in Chapter 1 are presented. In Section 6.3 a description of potential future work is provided. In Section 6.4 the final conclusion for this study is presented.

6.2 ANSWERING THE RESEARCH QUESTIONS

The research questions are presented below, together with a brief description of the answers to the research questions, found in this study.

6.2.1 What is the accuracy of the automated method and can a refinement tool aid to increase the accuracy of 3D person-specific volume conduction models of the human cochlea and electrode array?

Data from the automated method and the AAM were compared to data measured by an experienced anatomist. Using MAEs as a measure, it was determined that in some cases, the automated method trajectories deviated from the measured trajectories. Dissimilarities could be due to the smoothing of detected spirals, or landmarks which were incorrectly identified during the automated process. The AAM was successful in improving the accuracy of the automated method trajectories in these cases, with improved MAEs after the adaption process.

6.2.2 Which recommendations can be made regarding the 3D modelling of the human cochlea?

Three modifications to a 3D model were made to determine how variations affect T-levels. By determining the effects of these variations, recommendations could be made to aid future modelling work. For the first variation, it was determined that the exclusion of the OC does not have a noticeable effect on predicted T-levels. It is therefore recommended to exclude this geometry due to the unwarranted complexity it adds to the model. Secondly, the proposed modified CN geometry affects predicted T-levels at the basal and apical regions. Albeit higher than the predicted T-levels from the original CN model, the T-levels from the modified CN geometry illustrated an improved trend, compared to map T-levels. Finally, it was determined that the granularity of cochlear structures does not seem to have a pronounced influence on T-levels. Therefore, it is recommended to use faceted geometries since this would reduce geometric errors, meshing errors and overall complexities, while achieving similar predictions to the smooth geometry model.

6.2.3 Can a 3D model be used to rate a selection of FNS interventions based on their effectiveness in reducing FNS?

Two FNS interventions were investigated through a model of the electrically stimulated cochlea and were rated according to their effectiveness in reducing FNS. The EDRR was used as a measure of the effectiveness since a value larger than 1 would indicate that, on average, a useful dynamic range of 10 dB can be achieved without stimulating the FN. Increased pulse widths and AR stimulation were investigated as interventions. Models indicated that increasing the pulse width has limited benefit when treating FNS, but that the AR stimulation mode could be more effective. Furthermore, it was determined that a combination of increased pulse widths and AR stimulation would be most beneficial.

6.2.4 Does AR stimulation prove to be effective in reducing FNS in clinical experiments?

AR stimulation was investigated in this study as an FNS intervention, by evaluating the EMG signal energy, since Bahmer and Baumann (2016) suggested that artefact reduction supports the idea of reducing FNS. AR stimulation resulted in a reduced electrical artefact, compared to MP1+2 stimulation. Furthermore, the user reported no FNS symptoms during AR stimulation. This observation corresponds well with the hypothesis of Bahmer and Baumann (2016). Since both the electrical artefact and perceptual FNS were reduced, it can be concluded that AR stimulation is effective in reducing FNS for this particular CI user.

6.2.5 What is the effect of AR stimulation on perceptual T-levels and dynamic range?

AR stimulation resulted in reduced T-levels and increased C-levels, consequently increasing the dynamic range. An increase in dynamic range is widely associated with an increase in implant performance (Khater et al., 2015), which support the use of AR stimulation. The AR stimulation mode reduces FNS while improving T-levels and increasing dynamic range.

6.2.6 How successful is this model in predicting measured outcomes?

Predicted T-levels were significantly higher than the T-levels found during clinical testing. This is in line with the findings by Kalkman et al. (2016). Advancements in volume conduction models and modelling of neural excitations could potentially improve the accuracy of T-level predictions. Albeit invariably high predicted T-levels were found, a relative comparison between T-levels for different stimulation techniques could be used to rate FNS interventions.

6.3 FUTURE WORK

Although AR stimulation illustrated a reduction in FNS, it should be evaluated for a larger CI user cohort to determine whether the findings of this study can be generalized. Ideally, similar tests should be performed for all active electrodes, to determine whether FNS can be reduced without adversely influencing the dynamic range or auditory T-levels. In addition, CI performance should be evaluated by using one or more standardised speech perception tests to determine whether AR stimulation has an adverse effect on speech perception. During these tests, the severity of FNS should objectively be evaluated using EMG recordings.

6.4 FINAL CONCLUSION

In summation, the following can be concluded from this study:

- The accuracy of the model generated by the automated method relative to measured data could be improved using the proposed refinement tool.
- These refined models were utilised to evaluate FNS interventions, after which these interventions could be rated according to their effectiveness.
- Validation of the AR stimulation mode as an FNS intervention was done in a clinical environment, which demonstrated a reduced electrical artefact, reduced FNS symptoms, a decrease in perceptual T-levels and an increase in dynamic range.

REFERENCES

ABDELHAMED, M. 2019. Evaluation of the Triphasic Pulse Stimulation in Eliminating Facial Nerve Stimulation in Cochlear Implant Recipients. *Global Journal of Otolaryngology,* 19.

AGRAWAL, S., SCHART-MOREN, N., LIU, W., LADAK, H. M., RASK-ANDERSEN, H. & LI, H. 2018. The secondary spiral lamina and its relevance in cochlear implant surgery. *Ups J Med Sci,* 123**,** 9-18.

AHN, J. H., OH, S. H., CHUNG, J. W. & LEE, K.-S. 2009. Facial nerve stimulation after cochlear implantation according to types of Nucleus 24-channel electrode arrays. *Acta oto-laryngologica,* 129**,** 588-591.

ALHARBI, F. A., SPRENG, M. & ISSING, P. R. 2012. Facial Nerve Stimulation Can Improve after Cochlear Reimplantation and Postoperative Advanced Programming Techniques: Case Report. *International Journal of Clinical Medicine,* 3**,** 62-64.

BADENHORST, W., HANEKOM, T. & HANEKOM, J. J. 2017. Analysis of a purely conductance-based stochastic nerve fibre model as applied to compound models of populations of human auditory nerve fibres used in cochlear implant simulations. *Biol Cybern,* 111**,** 439-458.

BAHMER, A., ADEL, Y. & BAUMANN, U. 2017. Preventing facial nerve stimulation by triphasic pulse stimulation in cochlear implant users: intraoperative recordings. *Otology & Neurotology,* 38**,** e438-e444.

BAHMER, A. & BAUMANN, U. 2016. The underlying mechanism of preventing facial nerve stimulation by triphasic pulse stimulation in cochlear implant users assessed with objective measure. *Otology & Neurotology,* 37**,** 1231-1237.

BATTMER, R., PESCH, J., STÖVER, T., LESINSKI-SCHIEDAT, A., LENARZ, M. & LENARZ, T. 2006. Elimination of facial nerve stimulation by reimplantation in cochlear implant subjects. *Otology & neurotology : official publication of the American Otological Society, American Neurotology Society [and] European Academy of Otology and Neurotology,* 27**,** 918-922.

BELTRAME, M. A., BONFIOLI, F. & FRAU, G. N. 2000. Cochlear implant in inner ear malformation: double posterior labyrinthotomy approach to common cavity. *Updates in Cochlear Implantation.* Karger Publishers.

BERRETTINI, S., VITO, D. A., BRUSCHINI, L., PASSETTI, S. & FORLI, F. 2011. Facial nerve stimulation after cochlear implantation: our experience. *Acta otorhinolaryngologica Italica : organo ufficiale della Societa italiana di otorinolaringologia e chirurgia cervico-facciale,* 31**,** 11-6.

BIGELOW, D. C., KAY, D. J., RAFTER, K. O., MONTES, M., KNOX, G. W. & YOUSEM, D. M. 1998. Facial nerve stimulation from cochlear implants. *The American journal of otology,* 19**,** 163-9.

BOYER, E., KARKAS, A., ATTYE, A., LEFOURNIER, V., ESCUDE, B. & SCHMERBER, S. 2015. Scalar localization by cone-beam computed tomography of cochlear implant carriers: a comparative study between straight and periomodiolar precurved electrode arrays. *Otology & Neurotology,* 36**,** 422-429.

BROOMFIELD, S., MAWMAN, D., WOOLFORD, T. J., O'DRISCOLL, M., LUFF, D. & RAMSDEN, R. T. 2000. Non-auditory stimulation in adult cochlear implant users. *Cochlear implants international,* 1**,** 55-66.

CAMILLERI, A. E., TONER, J. G., HOWARTH, K. L., HAMPTON, S. & RAMSDEN, R. T. 1999. Cochlear implantation following temporal bone fracture. *The Journal of Laryngology & Otology,* 113**,** 454-457.

CLARK, G. M. 1973. A hearing prosthesis for severe perceptive deafness--experimental studies. *J Laryngol Otol,* 87**,** 929-45.

COHEN, N. L., HOFFMAN, R. A. & STROSCHEIN, M. 1988. Medical or Surgical Complications Related to the Nucleus Multichannel Cochlear Implant. *Annals of Otology, Rhinology & Laryngology,* 97**,** 8-13.

CROUS, H. G., HANEKOM, T. & HANEKOM, J. J. 2018. *Investigating the automation of the 3D computational model development workflow of the cochlear implant.* Masters Dissertation, University of Pretoria.

CUREOGLU, S., BAYLAN, M. Y. & PAPARELLA, M. M. 2010. Cochlear otosclerosis. *Current opinion in otolaryngology & head and neck surgery,* 18**,** 357-362.

CUSHING, S. L., PAPSIN, B. C. & GORDON, K. A. 2006. Incidence and characteristics of facial nerve stimulation in children with cochlear implants. *The Laryngoscope,* 116**,** 1787-1791.

DJOURNO, A. & EYRIES, C. 1957. Auditory prosthesis by means of a distant electrical stimulation of the sensory nerve with the use of an indwelt coiling. *Presse Med,* 65**,** 1417.

DOSHI, J., JOHNSON, P., MAWMAN, D., GREEN, K., BRUCE, I. A., FREEMAN, S. & LLOYD, S. K. W. 2015. Straight Versus Modiolar Hugging Electrodes: Does One Perform Better Than the Other? *Otology & Neurotology,* 36**,** 223-227.

ELFARNAWANY, M., ALAM, S. R., ROHANI, S. A., ZHU, N., AGRAWAL, S. K. & LADAK, H. M. 2017. Micro-CT versus synchrotron radiation phase contrast imaging of human cochlea. *Journal of microscopy,* 265**,** 349-357.

ERIXON, E., HÖGSTORP, H., WADIN, K. & RASK-ANDERSEN, H. 2009. Variational anatomy of the human cochlea: implications for cochlear implantation. *Otology & neurotology : official publication of the American Otological Society, American Neurotology Society [and] European Academy of Otology and Neurotology,* 30**,** 14-22.

ESHRAGHI, A. A., NAZARIAN, R., TELISCHI, F. F., RAJGURU, S. M., TRUY, E. & GUPTA, C. 2012. The cochlear implant: historical aspects and future prospects. *The Anatomical Record: Advances in Integrative Anatomy and Evolutionary Biology,* 295**,** 1967-1980.

ESPAHBODI, M., SWEENEY, A. D., LENNON, K. J. & WANNA, G. B. 2015. Facial nerve stimulation associated with cochlear implant use following temporal bone fractures. *Am J Otolaryngol,* 36**,** 578-582.

FRITZSCH, B., JAHAN, I., PAN, N., KERSIGO, J., DUNCAN, J. & KOPECKY, B. 2011. Dissecting the molecular basis of organ of Corti development: Where are we now? *Hear Res,* 276**,** 16-26.

GALVIN, J. J., 3RD & FU, Q.-J. 2005. Effects of stimulation rate, mode and level on modulation detection by cochlear implant users. *Journal of the Association for Research in Otolaryngology : JARO,* 6**,** 269-279.

GELFAND, S. A. 2017. *Hearing: An introduction to psychological and physiological acoustics,* CRC Press.

GRAHAM, J. M., PHELPS, P. D. & MICHAELS, L. 2000. Congenital malformations of the ear and cochlear implantation in children: review and temporal bone report of common cavity. *The Journal of Laryngology & Otology,* 114**,** 1-14.

GRAY, H. 1918. Anatomy of the human body. *Philadelphia: Lea & Febiger*.

GROSS, L., HANEKOM, T., HANEKOM, J. J. & BADENHORST, W. 2017. *3D modelling of post-cochlear implant facial nerve stimulation in a specific user*. Masters Dissertation, University of Pretoria.

HANEKOM, T. & HANEKOM, J. J. 2016. Three-dimensional models of cochlear implants: A review of their development and how they could support management and

maintenance of cochlear implant performance. *Network (Bristol, England),* 27**,** 67-106.

HO, E. C., PROOPS, D., ANDREWS, P. & GRAHAM, J. 2007. Unexpected exit of a cochlear implant electrode through the wall of the basal turn of the cochlea – a report on two patients. *Cochlear Implants International,* 8**,** 162-171.

HOCHMAIR, I., HOCHMAIR, E., NOPP, P., WALLER, M. & JOLLY, C. 2015. Deep electrode insertion and sound coding in cochlear implants. *Hearing research,* 322**,** 14-23.

HOFFMAN, R. A. & COHEN, N. L. 1995. Complications of cochlear implant surgery. *The Annals of Otology, Rhinology & Laryngology.Supplement,* 166**,** 420-422.

HOUSE, L. R. 1987. Cochlear implant: the beginning. *The Laryngoscope,* 97**,** 996-997.

IWASAKI, S., ATSUMI, K., OCHO, S. & MIZUTA, K. 1998. Facial nerve stimulation by a cochlear implant in a hemodialysis patient with bone of low mineral density. *European Archives of Oto-Rhino-Laryngology,* 255**,** 352-354.

JACKLER, R. K., LUXFORD, W. M. & HOUSE, W. F. 1987a. Congenital malformations of the inner ear: a classification based on embryogenesis. *The Laryngoscope,* 97**,** 2-14.

JACKLER, R. K., LUXFORD, W. M. & HOUSE, W. F. 1987b. Sound detection with the cochlear implant in five ears of four children with congenital malformations of the cochlea. *The Laryngoscope,* 97**,** 15-17.

KALKMAN, R. K., BRIAIRE, J. J., DEKKER, D. M. & FRIJNS, J. H. 2014. Place pitch versus electrode location in a realistic computational model of the implanted human cochlea. *Hear Res,* 315**,** 10-24.

KALKMAN, R. K., BRIAIRE, J. J. & FRIJNS, J. H. 2016. Stimulation strategies and electrode design in computational models of the electrically stimulated cochlea: an overview of existing literature. *Network: Computation in Neural Systems,* 27**,** 107-134.

KELSALL, D. C., SHALLOP, J. K., BRAMMEIER, T. G. & PRENGER, E. C. 1997. Facial nerve stimulation after Nucleus 22-channel cochlear implantation. *The American journal of otology.*

KEMPF, H. G., TEMPEL, S., JOHANN, K. & LENARZ, T. 1999. Complications of cochlear implant surgery in children and adults. *Laryngo-Rhino-Otologie,* 78**,** 529-537.

KHATER, A., EL SHENNAWAY, A. & ANANY, A. 2015. Improvement of cochlear implant performance: changes in dynamic range. *The Egyptian Journal of Otolaryngology,* 31**,** 36-41.

KLAWITTER, S., LANDSBERGER, D. M., BÜCHNER, A. & NOGUEIRA, W. 2018. Perceptual changes with monopolar and phantom electrode stimulation. *Hearing research,* 359**,** 64-75.

LANGMAN, A. W., QUIGLEY, S. M., HEFFERNAN, J. T. & BRAZIL, C. 1995. Use of botulinum toxin to prevent facial nerve stimulation following cochlear implantation. *The Annals of otology, rhinology & laryngology. Supplement,* 166**,** 426-8.

LEEK, M. R. 2001. Adaptive procedures in psychophysical research. *Perception & Psychophysics,* 63**,** 1279-1292.

LUCA, C. J. D. 2002. Surface Electromyography : Detection and Recording. *DelSys Incorporated,* 10**,** 1-10.

MAAS, S., BANCE, M., O'DRISCOLL, M., MAWMAN, D. & RAMSDEN, R. T. 1996. Explantation of a nucleus multichannel cochlear implant and re-implantation into the contralateral ear. A case report of a new strategy. *The Journal of laryngology and otology,* 110**,** 881-883.

MALHERBE, T. K., HANEKOM, T. & HANEKOM, J. J. 2013. Can subject-specific single-fibre electrically evoked auditory brainstem response data be predicted from a model? *Med Eng Phys,* 35**,** 926-36.

MALHERBE, T. K., HANEKOM, T. & HANEKOM, J. J. 2016. Constructing a three-dimensional electrical model of a living cochlear implant user's cochlea. *International Journal for Numerical Methods in Biomedical Engineering,* 32**,** e02751.

MANCINI, P., D'ELIA, C., BOSCO, E., DE SETA, E., PANEBIANCO, V., VERGARI, V. & FILIPO, R. 2008. Follow-up of cochlear implant use in patients who developed bacterial meningitis following cochlear implantation. *The Laryngoscope,* 118**,** 1467-1471.

MARSHALL, A. H., FANNING, N., SYMONS, S., SHIPP, D., CHEN, J. M. & NEDZELSKI, J. M. 2005. Cochlear Implantation in Cochlear Otosclerosis. *The Laryngoscope,* 115**,** 1728-1733.

MARTINS, G. D. S. Q., BRITO NETO, R. V., TSUJI, R. K., GEBRIM, E. M. M. S. & BENTO, R. F. 2015. Evaluation of intracochlear trauma caused by insertion of cochlear implant electrode arrays through different quadrants of the round window. *BioMed research international,* 2015.

MATTERSON, A. G., O'LEARY, S., PINDER, D., FREIDMAN, L., DOWELL, R. & BRIGGS, R. 2007. Otosclerosis: selection of ear for cochlear implantation. *Otology & neurotology : official publication of the American Otological Society, American Neurotology Society [and] European Academy of Otology and Neurotology,* 28**,** 438-446.

MCCLAY, J. E., TANDY, R., GRUNDFAST, K., CHOI, S., VEZINA, G., ZALZAL, G. & WILLNER, A. 2002. Major and minor temporal bone abnormalities in children with and without congenital sensorineural hearing loss. *Archives of Otolaryngology–Head & Neck Surgery,* 128**,** 664-671.

MERTES, J. & CHINNICI, J. 2006. Cochlear Implants - Considerations in Programming for the Pediatric Population.

MIRANDA, P. C., SAMPAIO, A., #XE9, LOPES, L., LOPES, R. A. F., RAMOS VENOSA, A. & OLIVEIRA, C. A. C. P. D. 2014. Hearing Preservation in Cochlear Implant Surgery. *International Journal of Otolaryngology,* 2014**,** 6.

MUCKLE, R. P. & LEVINE, S. C. 1994. Facial nerve stimulation produced by cochlear implants in patients with cochlear otosclerosis. *The American journal of otology.*

MYLANUS, E. A. M., ROTTEVEEL, L. J. C. & LEEUW, R. L. 2004. Congenital malformation of the inner ear and pediatric cochlear implantation. *Otology & neurotology : official publication of the American Otological Society, American Neurotology Society [and] European Academy of Otology and Neurotology,* 25**,** 308-317.

NIGAM, P. K. & NIGAM, A. 2010. Botulinum toxin. *Indian journal of dermatology,* 55**,** 8-14.

NIPARKO, J. K., OVIATT, D. L., COKER, N. J., SUTTON, L., WALTZMAN, S. B., COHEN, N. L. & IMPLANTATION, V. C. S. G. O. C. 1991. Facial nerve stimulation with cochlear implantation. VA Cooperative Study Group on Cochlear Implantation. *Otolaryngology-Head and Neck Surgery,* 104**,** 826-830.

NOBLE, J. H., LABADIE, R. F., MAJDANI, O. & DAWANT, B. M. 2011. Automatic segmentation of intracochlear anatomy in conventional CT. *IEEE transactions on bio-medical engineering,* 58**,** 2625-2632.

NOVAK, M. A., FIFER, R. C., BARKMEIER, J. C. & FIRSZT, J. B. 1990. Labyrinthine ossification after meningitis: its implications for cochlear implantation. *Otolaryngology--head and neck surgery : official journal of American Academy of Otolaryngology-Head and Neck Surgery,* 103**,** 351-356.

O'CONNELL, B. P., DEDMON, M. M. & HAYNES, D. S. 2017. Hearing Preservation Cochlear Implantation: a Review of Audiologic Benefits, Surgical Success Rates,

and Variables That Impact Success. *Current Otorhinolaryngology Reports,* 5**,** 286-294.

OCAK, E., KOCAOZ, D., ACAR, B. & TOPCUOGLU, M. 2018. Radiological Evaluation of Inner Ear with Computed Tomography in Patients with Unilateral Non-Pulsatile Tinnitus. *J Int Adv Otol,* 14**,** 273-277.

PAPSIN, B. C. 2005. Cochlear Implantation in Children With Anomalous Cochleovestibular Anatomy. *The Laryngoscope,* 115**,** 1-26.

PATEL, A. & GROPPO, E. 2010. Management of temporal bone trauma. *Craniomaxillofacial trauma & reconstruction,* 3**,** 105-13.

PFINGST, B. E., FRANCK, K. H., XU, L., BAUER, E. M. & ZWOLAN, T. A. 2001. Effects of electrode configuration and place of stimulation on speech perception with cochlear prostheses. *Journal of the Association for Research in Otolaryngology : JARO,* 2**,** 87-103.

PFINGST, B. E., ZWOLAN, T. A. & HOLLOWAY, L. A. 1997. Effects of stimulus configuration on psychophysical operating levels and on speech recognition with cochlear implants. *Hearing Research,* 112**,** 247-260.

PIETSCH, M., AGUIRRE DAVILA, L., ERFURT, P., AVCI, E., LENARZ, T. & KRAL, A. 2017. Spiral Form of the Human Cochlea Results from Spatial Constraints. *Sci Rep,* 7**,** 7500.

POLAK, M., ULUBIL, S. A., HODGES, A. V. & BALKANY, T. J. 2006. Revision cochlear implantation for facial nerve stimulation in otosclerosis. *Archives of otolaryngology--head & neck surgery,* 132**,** 398-404.

RAH, Y. C., YOON, Y. S., CHANG, M. Y., LEE, J. Y., SUH, M. W., LEE, J. H., OH, S. H., CHANG, S. O. & PARK, M. K. 2016. Facial nerve stimulation in the narrow bony cochlear nerve canal after cochlear implantation. *The Laryngoscope,* 126**,** 1433-1439.

RAMSDEN, R., ROTTEVEEL, L., PROOPS, D., SAEED, S., VAN OLPHEN, A. & MYLANUS, E. 2007. Cochlear Implantation in Otosclerotic Deafness. *Otosclerosis and Stapes Surgery*. Basel: KARGER.

RAYNER, M. G., KING, T., DJALILIAN, H. R., SMITH, S. & LEVINE, S. C. 2003. Resolution of facial stimulation in otosclerotic cochlear implants. *Otolaryngology - Head and Neck Surgery.*

REDA, F. A., MCRACKAN, T. R., LABADIE, R. F., DAWANT, B. M. & NOBLE, J. H. 2014. Automatic segmentation of intra-cochlear anatomy in post-implantation CT of unilateral cochlear implant recipients. *Medical image analysis,* 18**,** 605-615.

ROTTEVEEL, L. J., PROOPS, D. W., RAMSDEN, R. T., SAEED, S. R., VAN OLPHEN, A. F. & MYLANUS, E. A. 2004. Cochlear implantation in 53 patients with otosclerosis: demographics, computed tomographic scanning, surgery, and complications. *Otology & Neurotology,* 25**,** 943-952.

RUCKENSTEIN, M. J. 2012. Cochlear implants and other implantable hearing devices. 448.

RUIZ, H., ALMIRÓN, L., GRASSANO, C. & FILAS, E. 2006. Facial nerve protection. *Wiener Medizinische Wochensschrift,* 156**,** 1-192.

SARGENT, E. W. 2001. OTOSCLEROSIS: A Review for Audiologists Eric W. Sargent Medical & Surgical Hearing & Hearing Loss 1226. *Audiology Online*.

SCHATZER, R., VAN DE HEYING, P., MÜLLER, J., WEBER, B. P., WIESER, S., GERARD, J. M., ROUX-VAILLARD, S., SÜRTH, W. & ZIERHOFER, C. Selective suppression of facial nerve activation in ci patients with triphasic stimulation. 13th International Conference on Cochlear Implants and Other Implantable Auditory Implants (Book of Abstracts), 2014. 119.

SEEBER, B., FASTL, H. & BAUMANN, U. Akustische Lokalisation mit Cochlea-Implantat und Richtmikrofon-Hörgerät (Acoustical localization with cochlear implant and directional microphone hearing aid). Fortschritte der Akustik--DAGA'01, 2001.

SEEBER, B. U. & BRUCE, I. C. 2016. The history and future of neural modeling for cochlear implants. *Network: Computation in Neural Systems,* 27**,** 53-66.

SEMAAN, M. T., GEHANI, N. C., TUMMALA, N., COUGHLAN, C., FARES, S. A., HSU, D. P., MURRAY, G. S., LIPPY, W. H. & MEGERIAN, C. A. 2012. Cochlear implantation outcomes in patients with far advanced otosclerosis. *American Journal of Otolaryngology - Head and Neck Medicine and Surgery.*

SEYYEDI, M., HERRMANN, B. S., EDDINGTON, D. K., NADOL, J. B. & JR. 2013. The pathologic basis of facial nerve stimulation in otosclerosis and multi-channel cochlear implantation. *Otology & neurotology : official publication of the American Otological Society, American Neurotology Society [and] European Academy of Otology and Neurotology,* 34**,** 1603-9.

SHIN, K. J., GIL, Y. C., LEE, J. Y., KIM, J. N., SONG, W. C. & KOH, K. S. 2014. Three-Dimensional Study of the Facial Canal Using Microcomputed Tomography for Improved Anatomical Comprehension. *The Anatomical Record,* 297**,** 1808-1816.

SHIN, K. J., LEE, J. Y., KIM, J. N., YOO, J. Y., SHIN, C., SONG, W. C. & KOH, K. S. 2013. Quantitative analysis of the cochlea using three-dimensional reconstruction based on microcomputed tomographic images. *Anat Rec (Hoboken),* 296**,** 1083-8.

SHORT, M. 2016. Meningitis and encephalitis. *SAGE Journals,* 9**,** 589-596.

SMULLEN, J. L., POLAK, M., HODGES, A. V., PAYNE, S. B., KING, J. E., TELISCHI, F. F. & BALKANY, T. J. 2005. Facial nerve stimulation after cochlear implantation. *The Laryngoscope,* 115**,** 977-82.

STEENERSON, R. L., GARY, L. B. & WYNENS, M. S. 1990. Scala vestibuli cochlear implantation for labyrinthine ossification. *Otology & Neurotology,* 11**,** 360-363.

STJERNHOLM, C. & MUREN, C. 2002. Dimensions of the cochlear nerve canal: a radioanatomic investigation. *Acta oto-laryngologica,* 122**,** 43-48.

STODDART, R. L. & COOPER, H. R. 1999. Electrode complications in 100 adults with multichannel cochlear implants. *J Laryngol Otol Suppl,* 24**,** 18-20.

TECHNAVIO. 2016. The Number of Cochlear Implants Shipped Worldwide is Expected to Hit 96,000 by 2020.

THEUNISSE, H. J., PENNINGS, R. J., KUNST, H. P., MULDER, J. J. & MYLANUS, E. A. 2018. Risk factors for complications in cochlear implant surgery. *European Archives of Oto-Rhino-Laryngology,* 275**,** 895-903.

TRENTMAN, T. L., MALONEY, J. A., WIE, C. S., REBECCA, A. M. & ROSENFELD, D. M. 2015. Use of botulinum toxin injections to treat peripheral stimulator induced facial muscle twitching: a case report. *Springerplus,* 4**,** 671.

TSANG, W. S., YU, J. K., BHATIA, K. S., WONG, T. K. & TONG, M. C. 2013. The Bonebridge semi-implantable bone conduction hearing device: experience in an Asian patient. *J Laryngol Otol,* 127**,** 1214-21.

TUCCI, D. L., TELIAN, S. A., ZIMMERMAN-PHILLIPS, S., ZWOLAN, T. A. & KILENY, P. R. 1995. Cochlear implantation in patients with cochlear malformations. *Archives of otolaryngology--head & neck surgery,* 121**,** 833-8.

VAN BOXTEL, A. Facial EMG as a tool for inferring affective states. Proceedings of measuring behavior, 2010. Noldus Information Technology Wageningen, 104-108.

WANG, J., TANG, L. & BRONLUND, J. E. 2013. Surface EMG Signal Amplification and Filtering. *International Journal of Computer Applications,* 82**,** 975-8887.

WEISSGERBER, T., STÖVER, T. & BAUMANN, U. 2019. Speech perception in noise: Impact of directional microphones in users of combined electric-acoustic stimulation. *PLOS ONE,* 14**,** e0213251.

WILSON, B. S. & DORMAN, M. F. 2008. Cochlear implants: a remarkable past and a brilliant future. *Hearing research,* 242**,** 3-21.

XU, J., XU, S. A., COHEN, L. T. & CLARK, G. M. 2000. Cochlear view: postoperative radiography for cochlear implantation. *Am J Otol,* 21**,** 49-56.

YEUNG, A. H., BRODIE, H. A., TALAVERA, F., ROLAND, P. S., MEYERS, A. D. & SHOHET, J. A. 2017. Labyrinthitis Ossificans. *Medscape*.

YOO, S. K., WANG, G., RUBINSTEIN, J. T. & VANNIER, M. W. 2000. Three-dimensional geometric modeling of the cochlea using helico-spiral approximation. *IEEE Transactions on Biomedical Engineering,* 47**,** 1392-1402.

ZAHAK, M. 2012. Signal Acquisition Using Surface EMG and Circuit Design Considerations for Robotic Prosthesis. *Computational Intelligence in Electromyography Analysis - A Perspective on Current Applications and Future Challenges.* InTech.

ZHU, Z., TANG, Q., ZENG, F.-G., GUAN, T. & YE, D. 2012. Cochlear-implant spatial selectivity with monopolar, bipolar and tripolar stimulation. *Hearing research,* 283**,** 45-58.